

Journal Pre-proof

Neotectonics around the Ordos Block, North China: A review and new insights

Wei Shi, Shuwen Dong, Jianmin Hu



PII: S0012-8252(19)30291-0
DOI: <https://doi.org/10.1016/j.earscirev.2019.102969>
Reference: EARTH 102969

To appear in:

Received Date: 7 May 2019
Revised Date: 29 September 2019
Accepted Date: 29 September 2019

Please cite this article as: Shi W, Dong S, Hu J, Neotectonics around the Ordos Block, North China: A review and new insights, *Earth-Science Reviews* (2019), doi: <https://doi.org/10.1016/j.earscirev.2019.102969>

This is a PDF file of an article that has undergone enhancements after acceptance, such as the addition of a cover page and metadata, and formatting for readability, but it is not yet the definitive version of record. This version will undergo additional copyediting, typesetting and review before it is published in its final form, but we are providing this version to give early visibility of the article. Please note that, during the production process, errors may be discovered which could affect the content, and all legal disclaimers that apply to the journal pertain.

© 2019 Published by Elsevier.

Neotectonics around the Ordos Block, North China: A review and new insights

Wei Shi^{a,b,†}, Shuwen Dong^c, Jianmin Hu^a

^{a)} Institute of Geomechanics, Chinese Academy of Geological Sciences, Beijing 100081, China

^{b)} Key Laboratory of Neotectonic Movement and Geohazard, Ministry of Natural Resources, Beijing 100081, China

^{c)} Sinoprobe Center, Chinese Academy of Geological Sciences, Beijing 100037, China

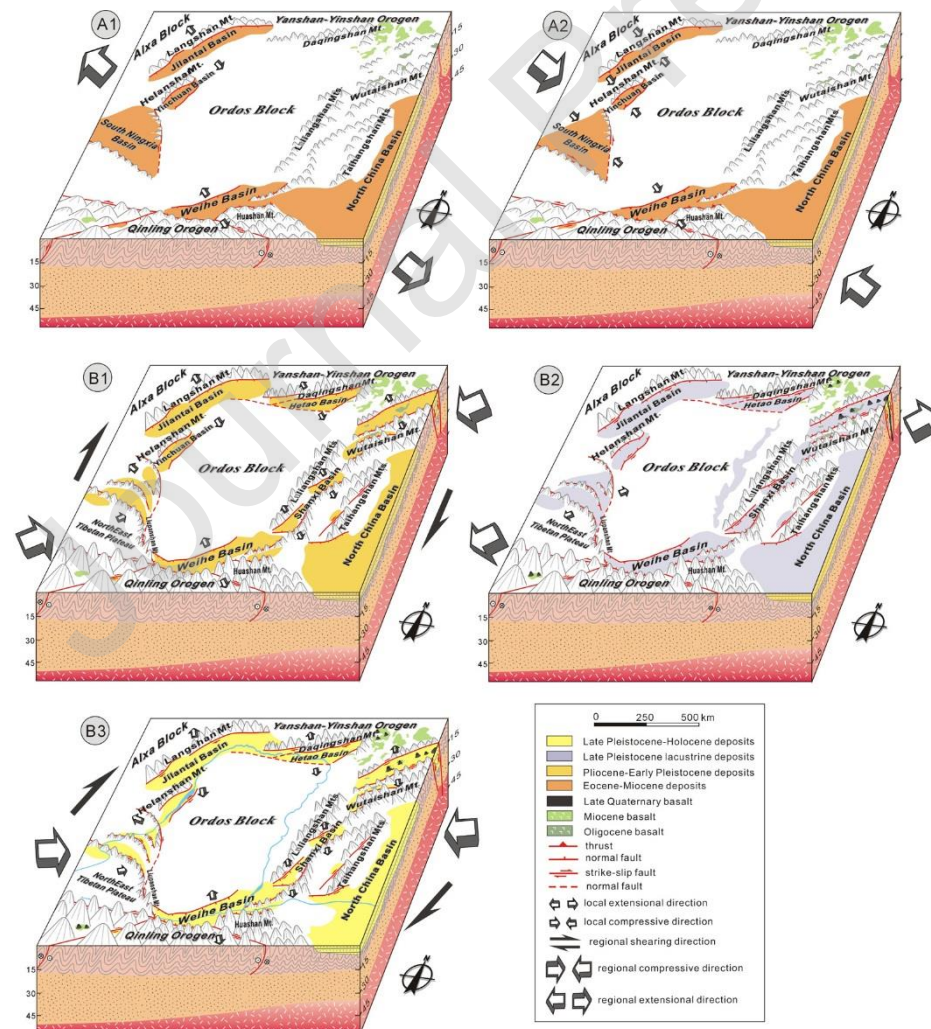
First author: Wei Shi

E-mail: shiweinmg@163.com

Tel: +86-10-88815102(O)

†Corresponding author: Wei Shi

Graphical abstract



Highlights

- Two-stage tectonic evolution of the faulted basins around the Ordos Block is rebuilt in the Cenozoic.
- The periphery of the Ordos Block is presented by pure shear deformation at the early stage and simple shear deformation at the late stage.
- The neotectonics of the periphery of the Ordos Block is originated from different driving.

Abstract The multiphase intensive intra-continental deformation of the Eurasian continent in the Cenozoic caused by Indo–Asian and Pacific–Asian collisions has been studied extensively. However, its Cenozoic intra-continental deformation process and dynamics remains poorly constrained. The western North China Plate of the Eurasian continent is characteristic of the Cenozoic faulted basin system around Ordos Block, and is a critical region to determine this deformation process. Here, new structural data and fault kinematic analysis, coupled with new geochronological results, delineates a two-stage Cenozoic tectonic evolution in the region, providing new structural evidence to decipher the intra-continental deformation due to Indo–Asian and Pacific–Asian collisions. The first stage is characterized by the formation of faulted basins in the northwestern and southeastern margins of the Ordos Block, dominated by a pure-shear mechanism. This stage further comprises the NW–SE extension spanning the Eocene to Late Miocene (ca. 10.5 Ma), and the subsequent basin inversion triggered by the NW–SE compression during the Late Miocene (ca. 10.5–9.5 Ma). Its tectonism is associated mainly with the far-field effect of the northwestward subduction of the Pacific Plate. The second stage is characterized by the development of the Shanxi and Hetao Basins in the eastern and northern parts of the Ordos Block, respectively, and an intensive mountain-building process in the western part since the Late Miocene (ca. 9.5 Ma), which is connected with a simple-shear mechanism. This stage is furthermore divided into three alternating episodes of shortening and extension events. These resulted predominantly from far-field responses to the northeastward growth of the Tibetan Plateau and partially from the Pacific subduction.

Key Words: North China; Ordos Block; neotectonics; faulted basin; intracontinental deformation; Indo–Asian collision; Pacific–Asian collision

1. Introduction

The Eurasian continent was subject to multiphase intensive intracontinental deformation in the Cenozoic. However, its Cenozoic intra-continental deformation process and the driving force has long been disputed, which is associated with the Indo–Asian collision (e.g., Molnar and Tapponnier, 1975; Wang et al., 1984; Jolivet et al., 1990; Avouac and Tapponnier, 1993; Tapponnier et al., 2001; Liu et al., 2004; Yin et al., 2010; Xu, J. et al., 2013; Zhao, W. et al., 2016), is caused by the Pacific–Asian collision (Cui, 1997; Schellart and Lister, 2005), or is connected with a combined effect of the Indo–Asian collision and the Pacific–Eurasia convergence (e.g., Ren et al., 2002; Li et al., 2010; Li, S. et al., 2015; Shi et al., 2015b; Liu et al., 2019a). The western part of the North China Plate in the interior of the Eurasian continent is characterized by the Cenozoic faulted basin system around the Ordos Block (Fig. 1A), which contains key information for deciphering the intra-continental deformation process of the Eurasian continent and its driving mechanism (RGAFSO, 1988; Zhang et al., 1998; Chen et al., 2018).

Previous studies have focused on the three-stage extensional deformation in conjunction with the sustained uplift of the Ordos Block, the development of the Weihe, Yinchuan, Jilantai, and Hetao Basins during the Eocene–Oligocene, the continued subsidence of the faulted basins and the development of the Shanxi Basin in the Miocene–Pliocene, and the lasting development of the rifted basins since the Quaternary (RGAFSO, 1988; Deng et al., 1999). The study indicates that the Paleogene and Neogene subsidence were driven by the westward subduction of the Pacific Plate and the growth of the Tibetan Plateau. Regional structural and stratal sequence analyses suggested that three phases of extensional deformation dominated on the periphery of the Ordos Block, i.e., the Eocene–Oligocene NW–SE extension and the formation of the basins (Weihe, Yinchuan, Jilantai, and Hetao Basins) in the north-northwestern and southeastern margins of the block (Deng et al., 1999), the Miocene NE–SW extension, and the Late Miocene NW–SE extension, as well as the development of the Shanxi Basin (Zhang et al., 1998, 2003, 2006). However, kinematic analysis of the Weihe Basin, which is connected to the Shanxi Basin in the northeast, is inconsistent with the findings of Zhang et al. (2003, 2006), and suggests more complicated, alternating extensional and compressive tectonic regimes since the middle Eocene (Mercier et al., 2013).

Remote sensing analysis and structural investigation has implied that the basin

formation has coincided with the counterclockwise rotation of the Ordos Block around a pole with respect to the Gobi-Mongolia region (Zhang et al., 1998) or differential rotation of the Ordos and Taihang blocks (Xu et al., 1992, 1993). However, analysis of the GPS data, as well as numerical simulation of crustal rheology, suggest that the rifted basins likely resulted from gravitational collapse and not the rotation of the blocks (He and Liu, 2002; He et al., 2004; Liu et al., 2004; Cui et al., 2016; Gao et al., 2017). Additionally, recent fault kinematic analysis of the eastern and western margins of the Ordos Block indicate no obvious rotation on its periphery (Shi et al., 2015b).

Here new structural data and fault kinematic analysis of the periphery of the Ordos Block, together with new geochronological results, allow us to evaluate the Cenozoic tectonic regime and deformation process, which provides more direct structural evidences in contrast to decipher the northeastward growth process of the Tibetan Plateau.

2. Geological setting

The western part of the North China Plate is characterized by a number of Cenozoic faulted basins around the Ordos Block, comprising Yinchuan and Jilantai Basins to the northwest, Hetao Basin to the north, Shanxi Basin to the east, as well Weihe Basin to the south, except for the depressed basin (South Ningxia Basin) to the southwest (RGAFSO, 1988; Zhang et al., 1995). Geophysical data show that the Ordos Block has a thick lithosphere (~200 km), and no evidence of stratal deformation (Menzies et al., 2007; Chen, 2010). The Moho beneath the basins, in contrast to the Ordos Block, is usually uplifted by 5–10 km along boundary faults, indicating a thinned lithosphere (ca. 100 km; Xu et al., 1993; Chen et al., 2009; Tang et al., 2010; Ren et al., 2012). The following subsections present the structural and stratal frames of the basins based on new previous studies (Fig. 2; Table 1).

2.1. South Ningxia Basin

The South Ningxia Basin is bounded by the Ordos Block to the west, the Tibetan Plateau to the south, and the Alxa Block to the north (Fig. 1B; IG and SBNX, 1990). It consists of three discrete intra-range basins characterized by Cenozoic strata (i.e., Haiyuan-Xingrenpu, Tongxin, and Hongsipu Basins) and four convex to the northeast arcuate faults along the fronts of these basins (i.e., the Haiyuan-Liupanshan, Xiangshan-Tianjinshan, Yantongshan, and Luoshan-Niushoushan faults) (Fig. 2; Deng et al., 1984).

The Cenozoic sedimentary rocks (overlain by Quaternary loess and sandy clay)

in the South Ningxia Basin can be divided into four lithostratigraphic units according to their depositional facies, paleontology, and paleomagnetic data, i.e., (from bottom to top) the Sikouzi, Qingshuiying, Zhangenpu, and Ganhegou formations (Fig. 3; Table 1; ECRGCN, 2017; Shen et al., 2001; Jiang et al., 2007; Lin et al., 2010; Wang et al., 2011). Unlike the other formations, the contact between the Zhangenpu and Ganhegou formations is disconformably (Liu et al., 2019b). The Sikouzi Fm. is the lowermost Cenozoic deposit in this basin, with a deposition age interval of ca. 30 to 26 Ma (late Early to Late Oligocene), as demonstrated by the new paleomagnetic data for the Sikouzi section (Wang et al., 2011). It is characterized by a series of terrestrial, red, coarse-grained sandstones, with inclined bedding and cross-stratification, and conglomerates (Fig. 3; Table 1). The Qingshuiying Fm., corresponding to the Late Oligocene–Early Miocene (ca. 26–21 Ma), is distributed widely in the area and consists of a thick series of salt-bearing lacustrine sediments marked by purple to red mudstones, as well as siltstones containing abundant layers of gypsum (Shen et al., 2001; Liu et al., 2019b) (Fig. 3). The Zhangenpu Fm. is typified by thick-bed lateritic mudstones, siltstones, and fine-grained sandstones, with intervals of reticular gypsum (Fig. 3; Jiang et al., 2007; Lin et al., 2010; Wang et al., 2011), and its formation age spans the period ca. 21 to 10 Ma (Fig. 3; Liu et al., 2019b). The Ganhegou Fm., the uppermost Cenozoic sedimentary rock unit in the area, comprises thin, yellowish-gray conglomerates and coarse-grained sandstones (Fig. 3), and corresponds to the Late Miocene–Pliocene (ca. 9.5 to 2.6 Ma). The formation shows a distinct change in the sedimentary facies from lacustrine to fluvial, and is marked by significant changes in the sedimentation rate and paleoflow directions (Jiang et al., 2007; Lin et al., 2010; Liu et al., 2019a). In addition, the Yumen Fm., characterized by Early Pleistocene gray conglomerate (ECRGCN, 2017), commonly deposited in gullies, and generally unconformably overlies the Ganhegou Fm. or other pre-Pleistocene strata in the South Ningxia Basin (Fig. 3; Table 1). Its lower limit age, as delimited by cosmogenic nuclide burial dating of the alluvial conglomerate, is ca. 1.0–0.6 Ma (Shi et al., 2019b).

Previous studies have defined that four major faults developed in the South Ningxia Basin (trending in the WNW–ESE or NW–SE direction toward the southeast), all of which finally converge with the Liupanshan Fault system in the southwestern margin of the Ordos Block (RGAFSO, 1988), presenting an oroclinal structure that protrudes to the southwest (Fig. 2). This characterizes the structural framework of the South Ningxia Basin (Zhang et al., 1990; Shi et al., 2015).

The Liupanshan Fault (F_{1-1}) has a length of ~180 km and primarily strikes NNW along the eastern sides of the Liupanshan Mt. (Shi et al., 2006). It is marked by thrusting in the north and normal faulting in the south (IG and SBNX, 1990; Zhang et al., 1991).

The Haiyuan Fault (F_{1-2}) extends for ~200 km and is the innermost fault of the basin. It connects with the Liupanshan Fault in the southeast, and its en échelon faults link with the Maomaoshan Fault to the northwest (IG and SBNX, 1990). Large-scale active fault mapping in the region has indicated eleven en échelon faults, with significant left-lateral strike-slip activity since the Late Pleistocene (Burchfiel et al., 1991; Lasserre et al., 2002; Zheng et al., 2013; Liu et al., 2015), as well eight Late Pleistocene intra-fault pull-apart basins along the Haiyuan Fault (Figs. 2, 5; IG and SBNX, 1990). The Xiangshan-Tianjingshan Fault (F_{1-3}) extends northwestward with a length of 150 km and a dip to the southwest (Ye et al., 2015), and crops out primarily along the northern or northeastern side of the Xiangshan-Tianjingshan Mt. Additionally, this fault links with the Guliang-Lenglongling Fault to the northwest and the Liupanshan Fault to the south in the Guyuan area (Figs. 1, 2; IG and SBNX, 1990; Li et al., 2019). The Yantongshan Fault (F_{1-4}) develops mainly along the northeastern front of the Yantongshan Mt. Its hanging wall comprises Cambrian–Devonian slates, limestones, and sandstones. Analysis of the geophysical section indicates the listric shape of the wall (Fig. 2; Wang et al., 2013). The Luoshan-Niushoushan Fault (F_{1-5}) is the northeasternmost fault in the area, and extends mainly in a nearly N–S direction along the eastern sides of Luoshan and Niushoushan Mts. Subsequently, it strikes NW–SE and likely connects with the Longshoushan Fault (IG and SBNX, 1990). This fault marks the western margin of the Ordos Block (Chen et al., 2013; Shi et al., 2013).

2.2. Yichuan Basin

The Yichuan Basin, limited by the Ordos Block to the east and the Helanshan Structural Belt to the west, strikes north-northeast, with a length of ~160 km and a width of ~60 km (Figs. 1B, 2). The Yellow River crosses the basin from south to north, and connects with the South Ningxia Basin to the south and the Jilantai Basin to the north. The geologic evidence and seismic reflection data reveals the basin is filled with ~7000 m-thick Paleogene-Neogene sediments and ~1600 m-thick Quaternary sediment (COC, 1983; Huang et al., 2016). The Paleogene-Neogene sedimentary sequences in the Yinchuan Basin are divided into four sets of lithostratigraphic units, named the Sikouzi Formation (E_2s), the Qingshuiying

Formation (E_{3q}), the Zhangnengpu Formation (N_{1z}), and the Ganhegou Formation (N_{1-2g}), respectively, which coincide with the stratal sequences of the South Ningxia Basin (Fig. 3; Table 1; ECRGCN, 2017). The Sikouzi Fm., the lowermost Cenozoic deposit in the basin, formed in the Eocene–late Oligocene, and consists of a series of terrestrial red conglomerates in the lower section and red, coarse-grained sandstones in the upper section (Fig. 3; ECRGCN, 2017). The Qingshuiying Fm., characterized by a thick series of medium–thin bedding, purple conglomerate interbedded with sandstone, and marlstone in the uppermost strata, conformably covers the Sikouzi Fm. The regional strata suggest that the Qingshuiying Fm. was deposited in the Late Oligocene–Early Miocene (Fig. 3; ECRGCN, 2017). The Zhangnengpu Fm. is marked by thick-bed, brick-red conglomerate in the lower section and sandstone interbedded with mudstone in the upper section. The contact with the underlying Qingshuiying Fm. is conformable. Drilling data, as well as regional strata analysis, delimit its deposition age to the Late Miocene (21–10 Ma) (Liu et al., 2019b). The Ganhegou Fm., the uppermost Cenozoic sedimentary rock unit in the area, typically comprises medium–thin, gray conglomerates and yellowish, coarse-grained sandstones. The new paleomagnetic studies suggest its formation interval as 9.6–2.8 Ma, corresponding with the Late Miocene–Pliocene (Liu et al., 2019b). It indicates a distinct change in the sedimentary facies from lacustrine to fluvial (ECRGCN, 2017; Liu et al., 2019b). Additionally, the Early Pleistocene strata (i.e., Yumen Fm.) comprise gray conglomerate and sand (Shi et al., 2019b).

The basin is bounded by the NNE-striking Yellow River Fault (F₂₋₁) to the east and the Helanshan Eastern Piedmont Fault (F₂₋₄) to the west (Fig. 2). The basin is cut by two NNE–SSW-striking faults (from east to west: the Yinchuan-Pingluo Fault (F₂₋₂) and the Luhutai Fault (F₂₋₃)), which are parallel to the orientation of the bounding faults (Fig. 2; RGAFSO, 1988). A seismic reflection investigation has shown that the Yellow River Fault extends along the Yellow River, and covers a distance of 130 km, and dips westward at an angle of 70° (Huang et al., 2016), likely triggering the occurrence of the 1739 M ~8.0 Pingluo earthquake (Lin et al., 2015b). The Helanshan Eastern Piedmont Fault, running along the eastern margin of the Helanshan Mt., forms the western margin of the Yinchuan Basin (Fig. 3; Huang et al., 2013). The fault is characterized by a high-angle near the surface, becoming low angle towards the middle crust, and is cut by the Yellow River Fault at a depth of 20 km, as revealed by deep seismic reflection data (Liu et al., 2017). The Yinchuan-Pingluo and Luhutai faults are characterized as blind faults, as there is no

observable morpho-tectonic evidence (Lei et al., 2016). The Luhutai Fault extends downward and merges with the Helanshan Eastern Piedmont Fault. The westward-dipping Yinchuan-Pingluo fault, as well as the eastward-dipping Luhutai Fault, controls the Cenozoic sedimentation in the Yinchuan Basin (Huang et al., 2016).

2.3. Jilantai Basin

The Jilantai Basin is bounded by the Helanshan Structural Belt to the east, the Langshan Structural Belt to the northwest, and the Seertengshan Mt. to the north (Figs. 1B, 2). It is a half graben limited by the Langshan Fault and the Seertengshan Fault (SF) to the northwest (S3 of Fig. 6), and is filled with four sets of Cenozoic deposits, i.e., (from bottom to top) the Wulate, Linhe, Wuyuan, and Wulantuke Fms. (Fig. 3; Table 1; Zhang, 1983; Fu et al., 1994). The Wulate Fm., the lowermost Cenozoic sedimentary rock unit in the area, has a thickness of ~200 m and is characterized by medium-thick bed, brownish to maroon red conglomerates, gravel-bearing sandstone, and siltstone with cross-stratification and inclined bedding (Fig. 3). The contact of this formation with the underlying Early Cretaceous or pre-Cretaceous strata is generally unconformable (ECRGCN, 2017). The vertebrate fossil and paleomagnetic data delineate its deposition age to the Late Eocene–Oligocene (Fu et al., 1994), which likely corresponds to the Sikouzi Fm. in the Yinchuan Basin (Fig. 3). The Linhe Fm. consists of gray-green to dark-gray mudstone and siltstone, with horizontally bedded marl and gypsum, and has a conformable contact with the Wulate Fm. It was deposited in the Oligocene and drilling data show a thickness of ~1000 m (Fig. 3; Zhang, 1983; Fu et al., 1994). The Wuyuan Fm. was deposited in the Middle Miocene and typically consists of gray-purple, to gray-green mudstone and siltstone, with horizontally interbedded marl and gypsum. Its thickness is ~1100 m, and it has a conformable contact with the Linhe Fm. (Fig. 3). The Wulantuke Fm., the uppermost Cenozoic sedimentary rock unit in the basin, comprises gypsum-containing, thin, yellowish-gray to light-gray, fine-grained sandstones interbedded with marl, as well as thin conglomerate with horizontal and inclined bedding. It corresponds to the Late Miocene–Pliocene, as limited by regional strata correlation (Fig. 3; Table 1). This formation with a thickness of ~2000 m disconformably contacts with the Wuyuan Fm. (Zhang, 1983; Fu et al., 1994).

The Langshan Fault (F_{3-1}) is a bounding fault to the west of the Jilantai Basin. It is ~160 km long and trends NE–SW, with a southeastward dip of ~50°–70° (Fig. 2;

RGAFSO, 1988). This fault developed during the Late Pleistocene and Holocene (Rao et al., 2016). The Seertengshan Fault (F₃₋₂) is located along the piedmonts of Seertengshan Mt., constituting north boundary of the Jilantai Basin (Fig. 2). It strikes east–west, with a length of 175 km and dips southward at 40°–60° (S4 of the Fig. 7; Liu et al., 2016). The fault has undergone normal slip since the Cenozoic, causing the formation of three-level terraces (Long et al., 2017).

2.4. Hetao Basin

The Hetao Basin lies to the north of the Ordos Block, and is bounded by the Daqingshan and Wulashan Mts. to the north (Fig. 2). The basin is 300 km wide and 40–80 km long (Figs. 1B, 3). This is a Cenozoic half-graben basin, as indicated by the bounding normal faults (S5 of the Fig. 7; Zhang et al., 2013). The basin is filled by two Cenozoic sedimentary units (from bottom to top), namely, the Wuyuan and Wulantuke formations (Fig. 3; Table 1; Gao, 2007).

The Wuyuan Fm. is the lowermost Cenozoic deposit in the Hetao Basin with a thickness of ~130 m. It is characterized by yellowish-brown, to brownish-red mudstone interbedded with medium- to coarse-grained sandstone, and medium- to thinly-bedded conglomerate at the bottom. The phytolytic and palynological evidence obtained from drilling indicate the Miocene age, coinciding with the Zhangeppu Fm. in the Yinchuan Basin (Fig. 3; Table1). The Wulantuke Fm. comprises brownish-red to brownish-yellow sandy mudstone and sandy conglomerate, with intervals of calcic concretions and reticular gypsum. It is ~190 m thick, and has unconformable contacts with the underlying Wuyuan Fm. The formation was deposited in the Pliocene, as suggested by its vertebrate fossils (Gao, 2007).

The main faults in the north of the basin strike ENE–WSW, and comprise, from west to east, the Wulashan Fault (F₃₋₅) and the Daqingshan Fault (F₃₋₆) (Fig. 2). The PF has a length of ~110 km, runs along the southern margin of the Wulashan Mt., and dips ~80° to the south (Ran, 2003). The east-northeast-striking Daqingshan Fault extends for ~170 km along the southern margin of the Daqingshan and dips to the south, and is marked by normal faulting in the Quaternary (Ma et al., 2000). The northeast-striking Helingeer Fault (F₃₋₇) forms the eastern boundary of the basin, is 120 km long, and dips northwest at an angle of 60~70°, with normal faulting (Ran, 2003).

2.5. Shanxi Basin

The Shanxi Basin is ~40–120 km wide, and extends for more than ~900 km

along the eastern margin of the Ordos Block. It consists of four en échelon ENE-trending basins (i.e., the Datong Basin (DTB), Xin-Ding Basin (XDB), Taiyuan Basin (TYB), and the Linfen Basin (LFB)) bounded by high-angle normal faults (Fig. 2, S7 of Fig. 8; RGAFSO, 1988; Xu and Ma, 1992; Shi et al., 2015a).

The average thicknesses of the Cenozoic sediments in the Shanxi Basin is ~2000–3800 m (Chen, 1987). The Shanxi Basin is generally covered by thickly-bedded Late Pleistocene Malan loess. The Luzigou Fm. of the Mid–Late Miocene is the oldest syn-rift sedimentary unit, representing a Miocene to Pliocene deposit associated with Hipparion red clays (i.e., Baode and Jingle formations; GSBSX, 2002). The Luzigou Fm. is characterized by gray-green to orange sandstone in the mid–upper section and coarse sandstone containing conglomerate at the bottom. It is mainly distributed in the TYB (Fig. 3), and is delineated to the Early Miocene by paleomagnetic data (21–12 Ma) (Zhu et al., 2008). The Baode Fm. indicates a sequence of orange to purplish red mudstone, with intervals of several layers of calcic concretions. The formation is deposited conformably on the Luzigou Fm., and corresponds with Hipparion red clays, developing in the Late Miocene (Yue et al., 2004; Zhu et al., 2008; Li et al., 2013). The Jingle Fm. lies conformably on the underlying Baode Fm., and consists of bright-red clay with calcic concretions. It was formed in the Pliocene with an age limitation of 5.1–2.5 Ma (Zhu et al., 2008).

Cenozoic basalts occur in the northern segment of the Shanxi Basin and comprise three units, namely, the Fanshi, Hannuoba, and Datong basalts. The Fanshi basalt includes thickly-bedded lava flows on Cambrian limestone or Precambrian basement, and comprises dolerite and olivine basalt. It is exposed well in the DTB and the northern XDB (S7 of Fig. 8). The K-Ar ages of the Fanshi basalt range from 35 to 25 Ma (Chen et al., 1985; Wang et al., 1988). The Hannuoba basalt is characterized by stratiform lava flows, and consists mostly of olivine and pyroxene basalts, with intervals of brick-red to purple clay or pebble-bearing sandy clay. The Hannuoba basalt is developed well along the northern margin of the Shanxi Basin, and indicates minor flows in the rift interior. This basalt generally overlies the pre-Cenozoic strata above an angular unconformity, and has an unconformable contact with the Pliocene red clay. The K-Ar ages, as well as the age-diagnostic flora and fauna fossils, indicate that this basalt erupted during the Late Oligocene to Late Miocene (ca. 10–25 Ma; Wang et al., 1988; Xie et al., 1989). The Datong basalt comprises alkaline and tholeiitic basalts, and originates primarily from the

asthenospheric mantle (Xie et al., 1989). This basalt occurs generally at the intersection of the NE- and NW-striking faults, as demonstrated by numerous volcanic cones in the basin (Cen et al., 2016). Abundant K-Ar isotopic data and magnetostratigraphic analysis constrain the age of the Datong volcanic activity to the Middle Pleistocene (ca. 0.73–0.11 Ma) (Wang et al., 1988).

2.6. Weihe Basin

The Weihe Basin runs along the southern margin of the Ordos Block, and comprises a ~30–100 km wide and ~400 km long structural belt between the North China Plate and the Qinling Orogenic Belt (Figs. 1B, 2). The basin extends to the east and connects with the Yuncheng and Sanmenxia Basins, as suggested by the correlation between the Cenozoic sedimentary thicknesses of the two basins (Xing et al., 2005). The Weihe Basin shows the characteristics of a half-graben, as it is bounded mostly by the Qinling Piedmont Fault (F₅₋₁) to its south and the Kouzhen Fault (F₅₋₃) to its north (S10 of Fig. 10; Rao et al., 2014).

The Weihe Basin is characterized by a terrestrial 4000–6000 m thick Cenozoic terrestrial clastic succession, as revealed by the seismic reflection profiles and boreholes (Zhang et al., 1995). The sequence is divided into the following five lithostratigraphic units according to the depositional facies, paleontology, and paleomagnetic data, from bottom to top, the Honghe, Bailuyuan, Lengshuigou, Koujiacun, Bahe, and Lantian formations (Zhang et al., 1978; Li et al., 2016). The Honghe Fm., the earliest sedimentary stratum in the basin, comprises purplish-red mudstones interbedded with yellow to gray-green sandstone and conglomerate at the bottom. The animal and plant fossil data indicate that the rock unit was deposited in the Late Eocene (Liu and Xu, 2004; Li et al., 2016). The Bailuyuan Fm. has a thickness of ~700 m and is characterized by gray-white, thickly-bedded sandstone interbedded with brownish-red mudstone. The vertebrate fossil and palynological data suggest that the Bailuyuan sediments were deposited in the Late Eocene–Early Oligocene (Zhang, 1978; Liu and Xu, 2004). The Lengshuigou Fm. comprises yellowish-brown to brownish-red sandstone interbedded with dark-red mudstone has with a thickness of ~70 m. The formation contacts the underlying Bailuyuan Fm. via an angular unconformity, and it was deposited in the Early–Mid Miocene, as deduced by mammals, spores and pollen (Li et al., 1984; Liu and Xu, 2004). The Koujiacun Fm. is 100 m thick, and it has a conformable contact with the Lengshuigou Fm. It consists of brown-yellow mudstone, sandstone, and sandy conglomerate at the bottom, and corresponds to the Middle Miocene (Zhang, 1978).

The Bahe Fm. is dominated by purple-brown to light-yellow clay, interbedded with sandy clay and intervals of gray-green clay. Paleomagnetic and vertebrate fossil data suggest that the Bahe Fm. was conformably deposited on the Koujiacun Fm. in the Middle Miocene (11–7 Ma) (Kaakinen and Lunkka, 2003; Wang et al., 2014). The Lantian Fm., the uppermost formation in the basin, consists primarily of brown-red clay, with limestone concretions and conglomerate at the bottom. The formation overlies the Bahe Fm. via an angular unconformity, and it has a paleomagnetic age span of ca. 7.0–2.6 Ma, in accordance with the Late Miocene–Pliocene (An et al., 2000; Wang et al., 2014).

A synthesis of sedimentation, paleomagnetic, and vertebrate fossil data for the Cenozoic basins around the Ordos Block indicates that the basins in the northwestern and southeastern margins of the Ordos Block (Yinchuan, Jilantai, and Weihe Basins) were the earliest to be filled by the Eocene coarse-grained sandstones and conglomerate. The South Ningxia Basin in the western margin of the Ordos Block was filled slightly later than the above-mentioned basins by the Late Eocene clastic deposits. The earliest deposits in the Shanxi and Hetao Basins are the Late Miocene clastic materials (Fig. 3; Table 1). The stratal sequences of the basins indicate that the basins around the Ordos Block occurred initially in the Eocene except the Late Miocene Shanxi and Hetao Basins.

3. Cenozoic structural investigation and fault kinematics

This section focuses on a structural investigation of the major faults in the basins, as well as comprehensive fault kinematic analysis based on extensive new structural data. Subsequently, the Cenozoic tectonic regime and the deformation process in the periphery of the Ordos Block have been reconstructed. These results facilitate the reconstruction of a Cenozoic tectonic evolution model.

3.1. South Ningxia Basin

This study focused on four primary WNW- to NW-directed faults (the Haiyuan-Liupanshan, Xiangshan-Tianjingshan, Yantongshan, and Luoshan-Niushoushan faults) to understand the Cenozoic structures in the South Ningxia Basin (Figs. 4, 5; IG and SBNX, 1990). The four faults are investigated systematically based on a few representative outcrop-scale examples (Figs. 4, 5), and the sequence and timing of the deformation are subsequently defined.

Cross section S₁ across the Liupanshan Fault (Fig. 4; see Fig. 2 for the location of Fig. 4) indicates that the Cretaceous Liupanshan Group thrust strongly WSW over the Cenozoic (E₂₋₃) red beds along the Daguanshan Fault (F_{1-1b}) because of nearly

E–W compression (Shi et al., 2006). The N–S-striking Liupanshan Fault is exposed along the Ordovician limestone at the southernmost section of the South Ningxia Basin (Loc. B15), and controlled the deposition of the Cenozoic red beds (E_{2-3}). These results suggest that this region is subject to extensive activity in the Cretaceous–Cenozoic, as shown by the unconformable contact between the Miocene–Pliocene red clay and the Ordovician limestone (Fig. 4A). The Early Cretaceous conglomerates thrust toward the northeast over the N_{1-2} red clay, and are underlain by the Late Pleistocene loess, indicating the NE–SW shortening of this region from the Pliocene to the Early–Late Pleistocene (Fig. 4A). The compression led to thrusting of the Late Cretaceous conglomerate over the Cenozoic sandstone and mudstone along the Liupanshan Fault (Shi et al., 2006). The paleomagnetic data and the paleocurrent measurements of the Miocene strata indicate that a compression led to the uplift of the Liupanshan Mt., which is initiated at 9.5 Ma and lasted until the early Quaternary (Zheng et al., 2006; Lin et al., 2010; Li et al., 2013). Here normal faulting in the Late Pleistocene loess likely demonstrates another extension posterior to the Late Pleistocene (Fig. 4A).

Faults with oblique slip motion affected the N_{1-2} red clay bed at Loc. B14 (near Loc. B15) and are covered by Holocene deposits. The fault striation data suggest that the nearly E–W shortening in the Liupanshan region occurred after the Pliocene and prior to the Holocene (Fig. 4B; Shi et al., 2006). Normal faulting at Loc. B11 (south of Loc. B15) affect the Late Pleistocene loess with an lower limit age of 54.5 ± 4.6 ka (OSL), which further verifies the occurrence of the extension at the end of the Late Pleistocene (Fig. 4E; Shi et al., 2006). Thus, a four-stage deformation was defined for the Liupanshan Fault, which are the extension in the Eocene–Early Miocene, NE–SW shortening in the Late Miocene (9.5 Ma) to Early Pleistocene, extension in the Late Pleistocene, and the nearly E–W compression at the end of the Pleistocene.

Cross section S_2 across the arc-shaped fault zone in the South Ningxia Basin shows that all the Cenozoic strata (i.e., the Sikouzi (E_{3s}), Qingshuiying (30–26 Ma), Zhangenpu (26–21 Ma), and Ganhegou (21–10 Ma) Formations) are folded synchronously in the region (Fig. 5). Location A of the eastern Haiyuan Fault (Fig. 3) shows that the syn-depositional normal faults developed in the red-gray mudstones of the Qingshuiying Fm., suggesting the occurrence of a NW–SE extension from the Late Oligocene to the Middle Miocene (Fig. 5A). The locality H118, near the eastern Haiyuan Fault of the north of the Yueliang Shan Mt., displays another set of

synsedimentary faults with a NW-SE strike in the Early Miocene red mudstone, which unconformably overlies the Lower Cretaceous gray gypsum-bearing mudstones and sandstones (Fig. 5B; the location is marked in Fig. 5). Here, this set of normal faults cut downwards the Lower Cretaceous strata, where fault slip vectors suggest a NW-SE extensional regime (Fig. 5B), indicating that the NW-SE extensional deformation occurred in this region in the Middle Miocene as well. These results indicate that the NW-SE extensional deformation in this region also occurred in the Middle Miocene. Furthermore, the Silurian phyllites at the western Haiyuan Fault thrust toward the SSW over the Late Miocene-Pliocene red conglomerates along the main Haiyuan Fault, with an azimuth/plunge of $354^{\circ}/31^{\circ}$, as deduced from the fault-slip vectors (Fig. 5C). This thrust fault is covered by undeformed Early Pleistocene conglomerates, indicating that the shortening occurred in the Late Pliocene-Early Pleistocene (Fig. 5C). Additionally, numerous WNW-ESE-striking folds developed in the Late Miocene-Pliocene red sandstones of the Laolongwan Basin (south of the western Haiyuan Fault) in response to this deformation. These folds are generally partially covered by the Early Pleistocene conglomerate (Shi et al., 2015b), confirming that the intensive NE-SW shortening of the Haiyuan Fault also occurred in the Late Pliocene-Early Pleistocene.

Two sets of faults cut through the Late Miocene red, medium- to thinly-bedded sandstones at Loc. H39 (Fig. 5) in response to the early NE-SW-directed compression and the late syn-directed extension, as suggested by the cross-cutting superposed relationships of the two fault planes (Fig. 5E). The structural observation in the interior of the main Haiyuan Fault (Loc. H144; Fig. 5) shows that the strike-slip activation of the major Haiyuan Fault occur after the Late Pleistocene. The subhorizontal striations in the fault gouge indicate a left-lateral strike-slip, attributed to ENE-WSW compression. This responds to the youngest activation of the fault due to its development in the Late Pleistocene loess (Fig. 5F), and coinciding with the seismic focal mechanism solution (IG and SBNX, 1990), as well with GPS observations (Wang et al., 2001; Zheng et al., 2013). Loc. H183 near the Xiangshan-Tianjingshan Fault is characterized by the occurrence of NW-SE-trending outcrop-scale folds in the Oligocene-Pliocene rocks, suggesting NE-SW shortening (Fig. 5G). Two sets of faults developed in the medium- to thinly-bedded mudstones of the Qingshuiying Fm. at this site. Dextral strike-slip and normal faults are associated with NE-SW compression and NE-SW extension, respectively, as identified by the fault-slip vectors. The NE-SW extensional event

evidently predated the strike-slip activation, as limited by the interrelationships of the faults (Fig. 5H).

The Structural observations near the Xiangshan-Tianjingshan Fault (Loc. H195) indicate that the Late Oligocene–Early Miocene red, thinly-bedded sandstone, with intervals of mudstone, is shortened intensively from southwest to northeast along a set of detachment layers comprising red, thinly-bedded mudstone. These thrust-and-fold structures are overlain unconformably by Late Pleistocene loess, suggesting that the origin of the shortening is likely prior to the Late Pleistocene (Fig. 5I). Therefore, two deformation stages have been determined from fault kinematic analysis. Furthermore, the cross-cutting relationship of the fault planes suggests that the NW–SE extension is followed by NE–SW shortening (Fig. 5I).

At Loc. H200 east of Tongxin, nearly upright faults in the mudstones of the Qingshuiying Fm. are characterized by dextral strike-slip movements (Fig. 5J), attributed to NE–SW compression (Fig. 5J₄). Two sets of gypsum veins grew in the red, medium- to thinly-bedded mudstones of the Qingshuiying Fm. One set consists of syntaxial veins marked by growing perpendicularly to the wall rock, which indicates a NW–SE extensional event (Figs. 5J₁, J₂). The other set shows gypsum veins that had been stretched because of subhorizontal shearing (Fig. 5J₁), thereby representing NE–SW compression (Fig. J₄). The NW–SE extension predates the NE–SW compression, as deduced by the cross-cutting of shear veins off syntaxial veins (Fig. 5J₁). Analysis of the fault-slip vectors indicates that the NE–SW compression resulted in a sinistral strike-slip fault that cut through the Late Miocene–Pliocene mudstones of the Ganhegou Fm. in the west of Niushoushan Mt. (Fig. 5K). This faulting likely occurred before the Late Pleistocene, as it did not affect the overlying Late Pleistocene (Qp³) loess (Fig. 5K). One generation consists of normal faults associated with NW–SE extensional deformation, whereas the other comprises strike-slip faults linked to ENE–WSW compressive events (Fig. 5L). The interrelationships of the fault planes further indicate that NW–SE extension predates ENE–WSW shortening.

In summary, detailed structural investigations and analyses of the four major faults are in agreement with our study findings on the South Ningxia Basin (Shi et al., 2015), five episodes of deformation events have been defined for the South Ningxia region, a long-lived NW–SE extensional event from the Oligocene to the Middle Miocene, a subsequent short-term NW–SE shortening in the Late Miocene, an intensive NE–SW shortening event during the Late Miocene–Early Pleistocene, a

gentle NE–SW extensional activity during the Late Pleistocene, and a youngest strike-slip activation on the four major faults since the end of the Late Pleistocene.

3.2. Yinchuan Basin

The Yinchuan Basin is situated at the northwestern periphery of the Ordos Block, and is separated by the Helanshan Structural Belt to the east from the Jilantai Basin to the west (S_3 of Fig. 6; Liu et al., 2017). The Yinchuan Basin is bounded by the Helanshan Eastern Piedmont Fault (F_{2-4}) to the west and the Yellow River Fault (F_{2-1}) to the east (Fig. 6A; Lin et al., 2015b). The southern segment of the Helanshan Eastern Piedmont Fault is mostly presented by fault scarps, and marked by two sets of striations on the fault planes, suggesting two-stage deformation. The old striations indicate NW–SE compression and the young striations suggest NE–SW extension (Fig. 6A). Location Y01 east of the Yellow River Fault shows syn-depositional normal faults in the Late Oligocene–Early Miocene mudstone interbedded with fine-grained sandstone (Qingshuiying Fm.), where the striations indicate NW–SE extension (Fig. 6B). Here local fault kinematic analysis delimits the NE–SW extension posterior to the NW–SE syn-sedimentary extension (Fig. 6B). At Loc. W04 near the Yellow River Fault, two sets of faults developed in the red sandstone of Qingshuiying Fm., with NE- and ~E–W-striking faults, which indicate a NW–SE extension and NE–SW compression, respectively (Fig. 6C). Here the NW–SE extension predates the ~E–W compression, as inferred from the cross-cutting relationships of fault planes (Fig. 6C). One generation of syn-depositional normal faults developed in the N_{1-2g} red conglomerate (Zhangenpu Fm.) in the interior of the Yinchuan Basin, which are associated with NW–SE extension, as suggested by the fault-slip vectors (Fig. 6D).

Normal and strike-slip faults are observed in the Miocene mudstone (N_{1z}) at Loc. E348 (southern margin of the Yinchuan Basin). The fault kinematic analysis, together with the interrelationships of the faults, shows early NW–SE extension and late NW–SE compression. The two stages of faulting likely occurred before the Early Pleistocene (~2.58 Ma), as deduced by the overlying on the faults by Early Pleistocene conglomerates (Fig. 6E; Chen et al., 2015). Additionally, proluvial fans that developed along the Helanshan piedmont are cut by most faults, indicating that normal faulting originated in the Holocene (Zhan, 1982; Lin et al., 2015b).

Thus, these new structural measurements and fault kinematic analysis, in conjunction with our previous results (Huang et al., 2013), allow us to delineates a five-stage Cenozoic tectonic evolution in the Yinchuan Basin. Firstly, the region is

marked by widespread formation of rifted basins from the Eocene to the Early Miocene (ca. 45–9.5 Ma) under a NW–SE extensional regime (Liu et al., 2019a). Subsequent basin inversion is triggered by the NW–SE compression in the Late Miocene. Next, a NW–SE extensional activity dominates the region in the Late Miocene–Pliocene, leading to the deposition of the Ganhegou Fm. in the basin. Subsequently, a gentle NE–SW extension likely governs the basin in the Late Pleistocene, as manifested by regional tectonic studies (Shi et al., 2015b). Finally, the youngest transtensional tectonic regime (NE–SW compression and NW–SE extension) has affected the region since the end of the Late Pleistocene. Apparent strike-slip activities on the primary faults in the basin are determined based on focal mechanism solution and fault kinematic analysis (Huang et al., 2013; Gong et al., 2016).

3.3. Jilantai Basin

The Jilantai Basin is situated at the northwestern periphery of the Ordos Block and curves from southwest to northeast, which indicates convex arc geometry (Figs. 2, 3). A NW-trending section across the basin indicates a graben structure, with the depocenter in the northwesternmost basin (Fig. 3; S₄ in Fig. 7). The basin is bounded by the Langshan Piedmont Fault (F₃₋₁) and Seertengshan Fault (F₃₋₂) to the northwest, and the Yellow River Fault (F₃₋₄) to the southeast (Fig. 7C; Rao et al., 2016). A few outcrop-scale structures that delimit the basin deformation are observed on the primary faults. At Loc. LS11 middle segment of the Langshan Fault, two cross-cutting sets of faults developed in the Oligocene–Early Miocene mudstone of the Qingshuiying Fm. The NE-striking normal faults are characterized by syn-depositional structures, attributing to NW–SE extension (Fig. 7A), suggesting extensive NW–SE extensional activity in the Oligocene–Early Miocene. Here early E–W-striking sinistral strike-slip faults cut the above-mentioned NE-striking normal faults, and are linked to the transtension characterized by NE–SW compression and NW–SE extension (Fig. 7A). The faults are covered by the Early Pleistocene conglomerate, suggesting that the late transtensive deformation postdates the Early Miocene and occurred prior to the Early Pleistocene (Fig. 7A).

The eastern margin of the basin (Loc. WH14) indicates NE-striking normal faults and NE-trending strike-slip faults that cut the Oligocene–Miocene mudstone, thereby corresponding to NW–SE extension and transtension (NE–SW compression and NW–SE extension), respectively (Fig. 7B). Furthermore, it is covered by the Holocene alluvial deposits, representing faults that developed prior to the Holocene.

At Loc. SE12 western segment of the SF, two sets of normal faults developed in the fault zone (Fig. 7C). Here one set of faults (F_1) has a 10-cm-thick gouge and cuts the Proterozoic gneisses. The faults are covered by Early Pleistocene conglomerate, suggesting that NW–SE extension occurred prior to the Early Pleistocene. Another set of normal faults (F_2) cuts the Early Pleistocene conglomerate and controls the Quaternary deposits in the Jilantai Basin, corresponding with early NE–SW extension and the late ~N–S extension (Fig. 7C). Loc. SE14 to east of Loc. SE12 shows two sets of normal faults in the Miocene mudstone, which connect with the NW–SE and NE–SE extensions, respectively (Fig. 7D). The faults do not cut the sand and loess layers with the OSL ages of 11.87–13.1 ka, suggesting that the two stages of extension likely occurred before the Late Pleistocene. Loc. SE10 to the west of SE12 is characterized by Late Pleistocene lacustrine sediments with an OSL age of 79.1 ka. Here two sets of normal faults in the strata attributed to the NE–SW and NNE–SSW extensions (Fig. 7E). Two groups of normal faults also developed in the Late Pleistocene lacustrine sediments of Loc. SE11, and are covered by Holocene alluvial deposits. These correspond to early NE–SW and late NNE–SSW extensions, respectively (Fig. 7F), suggesting two stages of extension in the Jilantai Basin during the Late Pleistocene.

In summary, four deformation episodes are defined for the Jilantai Basin, i.e., a long-term NW–SE extension from the Oligocene to the Pliocene (including a pure NW–SE extension from the Oligocene to the Early Miocene and a transtensional deformation marked by NE–SW compression and NW–SE extension in the Late Miocene–Pliocene, a gentle NE–SW extension in the Late Pleistocene, and a subsequent youngest normal and strike-slip activation on the major faults since the end of the Late Pleistocene.

3.4. Hetao Basin

The Hetao Basin strikes ENE–WSW and is separated from the Jilantai Basin by the Wulashan uplift to the west (Figs. 2, 7). The basin is a half-graben bounded by the Wulashan Fault (F_{3-4}), Daqingshan Fault (F_{3-5}), and Helinggeer Fault (F_{3-6}) to the east (section S₆; Fig. 7).

The Wulashan Fault developed locally along the Wulashan Mt., and is presented by typical fault scarps consisting of gneiss in the footwall and Early Pleistocene conglomerate in the hanging wall (Fig. 7G). At Loc. D17, the fault with a dip angle of 60° document three stage of extension, earliest NW–SE, followed NE–SW, and latest NNE–SSW extensions (Fig. 7H).

The Daqingshan Fault also cuts the Proterozoic gneiss, causing the formation of fault scarps along the Daqingshan Mt. (Figs. 7I, 7J). A fault scarp at Loc. D19 is marked by a dip of $191^{\circ}\angle 52^{\circ}$ and a set of dip-slip striations, indicating a nearly N–S extension (Fig. 7I). At Loc. 20 west of Loc. D19, a fault scarp with a dip of $170^{\circ}\angle 55^{\circ}$ crops out clearly, and is characterized by two sets of striations, corresponding to early NW–SE and late nearly N–S extensions, respectively (Fig. 7J). A NE-striking normal fault develops in the Late Pleistocene loess at the eastern segment of the Daqingshan Fault, and is covered by Holocene slopewash. Here its striations on the fault plane indicate a nearly N–S extension (Fig. 7K).

The above structural measurement suggests a three-stage extensional deformation in the Hetao Basin, i.e., a NW–SE extension likely occurring in the Miocene–Pliocene, a NE–SW extension in the Late Pleistocene, and a ~N–S extension since the end of the Late Pleistocene.

3.5. Shanxi Basin

The Shanxi Basin, a NNE-striking faulted basin along the eastern margin of the Ordos Block, comprises five en échelon subbasins (i.e., DTB, XDB, TYB, LFB, and YCB) bounded by high-angle normal faults (RGAFSO, 1988; Xu et al., 1992, 1993; Zhang et al., 1995, 1998; Shi et al., 2015a). This study focused on two subbasins, i.e., the DTB and LFB, which are located at the northernmost and southern parts of the Shanxi Basin, respectively.

The DTB is the largest faulted basin of the Shanxi Basin (Figs. 2, 8), and is bounded by the ENE–WSW-striking Yanggao-Fengzhen Fault (F_{4-1}) to the north, the NE-striking Kouquanshan Fault (F_{4-2}) to the east, and the NE-striking Liulengshan (F_{4-3}), Yuxian (F_{4-4}), and Hengshan (F_{4-5}) faults to the south, giving the basin a fan geometry that widens to the northeast (Fig. 8; Shi et al., 2015a).

A NW-trending section (S_7 ; Fig. 8) across the basin indicates a graben structure with a central uplift of the Oligocene–Early Miocene Fansi basalt and two flanking subbasins along the syn-depositional faults (i.e., the Kouquanshan and Liulengshan faults).

At Loc. D10 (Fig. 10), the Liulengshan Fault is marked by fault scarps exposing Jurassic granodiorite, with dip direction/angle of $306^{\circ}/46^{\circ}$ (Figs. 8A, B). Here dip-slip and oblique-slip striations develop on the fault plane, indicating NW–SE extension and NE–SW extension, respectively (Fig. 8B). Fault kinematic analysis, together with an examination of the crosscutting relationships of the striations,

indicates that NW–SE extension preceded NE–SW extension (Fig. 3E), evidenced by Late Cenozoic sedimentation and paleomagnetism in the eastern DTB (Liu et al., 2018). The latter NE–SW extension event is constrained to the late Pleistocene based on a K–Ar age (0.68 ± 0.13 ka) for basalt that erupted along the fault. At Loc. D30 (southern DTB), the Liulengshan Fault cuts the Jurassic granite with a fault scarp typical of 10–18 m high and a dip direction/angle of $356^\circ/56^\circ$ (Fig. 8C). Here one set of striations is observed on the fault plane, indicating normal dip-slip activity dominated by ~N–S extension that occurred during the Holocene, because the Holocene sandy clay deposits along the fault (Fig. 8C). The Kouquanshan Fault is exposed well at Loc. D45 of the western DTB, with a fault scarp 10–20 m high and a trend/dip of $127^\circ/67^\circ$ (Fig. 8D). The hanging wall comprises Holocene pebble-bearing sandy clay, whereas the footwall consists of Archean granite gneiss. The contact is marked by fault breccia and a fracture zone with a thickness of ~1 m. Here one generation of fine, oblique-slip striations cuts one group of coarse dip-slip striations on the Kouquanshan Fault plane, indicating an early NW–SE extension and late NNW–SSE extension, as calculated from the fault-slip vectors (Fig. 8D).

The Linfen Basin is separated from the Yuncheng Basin by the Emei uplift to the south, and by the Lingshi push-up swell from the Taiyuan Basin (Fig. 2; Shi et al., 2015a). The basin is bounded primarily by the Luoyunshan Fault (F₄₋₁₁) to the west, and is a half-graben structure, as shown by the structural section (S₈; Fig. 9). The Luoyunshan Fault extends southward, cuts the thickly-bedded Cambrian limestone at Loc. HS86 (Fig. 9). It is marked by numerous fault scarps between the Linfen Basin and the Luoyunshan Mt. (Fig. 9A). The fault records a change at Loc. HS86 from pure dip-slip to oblique-slip movement, indicating the occurrence of NW–SE and NNW–SSE extensions, respectively (Fig. 9B). To the south of the Linfen Basin (Loc. HS90), an E–W-trending normal fault cuts the Early Cambrian marl. The fault-slip vectors attribute its development to NE–SW extension. Furthermore, extensional activity affects the local deposition of the Late Pleistocene (Q_P³) loess, thereby constraining timing of the extension to Late Pleistocene (Fig. 9C).

The structural analysis conducted in this study, as well as the results from previous studies (Cen et al., 2015; Shi et al., 2015a; Liu et al., 2018), has delimited a three-stage Cenozoic extension event in the Shanxi Basin, i.e., a NW–SE extension in the Late Miocene–Early Quaternary, a subsequent and weaker NE–SW extension in the Mid–Late Pleistocene, and a NNW–SSE extension since the end of the Late

Pleistocene.

3.6. Weihe Basin

The Weihe Basin is located to the south of the Ordos Block and to the north of the Qinling Orogenic Belt, and connects with the Yuncheng (S₉; Fig. 10) and Sanmengxia Basins toward the east. The basin is bounded by the Qinling Piedmont Fault (F₅₋₁) and the Huashan Piedmont Fault (F₅₋₄) to the south, and the Kouzhen (F₅₋₃) and Hancheng faults (F₅₋₇) to the north (S₁₀; Figs. 2, 10).

A NE-striking fault marked by syn-depositional normal faulting developed along the HPF and affected the deposition of the Eocene Honghe Fm. (Fig. 10). A group of syn-depositional faults with dominant NW or SE trends developed in the Honghe Fm. at Loc. HS123, suggesting NW–SE extension in the Eocene. Locally, a SE-trending normal fault cuts the syn-depositional fault, indicating sustained NW–SE extension after the Eocene (Fig. 10A). An E–W-striking blind fault, limited by the Huashan Piedmont Fault to the east, developed in the interior of the basin (Fig. 10). It is uncovered during artificial construction near the Weihe River, and has a fault scarp with height of ~5 m (Fig. 10B; Rao et al., 2014; Lin et al., 2015b). Extensive activity likely occurred in the Late Pleistocene, as it affected the Late Pleistocene sandy soil with a ¹⁴C age of 18270 yr B.P.), and do not cut the silty soil with a ¹⁴C age of 6865 yr B.P. (Rao et al., 2014; Lin et al., 2015b). A NW-striking fault with normal activity develops in the Middle Pleistocene interbedded sandstone and gravel near the Qinling Piedmont Fault (Loc. HS29), determining NE–SW extension in the Late Pleistocene (Fig. 10C).

At Loc. HS25, the Qinling Piedmont Fault crops out as a typical fault scarp, on which two sets of striations (dip-slip and subhorizontal sinistral) developed because of early NW–SE and the late NE–SW extensions, respectively (Fig. 10D). At Loc. HS31 (western segment of the HPF), a fault scarp comprising Proterozoic gneiss is marked by a group of striations, indicating nearly N–S extension (Fig. 10E). The Kouzhen Fault (north of the Weihe Basin) affected the deposition of loess (Lin et al., 2015a), on which two sets of striations developed, indicating early NW–SE and late nearly N–S extensions, respectively (Fig. 10F). Additionally, normal dip-slip activity and subhorizontal NNW–SSE-directed extension occurred during the Holocene, as suggested by the deposition of the Holocene sandy clay along the fault.

The Hancheng Fault (F₅₋₇) located in northeast of the Weihe Basin is marked by a fault scarp with a trend/dip angle of 132°/43°. Fault breccia comprising Ordovician limestone is observed at Loc. SX4 (Fig. 10G). A set of dip-slip striations is

developed on the fault plane covered by the Late Pleistocene loess, indicating that the NW–SE-striking extension occurred prior to the Late Pleistocene. The fault has a trend/dip angle of $145^{\circ}/51^{\circ}$ in the Late Pleistocene loess, and is covered by the Holocene sandy clay, indicating NNW–SSE-directed extension in the Holocene (Fig. 10G).

At Loc. H97 near the North Zhongtiaoshan Fault, a group of high-angle normal faults cross-cuts Late Pleistocene loess and gravel-bearing sandy clay. Fault kinematic analysis suggests that the NNW–SSE extension occurred posterior to the Late Pleistocene (Fig. 10H). Late Miocene–Pliocene red clay is deposited at Loc. H92 along the North Zhongtiaoshan Fault (Wang et al., 2002). A cluster of normal faults are characterized by dip-slip and oblique-slip activities, related to early NE–SW and late NNW–SSE extensions, respectively (Fig. 10I).

Fault kinematic analysis of the boundary faults in the Weihe Basin indicates three-stage deformation since the Eocene. The earliest stage involved long-term NW–SE extension from the Eocene to Pliocene (ca. 40–2.6 Ma). A subsequent weaker NE–SW extension in the Mid–Late Pleistocene caused regional subsidence in the interior of the Weihe Basin. Finally, NNW–SSE extension has dominated the basin since the end of the Late Pleistocene, as deduced by the evident subsidence in the basin and the dextral shear deformation along the boundary faults of the Weihe Basin.

4. Cenozoic stress fields

A stress field is generally sustained over a certain region for sufficient periods of time, which allows us to determine stress field sequences through fault kinematic analysis, and subsequent reconstruct the tectonic evolution of the region (Angelier, 1984; Ratschbacher et al., 2003; Zhang et al., 2003; Shi et al., 2012).

Inversion of the tectonic stress field is usually based on the Wallace-Bott hypothesis, which suggests that the fault-slip orientation is parallel to the orientation of the maximum shearing stress (Wallace, 1951; Bott, 1959; Mercier et al., 1991). Given that the hypothesis excludes numerous preexisting faults, recent research has suggested that a modified Anderson model could be more suitable for interpreting the reactivation of preexisting faults (Tong and Yin, 2011). A stress field, represented by three principal stress axes (maximum (σ_1), intermediate (σ_2), and minimum (σ_3) stresses, where $\sigma_1 > \sigma_2 > \sigma_3$) and stress ratio ($R = (\sigma_2 - \sigma_3)/(\sigma_1 - \sigma_3)$, $0 \leq R \leq 1$), is usually reconstructed by fault kinematic analysis of numerous fault-slip vectors obtained from different outcrops (Angelier, 1984; Mercier et al., 1991; Ritz and

Taboada, 1993; Zhang et al., 2003). The sequences of paleostress fields have been reconstructed primarily by analyzing the superposition relationships of multiple slip vectors on a single fault/foliation surface and by observing the cross-cutting relationships of truncated fault/foliation surfaces, which provide a relative chronology of the stress fields (Mercier et al., 1997; Ratschbacher et al., 2003; Zhang et al., 2003). Furthermore, the deformation time limits of brittle fabrics are generally determined by analyzing the youngest strata that contributed to faulting, unconformable relationships, and regional tectonics (Mercier et al., 1997).

In this study, a five-phase stress field sequence around the Ordos Block since the Cenozoic is determined based on our previous work on stress fields in the eastern and western sides of the Ordos Block (Shi et al., 2015a, 2015b). This sequence is characterized by episodic changes in the principal stress directions as follows: (1) Tectonic transtension since the end of the Late Pleistocene (Fig. 11; Table S1), (2) Late Pleistocene NE–SW extension (Fig. 12; Table S2), (3) Late Miocene–Early Pleistocene NE–SW compression (Fig. 13; Table S3), (4) Late Miocene NW–SE compression (Fig. 14; Table S4), and (5) Eocene–Late Miocene NW–SE extension (Fig. 15; Table S5).

4.1. Late Pleistocene transtensional stress regime with NNW–SSE extension and ENE–WSW compression

Our previous work shows that the youngest compressive stress field is located in the South Ningxia Basin (Shi et al., 2015b). The σ_1 , σ_2 , and σ_3 are at 078°/02°, 200°/72°, and 172°/14°, respectively (Fig. 11A). Additionally, the transtensional stress field in the Shanxi Basin is marked by σ_1 , σ_2 , and σ_3 at 199°/88°, 081°/01°, and 350°/01°, respectively, since the end of the Late Pleistocene (Fig. 11B; Shi et al., 2015a). Here analyses of fault-slip vectors of the major faults at the periphery of the Ordos Block and the tectonic transpression in the Weihe Basin (Ye et al., 1987; Cheng et al., 2018) suggests a transtensional regime with NNW–SSE extension and ENE–WSW compression in the faulted basins around the Ordos Block since the end of the Late Pleistocene (see section 3). The transtensional stress field is characterized by a subvertical maximum principal stress axis (σ_1) with an azimuth/plunge at 082°/61°, a subhorizontal intermediate principal stress axis (σ_2) with an azimuth/plunge at 260°/19°, and a nearly horizontal minimum principal stress axis (σ_3) with an azimuth/plunge at 171°/02° (Fig. 11C; Table S1). These results indicate the occurrence of a regional transtensional tectonic event. The stress regime caused a left-lateral strike-slip motion with a reverse component along the

major WNW- to NW-striking faults in the South Ningxia Basin since the end of the Late Pleistocene (Shi et al., 2015b). At same time it led to normal faulting and strike-slip activity along the boundary faults of the faulted basins (e.g., Yinchuan, Jilantai, Hetao, Shanxi, and Weihe Basins) around the Ordos Block (Xu et al., 1992; Shi et al., 2015a).

This tectonic transpression is the youngest stress field in this region, representing the modern state of stress in this region, which is deduced by analyses of the youngest fault slipping affecting the Holocene strata except for the Late Pleistocene loess (Shi et al., 2006b, 2013, 2015a, 2015b; Chen et al., 2013). In addition to direct structural evidence, this tectonic stress regime has also been inferred from the focal mechanisms of earthquakes (Xue and Yan, 1984; Deng and Sheng, 2015; Guo et al., 2017), GPS data (Zhu et al., 2000; Wang et al., 2001; Cui et al., 2016; Gao et al., 2017; Cheng et al., 2018), and tectonic stress (Xie et al., 2004), indicating the transpressional event has likely lasted to the present day.

4.2. Late Pleistocene NE–SW extension

Structural measurements and analyses, as well as results from previous studies (Shi et al., 2013, 2015a, b; Xu et al., 2013), suggest that the transtensional stress field is succeeded by a NE–SW extension in the periphery of the Ordos Block. The NE–SW-striking extensional stress field is characterized by σ_1 at $303^\circ/87^\circ$, σ_2 at $136^\circ/02^\circ$, and σ_3 at $226^\circ/03^\circ$ (Fig. 12; Table S2). The NE–SW extension occurred in the Late Pleistocene, as deduced by the development of syn-depositional normal faults in the Late Pleistocene lacustrine deposits of the western Ordos Block (Chen et al., 2013; Shi et al., 2015b), as well as the appearance of the Tongxin paleolake in the western Ordos Block (Xu et al., 2013).

4.3. Late Miocene–Early Pleistocene transtensional stress regime with NW–SE extension and NE–SW compression

Our previous studies on paleostress have indicated that NE–SW compressive structures with σ_1 at $044^\circ/04^\circ$, σ_2 at $129^\circ/06^\circ$, and σ_3 at $88^\circ/85^\circ$ were developed widely in the South Ningxia region in the Late Miocene–Early Pleistocene (Fig. 13A; Shi et al., 2015b). Additionally, a transtensional stress regime of NW–SE extension and NE–SW compression, with σ_1 at $237^\circ/73^\circ$, σ_2 at $033^\circ/01^\circ$, and σ_3 at $134^\circ/09^\circ$ dominated the basins around the Ordos Block during the same period (Fig. 13B; Shi et al., 2015a). Here, The synthesis of the paleostress analysis of the basins around the Ordos Block suggest a transtensional stress regime with σ_1 , σ_2 , and σ_3 orienting at $224^\circ/28^\circ$, $259^\circ/10^\circ$, and $134^\circ/18^\circ$, respectively, in accordance with NW–SE

extension and NE–SW compression (Fig. 13C; Table S3; Zhang et al., 2006).

The timing of this transtensional stress field is constrained further based on the following evidence. As stated in our previous work, the Late Miocene Luzigou Fm. is the lowermost strata filling the Shanxi Basin and is controlled by the transtensional stress field, suggesting that the stress regime is initiated in the Late Miocene (~10 Ma) (Shi et al., 2015a). The timing of this stress regime can be also determined by structural analysis as mentioned in Section 3. Here the youngest strata responsible to NE-SW shortening in the west of Ordos Block are the Late Miocene–Pliocene strata of the Ganhegou Fm. with the deposition span of ca. 9.5–2.6 Ma (Fig. 5; Liu et al., 2019b), denoting that this stress regime probably initiated in the Late Miocene (ca. 9.5 Ma), coinciding with the low-temperature thermochronological data from Zheng et al. (2006) and Duvall et al. (2013), as well as the timing of distinctive changes in sedimentary facies, sedimentation rates, and paleoflow directions (Jiang et al., 2007; Lin et al., 2010; Wang et al., 2011). The folds related to this shortening are commonly unconformably overlain by undeformed Early Pleistocene conglomerates with a probable lower limit age of ca. 1.0 Ma, standing for a regional angular unconformity (Figs. 5, 6; Shi et al., 2019b), in which chronological evidence provides the upper limit time of the transtensional regime prior to the Early Quaternary.

4.4. Late Miocene NW–SE compression

Fault kinematic inversions from numerous individual sites suggest another compressional stress regime characterized by mean stress orientations of $141^{\circ}/08^{\circ}$ for σ_1 , $044^{\circ}/24^{\circ}$ for σ_2 , and $046^{\circ}/69^{\circ}$ for σ_3 (Fig. 14; Table S4).

The crosscutting relationships of the various faults clearly confirm that this NW-SE compression occurs prior to the NE-SW compression, and posterior to the NW-SE extension, as analyzed above (Figs. 5, 6; Shi et al., 2015b, 2019a). This compressional stress regime is recorded preliminarily in the basins at the northwestern and southeastern margins of the Ordos Block, as well as in the South Ningxia Basin, which are filled by Eocene–Early Miocene deposit (Table 1), whereas is not occurred in the Shanxi and Hetao basins filled by the Late Miocene–Pliocene strata (Fig. 14). These results imply that the stress regime likely predated the Late Miocene.

The youngest strata responding to this shortening are the mudstones of the Hongliugou Fm. with an age span of 16.7–10.5 Ma, as suggested by the above structural analysis (Shi et al., 2015b). Combined with the depositional gap between

the Hongliugou and Ganhegou Fms. at ca. 10.5–9.5 Ma (Shen et al., 2001; Guo et al., 2002; Liu et al., 2019b), we suggest that the NW-SE shortening dominated this region for a short time during the Late Miocene from ca. 10.5 to 9.5 Ma.

4.5. Oligocene–Middle Miocene NW–SE extension

Structural investigations on NW–SE extensive structures are conducted most widely in the northwestern and southeastern margins of the Ordos Block (Shi et al., 2015b), and the Weihe Basin (Zhang et al., 1998; Shi et al., 2019a). Fault kinematic inversions show that the extensional stress regime is characterized by mean stress orientations of $148^{\circ}/86^{\circ}$ for σ_1 , $223^{\circ}/01^{\circ}$ for σ_2 , and $313^{\circ}/03^{\circ}$ for σ_3 (Fig. 15; Table S5). The cross-cutting relationships clearly delimited NW–SE extension prior to the NW–SE compression (Figs. 5, 6; Shi et al., 2015b). Furthermore, significant chronological evidence for this extensional stress regime is as follows. As discussed above, a number of NE-striking syn-depositional normal faults developed in the Late Oligocene–Middle Miocene mudstones of the Qingshuiying and Zhanganpu formations, indicating that NW–SE extension occurred from the Late Oligocene to the end of the Middle Miocene (Fig. 5; Shi et al., 2015b). Structural investigations confirmed that the syn-depositional normal faults related to NW–SE extension also developed in the Late Oligocene–Early Miocene mudstones (Qingshuiying Fm.) at the eastern margin of the Yinchuan Basin (Fig. 6B; Huang et al., 2013). Additionally, a group of NE-striking syn-sedimentary normal faults developed along the Huashan Piedmont Fault in the Weihe Basin, which affected the deposition of the Eocene Honghe Fm. (Fig. 10). These results suggested that the NW–SE extension regime dominated the northwestern and southeastern parts of the Ordos Block from the Eocene to the Oligocene. This extensional event is probably associated with the long-term eruption of the Cenozoic basic–ultrabasic volcanic rocks with Ar–Ar ages of 23–9.6 Ma in West Qinling (Yu et al., 2011) and the Fansi basalt with K–Ar ages of 40–30 Ma in the Datong Basin (Wang et al., 1988). Thus, the Ordos Block was dominated by long-term NW–SE extension that spanned the Eocene to the end of the Early Miocene.

Therefore, the synthesis of the above analyses of the stress regime shows that complex stress fields have orderly dominated the Ordos Block since the Eocene. There stress regimes are featured not by the changes in the orientations of the principal stress axes, but by alternating compression and extension (Fig. 16), and the distinct changes is are presented by the transformation from pure NW–SE compression to transtensional regime in the Late Miocene.

5. Formation and evolution of Cenozoic basins around the Ordos Block extension and basin formation

Fault kinematic analyses of the principle faults of the Cenozoic basins around the Ordos Block, as well as geochronological data, suggests that a two-stage Cenozoic deformation event, associated with related tectonic stress fields, features the Cenozoic tectonic evolution in the periphery of the Ordos Block (Figs. 16, 17). Tectonic-sedimentary responses and evident changes in the stress orientations (from NW–SE to NE–SW) imply the occurrence of two episodes of deformation events during the tectonic evolution and different dynamic settings.

5.1. NW–SE extension and basin formation in the Eocene to Late Miocene (~45–9.5 Ma)

As discussed above, a regional NW–SE extensional stress regime dominated the periphery of the Ordos Block from the Eocene to the Late Miocene. This stress regime caused long-term successive rifting around the Ordos Block, as shown by the NE–SW-oriented syn-sedimentary normal faults that cut the Eocene to Late Miocene deposits (Honghe, Qingshuiying, and Zhangerpu Formations) along the boundary faults in the rifted basins (Figs. 6, 10). The extension led to the initial occurrence of rifted basins (Jilantai, Yinchuan and Weihe Basins) in the northwestern and southeastern parts of the Ordos Block during the Eocene (Figs. 16, 17A₁) due to their optimal fracture conditions (Wang et al., 1984; Cui and Li, 1986; Huang et al., 2013). The Helanshan and Qinling Mountains uplifted rapidly in the Eocene (~45–30 Ma), as identified by the fission track low-temperature thermochronology (Yin et al., 2001). The Late Miocene deposition of the Baihe Fm. (Weihe Basin) is the youngest stratum involved during NW–SE extension, indicating an upper limit time of ca. 10 Ma for this deformation (Bellier et al., 1988). This suggests that the intensive rifting has lasted until the Late Miocene. Controlled by the NW–SE extension, the South Ningxia region situated in the flank of the stable block, or the westernmost regions, is successively filled by Oligocene–Early Miocene fluvial and lacustrine deposits and conformable contacts (Shi et al., 2015b; Fang et al., 2019). These results are related to the NE-oriented syn-depositional normal faults that cut the Oligocene–Early Miocene deposits (Qingshuiying and Zhangerpu Formations) in the region (Fig. 5; Shi et al., 2015b). The sources of the Oligocene–Early Miocene strata (i.e., the Sikouzi, Qingshuiying, and Zhangerpu Formations) predominantly derive from the western margin of the Ordos Block (Zhang et al., 2006; Wang et al., 2013).

The extension to the northeast and southwest of the Ordos Block lead to a break in the weak belt, marked by a generation of deep faults and the eruption of basalt along the faults (Fig. 17A2). For instance, numerous Cenozoic basic–ultrabasic volcanic rocks erupted along NE–SW-striking faults in West Qinling with Ar–Ar ages of 23–9.6 Ma (Yu et al., 2011). The Fanshi and Hannuoba basalts with K–Ar ages ranging from ~35 to ~10 Ma are exposed widely in the northeast of the Ordos Block (Chen et al., 1985; Wang et al., 1988; Xie et al., 1989), corresponding to the Oligocene–Late Miocene. Therefore, the intensive extension and sedimentation in the northeast and southwest of the Ordos Block occurred at ca. 30–10 Ma.

Fault kinematic analysis suggests that the extensional event is followed by a gentle short-term NW–SE shortening that led to the inversion of rifted basins around the Ordos Block, as well as short-term local uplift in the western Ordos Block. This is corroborated by the gentle inversion of the Oligocene–Middle Miocene sedimentary basins (Figs. 16, 17A2). The timing of the shortening is deduced primarily from the age of the youngest involved strata and the sedimentary discontinuity. The youngest strata involved in the shortening is the Early Miocene deposits of the Zhanggenpu Fm. with a paleomagnetic age of ~9.58 to ~2.77 Ma (Liu et al., 2019b), which indicates that its lower limit age is posterior to the Early Miocene (Shi et al., 2015b). As shown by the sedimentary studies, paleocurrent directions, and provenance of clasts from the west of the Ordos Block, a short break in the sedimentary process occurred in the Late Miocene, coincidental with a gentle paraconformity between the Late Miocene Zhanggenpu Fm. and the Late Miocene–Pliocene Ganhegou Fm. with the age interval of ca. 10.5 to 9.5 Ma (Shen et al., 2001; Liu et al., 2019). This likely corresponds with the short-term shortening, indicating the deformation occurred in Late Miocene (ca. 10.5 to 9.5 Ma).

5.2. Shearing deformation and pull-apart basin formation since the end of the Late Miocene (~9.5 Ma)

Previous structural analyses of faults in the western Ordos Block delineate a NE–SW compressive tectonic regime in the Late Miocene–Early Pleistocene (~9.5–~1.8 Ma) (Chen et al., 2015; Shi et al., 2015b). Additionally, a transtensional stress regime with NW–SE extension and NE–SW compression is defined for the Ordos Block during this period (Shi et al., 2019a). The transtensional stress regime is characterized by a NE-trending right-lateral shear stress regime along the eastern and western peripheries of the Ordos Block and a NW-striking left-lateral shear stress regime along the northern and southern peripheries, as suggested by numerical

simulations (RGAFSO, 1988). The crust of the eastern margin of the Ordos Block fracture in response to this transtensional stress generates a series of left-stepping en échelon pull-apart basins (Shanxi Basin) between the Taihangshan and Lüliangshan Mts. (Fig. 17B₁; Xu et al., 1993; Zhang et al., 2003; Cen et al., 2015; Shi et al., 2015a).

Apatite fission track thermal simulation shows that the Lüliangshan Mt. has been subject to a rapid uplift process at 10 Ma (Chen et al., 2012). The Kouzhai Fm., the oldest Cenozoic syn-rift stratum in the Shanxi Basin, is associated with Hipparion red clay, with a paleomagnetic age span of ca. 10–2.0 Ma (Yue et al., 2004; Li et al., 2009). These studies suggest that the Shanxi Basin formed in the Late Miocene–Early Quaternary (Figs 16, 17B₁). The stress regime also affect the periphery of the Ordos Block and led to the formation of the Hetao Basin. The basins to the northwest and southeast of the block (Jilantai, Yinchuan, and Weihe basins) have been successively stretched during this time (Fig. 17B₁; Huang et al., 2013). Furthermore, the mountains around the basins (Helanshan, Daqingshan, Lüliangshan, Liupanshan, and Qinling Mts.) are also marked by accelerated exhumation during the same time period, as suggested by numerous low-temperature thermochronometric studies (Enkelmann et al., 2006; Zheng et al., 2006; Chen et al., 2012; Li et al., 2013; Liu et al., 2013; Heberer et al., 2014; Chen et al., 2015; Sun et al., 2017; Xu et al., 2017).

The NE–SW shortening, characteristic of a subhorizontal compressive stress regime, predominately controlled the South Ningxia region from the Late Miocene to the Early Pleistocene (Shi et al., 2015b). Integration of detailed paleomagnetic data and vertebrate fossils from the Hejiakouzi and Sikouzi areas in the South Ningxia region indicate a distinct change in the sedimentary facies from fluvio-lacustrine to fluvio-piedmont since the end of the Middle Miocene (ca. 10 Ma) (Shen et al., 2001; Jiang et al., 2007; Lin et al., 2010; Wang et al., 2011; Liu et al., 2019b). This change is accompanied by an abrupt transformation in the paleoflow direction of this region (from N or SW to E and NE), and corresponds to an evident increase in the rate of sedimentation (Jiang et al., 2007; Lin et al., 2010; Wang et al., 2011, 2013; Liu et al., 2019b), which is associated with an intensive regional uplift, as indicated by low-temperature thermochronological studies on the Haiyuan Fault (Zheng et al., 2006; Duvall et al., 2013). Subsequently, the successive compression led to the formation of NW- to WNW-striking basin-and-range structures, characterized by four mountain ranges separated by Cenozoic sedimentary basins

(IG and SBNX, 1990; Shi et al., 2015b). This shortening event terminated in the Early Pleistocene (ca. 2.5 Ma), as shown by regional stratigraphic unconformities between the Late Miocene–Pliocene Ganhegou Fm. and the Early Pleistocene conglomerate (Shi et al., 2015b, 2019b).

Structural measurements and analysis show that NE–SW shortening had been followed by NE–SW extension in the Late Pleistocene (Figs. 12, 16). This is demonstrated by the development of syn-depositional normal faults in the Late Pleistocene lacustrine deposits (Chen et al., 2013) and the widespread normal faulting activity on the four NW- or NNW-striking faults in the western part of the Ordos Block (Shi et al., 2015b). The most apparent change is marked by the occurrence of a series of paleolakes (Jilantai, Hetao, and Salawusu paleolakes) in the faulted basins during this period (Li, J.B., et al. 2005; Chen, F.H., et al., 2008; Fan et al., 2011), as well as the appearance of the Tongxin paleo-lake between the Xiang Shan-Tianjingshan and the Yantongshan Mts. (Figs. 16, 17B2; Xu, T. et al., 2013).

The eruption of the late Quaternary basalts (ca. 70 ka) along the main fault in the northeastern part of the Ordos Block could be attributed to the downcutting of the preexisting faults to the lower crust, which accompanies the extensional event. These results confirm that the NE–SW extension occurred in the Middle Pleistocene. Furthermore, extensional deformation likely contribute to the widespread flow of basalt (0.73–0.11 Ma) (Wang et al., 1988; Fan et al., 2015) along the NE-striking faults (primarily at the intersection of NW- and NE-striking faults), as deduced by the clusters of volcanic cones across the Datong Basin (Li et al., 1998; Cen et al., 2015; Shi et al., 2015a). The ^{14}C dating of gouge from normal faults to the east of Luoshan Mt. (Chen et al., 2013), as well as fossil snails from the uppermost lacustrine deposits of the Late Pleistocene paleo-lake, suggests that the youngest age for this activity was ca. 18 ka (Xu, T. et al., 2013). However, the lower limit age for this extensional event remains unclear.

The tectonic regime subsequently changes into a transtensional activity, with ENE-trending subhorizontal maximum principal stress axes (σ_1) at the end of the Late Pleistocene (most likely after 18 ka) (Fig. 11; Shi et al., 2015b). This tectonic stress regime has dominated this region to the present time and coincides with the focal solutions of earthquakes (IG and SBNX, 1990), GPS data (Wang et al., 2001; Zheng et al., 2013), and geostresses (Xie et al., 2004), and represents the youngest stress field in the South Ningxia region (Shi et al., 2013, 2015b). Structural analyses and numerical simulations suggest that subsequent ENE–WSW compression in the

southwestern part of the Ordos Block generated a transtensional stress regime (ENE–WSW compression and NNW–SSE extension) around the Ordos Block (Xue and Yan, 1983; RGAFSO, 1988; Deng and Sheng, 2015; Guo et al., 2017). This regime is characterized by an ENE–WSW right-lateral shear regime in the northern and southern margins of the Ordos Block and an NNW–SSE left-lateral shear regime in the eastern and western sides of the block (Fig. 17B3; RGAFSO, 1988).

Furthermore, the preexisting NNE- and ENE-striking boundary faults along the basins of the Ordos Block have reactivated in response to the transtensional stress, and have been featured by dextral and sinistral oblique slips, respectively, as indicated by the lateral offset observed in the gullies (Zhang et al., 1998), the rapid deposition of the Late Quaternary–Holocene sandy clay along the faults (RGAFSO, 1988; Xu et al., 1993), and the disappearance of the paleolakes along the faults (Figs. 16, 17B3).

The amount of offset is consistent with the upstream length of the gullies, as shown by large-scale fault mapping in the central Shanxi Basin (Zhang et al., 1998). For instance, SPOT image analysis suggested that the Xizhoushan Fault (F₇) showed an offset of 50–250 m on gullies of variable lengths (Zhang et al., 1998). An average slip rate of 5.68 mm/yr during the Holocene likely contributed to the renewal of the Late Quaternary uplift of the Shiguangling and Lingshi push-up swells in the central Shanxi Basin (Xu et al., 1993).

In contrast with the eastern Ordos Block, the slip rate is largely in agreement with that of the left-lateral strike on the NW- to WNW-trending faults (Yantongshan, Xiangshan-Tianjingshan, and Haiyuan faults). It is also consistent with the right-lateral strike-slip movement on the NNW–SSE-striking Luoshan-Niushoushan Fault (RGAFSO, 1988; Deng et al., 1989; IG and SBNX, 1990; Zhang et al., 1990; Chen et al., 2013; Zheng, et al., 2013; Shi et al., 2015b). The strike-slip faulting on the Xiangshan-Tianjingshan Fault obliquely truncates the early NW-striking folds (Fig. 2), suggesting that early ENE–WSW shortening is imprinted by left-lateral strike-slip faulting at the end of the Late Pleistocene with a fault-slip offset of ~10 m (Chu et al., 2009). This likely contributed to the extremely limited westward extrusion of mini blocks in the area. However, the most intensive deformation in response to this tectonic transpression occurred along the Haiyuan Fault due to its closest situation of the Tibetan Plateau (Shi et al., 2013). The deformation is featured by the occurrence of small-scale pull-apart basins (e.g., Shenjiazhuang, Huangliangtan, Shaoshui, Dayingshui, Sanjiaocheng, Ganyanchi, Laohuyaoxian,

and Xiaonanchuan basins) along the main fault (see IG and SBNX (1990) for details). These results suggested that the maximum strike-slip displacement on the Haiyuan Fault since the end of the Late Pleistocene is greater than ~8 km and smaller than 15.5 km, as deduced from the offset of granite markers along the fault (Burchfiel et al., 1991). In addition, the total Holocene strike-slip displacement along the Haiyuan Fault has been calculated as 20–55 m at a slip rate of 2.5–9.0 mm/a. The maximum co-seismic offset of 8–16 m is associated with the Haiyuan earthquake in 1920 (Deng et al., 1989; IG and SBNX, 1990; Lasserre et al., 1999; Jolivet et al., 2013; Zheng, et al., 2013).

6. Formation regimes of the faulted basins

The above deformation process and their paleotectonic stress field proposes a two-stage tectonic evolution around the Ordos Block in the Cenozoic. The first stage is marked by faulting or rifting initiated in the northwestern and southeastern margins of the Ordos Block in the Eocene–Late Miocene under a NW–SE extensional regime (Zhang et al., 2003; Shi et al., 2015b). Investigation and analysis of tectonic stress suggest that the optimum direction of tectonic extension (σ_3) is $312^\circ/03^\circ$ and the attitude of the maximum principal compressive stress (σ_1) is $138^\circ/87^\circ$ (Fig. 15), which implies a pure shear deformation pattern around the Ordos Block during this period (Figs. 18A₁, A₂). The peripheries of the Ordos Block are controlled by the regional NW–SE extension. As stronger extension occurred on its northwestern and southeastern margins than on the other parts, the areas broke up, and are pulled apart (Wang et al., 1984; Cui and Li, 1986). A set of red lacustrine facies detritus is deposited in the region leading to the formation of the Jilantai, Yinchuan, and Weihe basins (Fig. 17A₁; Deng et al., 1999).

The second stage is characterized by the formation of pull-apart basins in the northeastern and eastern margins of the Ordos Block in the Late Miocene. It is dominated primarily by the transtensional stress regime in accordance with NW–SE extension and NE–SW compression, with σ_1 , σ_2 , and σ_3 orienting at $227^\circ/22^\circ$, $097^\circ/03^\circ$, and $135^\circ/21^\circ$, respectively (Fig. 13). The stress field indicates that simple shearing controlled the periphery of the Ordos Block, which is featured by a right-lateral Riedel shears (R) in the eastern and western sides of the block, and a left-lateral conjugate Riedel shear (R') in the southern and northern edges of the Ordos Block (Figs. 18B₁, B₂; Deng et al., 1999), as shown by previous studies on regional Riedel shear zones (Ghosh and Ramberg, 1976; Ahlgren, 2001; Katz et al., 2004). Here the optimum direction of maximum principal stress (σ_1) is $227^\circ/22^\circ$,

which is identical to loading compression along the N47°E strike in a planar model. Moreover, an internal friction angle of 15° is utilized in this study (Harding, 1974), and R and R' are estimated at N21°E and N77°E, respectively. The NNE-striking Riedel shears resulted in dextral strike-slip in the eastern margin of the Ordos Block and formed a series of NE-trending pull-apart basins (Shanxi Basin), which present left-stepping échelon (Fig. 18A₂). In addition, the Jilantai and Yinchuan basins are influenced by this regime and generated continuous faulting and deposition. The ENE-striking Weihe and Hetao basins are subjected to the ENE-trending conjugate Riedel shears with left-lateral shear action, which lead to the formation of the Hetao Basin and the extension in the Weihe Basin (Fig. 18A₁). The mechanism shows a ~~shear~~ shearing activity surrounding the Ordos Block except for the shortening in its southwestern margin, characteristic of a dextral shear along its eastern and western margins and a sinistral shear along its southern and northern edges, leading to the formation of the special structure comprising the stable Ordos Block as the center and a group of the basins (e.g., Yinchuan, Jilantai, Hetao, Weihe, Shanxi basins) as the edges (Deng et al., 1999). Therefore, the results show no obvious overall rotation activity for the Ordos Block (Xue and Yan, 1984; Cui et al., 2016), not corresponding with the block rotation hypothesis. Here it is likely that the intense shear deformation principally result from the northeastward growth of the Tibetan Plateau (Xue and Yan, 1983; Shi et al., 2015b).

7. Discussion

The results of this study suggest that a two-stage deformation process controlled the Ordos Block, i.e., (1) the Eocene to Mid–Late Miocene (~45–~9.5 Ma) NW–SE extension and formation regimes of basins, and (2) shearing deformation and pull-apart basin formation at the end of the Late Miocene (~9.5 Ma). These processes are characterized by different dynamic backgrounds because the North China Block is likely affected by the Indo–Asian and Pacific–Asian collisions (Ren et al., 2002).

The first stage is characterized by regional NW–SE extensional stress regimes from the Eocene to the Mid–Late Miocene, which leads to the occurrence of NE-striking faulted basins in the northwestern and southeastern margins of the Ordos Block (Huang et al., 2013; Shi et al., 2015b; Liu et al., 2019b). This lengthy period of extension is likely responsible for the development of NE-striking rift basins, such as the northwest China (Fan et al., 2019), Baikal basin (Ufimtsev, 1999) and the Japan Sea (Otofujii et al., 1985; Jolivet, 1994).

Tectono-sedimentation studies on the South Ningxia region suggested that the

material sources for the Oligocene–Early Miocene strata (Sikouzi, Qingshuiying, and Zhangenpu Fms.) predominantly originated from the western margin of the Ordos Block (Li et al., 2013; Wang et al., 2013; Liu et al., 2019a). Further, these studies have suggested no obvious uplift in the South Ningxia region prior to the Late Miocene (ca. 10 Ma), likely indicating that the growth of the Tibetan Plateau did not clearly imprint on the South Ningxia region during this period. These results are also supported by the presence of the Miocene aeolian deposits on the western Loess Plateau (Guo et al., 2002; Lease et al., 2011; Zhan et al., 2011). Comprehensive analyses of sedimentation, deformation, and tectonic stress regimes of the Japan Sea opening (Otofuji et al., 1985; Celaya and McCabe, 1987; Choi, 2012) suggest that the long-term extensional event is predominately linked dynamically with the far-field effects of the northwestward subduction of the Pacific Plate, in agreement with the extension in northwest China (Fan et al., 2019).

The second stage is presented by mountain building in the western margin of the Ordos Block and the opening of the Shanxi and Hetao basins in the Late Miocene in response to the transtensional stress regime (Ye et al., 1987; Zhang et al., 2006). Integrated analysis of sedimentary and paleomagnetic studies on the South Ningxia region (Shen et al., 2001; Jiang et al., 2007; Lin et al., 2010) indicates a distinct change in the sedimentary facies from fluvio-lacustrine to fluvio-piedmont since the Late Miocene (ca. 9.5 Ma) (Jiang et al., 2007; Lin et al., 2010; Wang et al., 2011; Liu et al., 2019a). This change is accompanied by an abrupt transformation in the paleo-flow direction in the region (from N or SW to E and NE), and coeval with an evident increase in the sedimentation rate (Jiang et al., 2007; Lin et al., 2010; Wang et al., 2011, 2013; Liu et al., 2019b). Additionally, it is associated with an intensive regional uplift in the southwestern margin of the Ordos Block, as suggested by numerous low-temperature thermochronological studies on the Haiyuan Fault (Zheng et al., 2006; Duvall et al., 2013). In fact, almost synchronous uplift and intensive crustal shortening along the periphery of the Tibetan Plateau in the Late Miocene (ca. 10 Ma) has been suggested by both extensive tectono-sedimentation studies (Kirby et al., 2002; Charreau et al., 2005; Fang et al., 2005; Dayem et al., 2009; Godard et al., 2009, 2010; Clark et al., 2010; Liu et al., 2010; Zhang et al., 2010; Ge et al., 2012; Ma et al., 2013; Shi et al., 2013, 2015b; Wang, X.X. et al., 2013), and low-temperature thermochronometric work (Kirby et al., 2002; Enkelmann et al., 2006; Godard et al., 2009, 2010; Liu et al., 2010, 2013; Wang E.Q. et al., 2012; Heberer et al., 2014; Yang et al., 2014). Such mechanisms contribute to

the paleoenvironmental changes around the Tibetan Plateau (Qiang et al., 2001; Dettman et al., 2003; Hough et al., 2011). The comprehensive studies on stratigraphic, geochronological, and paleoenvironmental changes in the South Ningxia Basin of the northeastern Tibetan Plateau showed the onset of a significant tectonic regime in this region since the Late Miocene (~9.5 Ma), which is attributed to the significantly evident growth of the Tibetan Plateau. The Shanxi faulted basin in the eastern margin of the Ordos Block formed in the Late Miocene–Early Pleistocene due to a transtensional stress regime (Shi et al., 2015a), which is likely restricted by the Pacific Plate to the west (Northrup et al., 1995; Park et al., 1998). Tectono-sedimentation analysis suggests that the deformation of the periphery of the Ordos Block could be attributed predominantly to the Indo–Asian collision (Jolivet et al., 1994; Bao et al., 2013) and partially to the northwestward subduction of the Pacific Plate (Li et al., 2010), which coincided with the lithospheric velocity structure beneath the Ordos Block (Chen et al., 2018).

8. Conclusions

The following conclusions can be drawn based on analysis of fault kinematics, field investigations, and formation regimes.

(1) The two-stage tectonic evolution of the faulted basins around the Ordos Block in the Cenozoic is reconstructed. The first stage is featured by rifting in the northwestern and southeastern peripheries of the Ordos Block in the Eocene–Late Miocene (~50–10.5 Ma), leading to the formation of the Jilantai, Yinchuan, and Weihe Basins. The stage ended with a gentle short-term NW–SE shortening in the Late Miocene (~10.5–~9.5Ma). The second stage is marked by pull-apart basin formation in the eastern and northern margins of the Ordos Block, as well an intensive mountain-building process in the western margin of the block since the Late Miocene (~9.5 Ma). This stage further comprises the formation of the Shanxi and Hetao Basins in the northeastern and eastern margins of the block in the Late Miocene to Early Pleistocene (ca. 9.5–2.58 Ma) due to a transtensional stress regime, respectively. A subsequent widespread occurrence of paleolakes in the faulted basins in the Late Pleistocene was caused by a gentle NE–SW extension, evident strike-slip activities in the periphery of the Ordos Block since the end of the Late Pleistocene because of youngest tectonic transtensional regime.

(2) The periphery of the Ordos Block is characterized by pure-shear deformation at the early stage and simple-shear deformation at the late stage.

(3) The periphery of the Ordos Block is generally subject to two-stage tectonic

deformation in the Cenozoic, which originate from different driving forces. The formation of the faulted basins in the first stage is probably linked to the effects of the northwestward subduction of the Pacific Plate. The formation of the pull-apart basins in the second stage is attributed predominantly to the northeastward growth of the Tibetan Plateau and partially to the northwestward subduction of the Pacific Plate.

Conflict of interest statement

None

Acknowledgments

The data supporting Figures 11, 12, 13, 14, 15 in this paper are available in Supporting Information (SI) Tables S1, S2, S3, S4, S5, respectively, or are available by contacting the corresponding author. This study is supported by the National Science Foundation of China (Grant numbers 41672203), and China Geological Survey (CGS) (Grant numbers DD20190018, DD20160060, 1212011120099, 1212011120100, 1212011220259). We acknowledge Drs. Chen, H., Huang, X.F., Cen, M., Chen, L., Chen, P., Chen, X.Q., Li, H.Q., Wang, Y.C., Gong, W.B., Li, J.Y. and others for assistance in the field. We are grateful to the editors and reviewers for their critical and constructive comments to improve the manuscript, as well as to Dr. Richard W. Allmendinger for Faultkin 7.4.1 in calculating the fault-slip vectors (<https://macdownload.informer.com/faultkin/>).

References

- Ahlgren, S. G., 2001. The nucleation and evolution of Riedel shear-zones as deformation bands in porous sandstone. *Journal of Structural Geology* 23, 1203-1214.
- An, Z. S., Sun, D. H., Chen, M. Y., Sun, Y. B., Li, L., Chen, B. Q., 2000. Red clay sequences in Chinese Loess Plateau and recorded paleoclimate events of the Later Tertiary. *Quaternary Sciences* 20 (5), 435-446.
- Angelier, J., 1984. Tectonic analysis of fault slip data sets. *Journal of Geophysical Research* 89, 5835-5848.
- Avouac, J. P., Tapponnier, P., 1993. Kinematic model of active deformation in central Asia. *Geophysical Research Letters* 20, 895-898.

- Bellier, O., Mercier, J. L., Vergely, P., Long, C. X., Ning, C. Z., 1988. Cenozoic sedimentary and tectonic evolution of the Weihe graben (Shaanxi Country, Northern China). *Bull. Soc. Geol. Fr.* 4, 979-994.
- Bott, M. H. P., 1959. The mechanisms of oblique slip faulting. *Geological Magazine* 96, 09-117.
- Burchfiel, B. C., Zhang, P. Z., Wang, Y. P., Song, F. M., Deng, Q. D., Molnar, P., Royden, L., 1991. Geology of the Haiyuan Fault zone, Ningxia-Hui Autonomous Region, China, and its relation to the evolution of the northeastern margin of the Tibetan Plateau. *Tectonics* 10, 1091-1110.
- Cen, M., Dong, S. W., Shi, W., Zhou, T. F., Chen, L., Chen, X. Q., 2015. Structural analysis on the formation mechanism of Datong basin. *Geological Review* 61 (6), 1235-1247.
- Changqing Oilfield Company, Petro China (COC), 1983. Alas of the advances in oil-gas exploration. Petroleum Industry Press, Beijing, pp. 1-166.
- Chen, F. H., Fan, Y. X., Madsen, D. B., Chun, X., Zhao, H., Yang, L. P., 2008. Preliminary study on the formation mechanism of the “Jilantai-Hetao” mega lake and the lake evolutionary history in Hetao region. *Quaternary Sciences* 28 (5), 866-873.
- Chen, G. A., 1987. On the geotectonic nature of the Fen-Wei Rift system. *Tectonophysics* 143, 217-223.
- Chen, G., Ding, C., Xu, L. M., Zhang, H. R., Hu, Y. X., Yang, P., Li, N., Mao, X. N. 2012. Analysis on the thermal history and uplift process of Zijinshan intrusive complex in the eastern Ordos basin. *Chinese J. Geophys.* 55 (11), 3731-3741.
- Chen, H., Hu, J. M., Gong, W. B., Kang, R., Li, L. B., 2015. Characteristics and transition mechanism of late Cenozoic structural deformation within the Niushou Shan–Luoshan fault zone at the northeastern margin of the Tibetan Plateau. *Journal of Asian Earth Sciences* 114, 73-88.
- Chen, H., Hu, J. M., Gong, W. B., Li, L. B., 2013. Cenozoic deformation and evolution of the Niushou Shan-Luo Shan fault zone in the northeast margin of the Tibet Plateau. *Earth Science Frontiers* 20, 18-35.
- Chen, H., Hu, J. M., Wu, G. L., Shi, W., Geng, Y. Y., Qu, H. J., 2015. Apatite fission-track thermochronological constraints on the pattern of late Mesozoic–Cenozoic uplift and exhumation of the Qinling Orogen, central China. *Journal of Asian Earth Sciences* 114, 649–673.
- Chen, L., 2010. Concordant structural variations from the surface to the base of the upper mantle in the North China Craton and its tectonic implications. *Lithos* 120, 96–115.
- Chen, L., Cheng, C., Wei, Z.G., 2009. Seismic evidence for significant lateral variations in lithospheric thickness beneath the central and western North China Craton. *Earth Planet. Sci.*

Lett. 286 (1), 171–183.

- Chen, W. J., Liu, R., Sun, J., 1985. The temporal and spatial distribution of Cenozoic basalts and the evolution of north China basin. *Res. Recent Crust Movement* 1, 41-49.
- Chen, Z. H., Wang, C. Y., Lou, H., 2018. Crust and upper mantle velocity structure beneath the Ordos Block and its tectonic significance. *Chin. Sci. Bull* 63, 327-339.
- Cheng, Y. L., He, C. Q., Rao, G., Yan, B., Lin, A. M., Hu, J. M., Yu, Y. L., Yao, Q., 2018. Geomorphological and structural characterization of the southern Weihe Graben, central China: Implications for fault segmentation. *Tectonophysics* 722, 11-24.
- Chu, Q. Z., 2009. Classification of faults in the Zhongwei fault zone and its tectonic implication. *Acta Geologica Sinica* 83, 1221-1232.
- Cui, D. X., Hao, M., Li, Y. H., Wang, W. P., Qin, S. L., Li, C. J., 2016. Present-day crustal movement and strain of the surrounding area of Ordos block derived from repeated GPS observations. *Chinese Journal of Geophysics* 59 (10), 3646-3661.
- Cui, S. Q., 1997. Formation and evolution of Cenozoic continental rift belts in East Asia. In: 30th International Geological Congress. Xiao, X., Liu, F. (Eds.). 6, 15-36.
- Cui, S. Q., Li, J. R., 1986. Comparative tectonic analysis of Fen-Wei graben and Baikal rift system. *Bulletin of the Chinese Academy of Geological Sciences* 15, 21-31.
- Davis, G. H., Bump, A. P., Garcí'a, P. E., Ahlgren, S. G., 1999. Conjugate Riedel deformation band shear zones. *Journal of Structural Geology* 22, 169-190.
- Dayem, K. E., Molnar, P., Clark, M. K., Houseman, G. A., 2009. Far-field lithospheric deformation in Tibetan during continental collision. *Tectonics* 28, 1-9.
- Deng, Q. D., Chen, S. P., Min, W., Yang, G. Z., Reng, D. W., 1999. Discussion on Cenozoic tectonics and dynamics of the Ordos block. *Journal of Geomechanics* 5 (3), 13-21.
- Deng, Q. D., Sung, F. M., Zhu, S. L., Li, M., Wang, T., Zhang, W., Burchfiel, B. C., Molnar, P., Zhang, P. Z., 1984. Active faulting and tectonics of the Ningxia-Hui autonomous region, China. *J. Geophys. Res.* 89 (B6), 4427-4445.
- Deng, S. Q., Sheng, S. Z., 2015. The crustal stress field around the Ordos Block. *North China Earthquake Sciences* 33 (2), 55-62.
- Duvall, A. R., Clark, M. K., Kirby, E., Farley, K. A., Craddock, W. H., Li, C. Y., Yuan, D. Y., 2013. Low temperature thermochronometry along the Kunlun and Haiyuan faults, NE Tibetan Plateau: Evidence for kinematic change during late stage orogenesis. *Tectonics* 32, 1190-1211.
- Editorial Committee of the Regional Geology of China, Ningxia (ECRGCN), 2017. The Regional Geology of China, Ningxia. Geological Publishing House, Beijing, pp. 1-916.
- Enkelman, E., Ratschbacher, L., Jonckheere, R., Nestler, R., Fleischer, M., Gloaguen, R., Hacker,

- B. R., Zhang, Y. Q., Ma, Y. S., 2006. Cenozoic exhumation and deformation of northeastern Tibetan and the Qinling: Is Tibetan lower crustal flow diverging around the Sichuan Basin? *Geological Society of America Bulletin* 118, 651-671.
- Fan, L. G. Meng, Q. R., Wu, G. L., Wei, H. H., Du, Z. M., Wang, E. C., 2019. Paleogene crustal extension in the eastern segment of the NE Tibetan plateau. *Earth and Planetary Science Letters* 514, 62-74.
- Fan, Q. C., Zhao, Y. W., Chen, S. S., Li, N., Sui, J. L., 2015. Quaternary volcanic activities in the west of the Daxing'anling-Taihangshan gravity lineament. *Bulletin of Mineralogy, Petrology and Geochemistry* 34 (4), 674-681.
- Fan, T. L., Fan, Y. X., Wei, G. X., 2011. New findings and dating of lacustrine sediments in the Xishanzui subuplift, Hetao Basin. *Acta Geographica Sinica* 5, 698-708.
- Fang, X. M., Fang, Y. H., Zan, J. B., Zhang, W. L., Song, C. H., Appel, E., Meng, Q. Q., Miao, Y. F., Dai, S., Lu, Y., Zhang, T., 2019. Cenozoic magnetostratigraphy of the Xining Basin, NE Tibetan Plateau, and its constraints on paleontological, sedimentological and tectonomorphological evolution. *Earth-Science Reviews* 190, 460-485.
- Fu, Z. Y., Yuan, X. Q., Geng, G. C., 1994. The Tertiary of the Hetao Basin and its biotas. *Journal of Stratigraphy* 18 (1), 24-29.
- Gao, L. X., Han, X. M., Dai, Y., Li, J., Yang, H. Y., 2017. Movement characteristics and present seismic behavior of the Ordos block. *Journal of geodesy and geodynamics* 37 (4), 349-354.
- Gao, S. L., 2007. Research about geological conditions of shallow gas (biogenic gas) accumulation in Hetao Basin. Northwest University, Xi'an, pp. 1-173.
- Geological Survey Bureau of Shanxi Province (GSBSX), 2002. Regional Geology of Yingxian (1:250000). Geological Publishing House, Beijing, pp.106-127.
- Ghosh, S. K. Ramberg, H., 1976. Reorientation of inclusions by combination of pure shear and simple shear. *Tectonophysics* 34 (1-2), 1-70.
- Gong, W. B., Shi, W., Chen, H., Qiu, S. D., Yin, Y. G., Zhao, Y., 2016. Quaternary active characteristics of the Liumugao Fault in the northern segment of the Niushoushan-Luoshan fault. *Journal of Geomechanics* 22 (4), 1004-1014.
- Guo, X. Y., Jiang, C. S., Wang, X. S., Tian, X., 2017. Characteristics of small to moderate focal mechanism solutions stress field of the circum Ordos block. *Journal of geodesy and geodynamics* 37 (7), 675-685.
- He, J. K., Cai, D. S., Li, Y. X., Gong, Z., 2004. Active extension of the Shanxi rift, north China: Does it result from anticlockwise block rotations? *Terra Nova* 16, 38-42.
- Heberer, B., Anzenbacher, T., Neubauer, F., Genser, J., Dong, Y. P., Dunkl, I., 2014. Polyphase exhumation in the western Qinling Mountains, China: Rapid Early Cretaceous cooling along

- a lithospheric-scale tear fault and pulsed Cenozoic uplift. *Tectonophysics* 617, 31-43.
- Huang, X. F., Feng, S. Y., Gao, R., Li, W. H., 2016. Development of Yinchuan Basin: Deep seismic reflection profile revealed the linkage between shallow geology and deep structure. *Chinese Journal of Geology* 51(1), 53-66.
- Huang, X. F., Shi, W., Li, H. Q., Chen, L., Cen, M., 2013. Cenozoic tectonic evolution of the Yinchuan Basin: Constrains from the deformation of its boundary faults. *Earth Science Frontiers* 20, 199-210.
- Institute of Geology, State Seismological Bureau (IG), Seismological Bureau of Ningxia Hui Autonomous Province (SBNX), 1990. Haiyuan Active Fault. Seismological Press, Beijing, pp. 1-286.
- Jiang, H. C., Ding, Z. L., Xiong, S. F., 2007. Magnetostratigraphy of the Neogene Sikouzi section at Guyuan, Ningxia, China. *Palaeogeography, Palaeoclimatology, Palaeoecology* 243, 223-234.
- Jolivet, L., Davy, P., Cobbold, P., 1990. Right-lateral shear along the Northwest Pacific Margin and the India-Eurasia Collision. *Tectonics* 9 (6), 1409-1419.
- Jolivet, L., Tamaki, K., Fournier M., 1994. Japan Sea, opening history and mechanism: A synthesis. *Journal of Geophysical Research* 99, 22237-22259.
- Jolivet, R., Lasserre, C., Doin, M. P., Peltzer, G., Avouca, J. P., Sun, J., Dailu, R., 2013. Spatio-temporal evolution of a seismic slip along the Haiyuan fault, China: Implications for fault frictional properties. *Earth and Planetary Science Letters* 377-378, 23-33.
- Kaakinen, A., Lunkka, J. P., 2003. Sedimentation of the Late Miocene Bahe Formation and its implications for stable environments adjacent to Qinling Mountains in Shaanxi, China. *Journal of Asian Earth Sciences* 22, 67-78.
- Katz, Y., Weinberger, R., Aydin, A., 2004. Geometry and kinematic evolution of Riedel shear structures, Capitol Reef National Park, Utah. *Journal of Structural Geology* 26, 491-501.
- Lasserre, C., Gaudemer, Y., Tapponnier, P., Meriaux, A. S., Van der Woerd, J., Yuan, D., Ryerson, F. J., Finkel, R. C., Caffee, M. W., 2002. Fast late Pleistocene slip rate on the Lenglongling segment of the Haiyuan fault, Qinghai, China. *Journal of Geophysical Research* 107 (B11), 2276.
- Lei, Q. Y., Zhang, P. Z., Zheng, W. J., Chai, C. Z., Wang, W. T., Peng, D. U., 2016. Dextral strike-slip of Sanguankou-Niushoushan fault zone and extension of arc tectonic belt in the northeastern margin of the Tibet Plateau. *Science China Earth Sciences* 59 (5), 1025-1040.
- Li, C. K., Wu, W. Y., Qiu, Z. D., 1984. Chinese Neogene: Subdivision and correlation. *Vertebrata Pal Asiatica* 22 (3), 163-172.
- Li, J. B., Ran, Y. K., Guo, W. S., 2005. Research on the lacustrine strata of the Tuoketuo mesa,

- Hetao Basin, China. *Quaternary Sciences* 25 (4), 630-639.
- Li, J. X., Liu, C. Y., Yue, L. P., Wang, J. Q., 2015. Apatite fission track evidence for the Cenozoic uplift of the Lüliang Mountains and a discussion on the uplift mechanism. *Geology in China* 42 (4), 960-972.
- Li, J. X., Yue, L. P., Liu, C. Y., Wang, X. Y., Li, G. F., 2013. The tectonic-sedimentary evolution of the Lüliang Mountains since the Miocene. *Journal of Stratigraphy* 37 (1), 93-100.
- Li, J. X., Yue, L. P., Xu, Y., Sun, B., Sun, L., Wang, X. Y., 2009. New advances in the study of the late Neogene stratigraphy in the Lvliang Mountain. *Journal of Stratigraphy* 2, 68-73.
- Li, S. Z., Guo, L. L., Xu, L. Q., Somerville, I. D., Cao, X. Z., Yu, S., Wang, P. C., Suo, Y. H., Liu, X., Zhao, S. J., 2015. Coupling and transition of Meso–Cenozoic intracontinental deformation between the Taihang and Qinling Mountains. *Journal of Asian Earth Sciences* 114, 188-202.
- Li, S. Z., Suo, Y. H., Dai, L. M., Liu, L., Chong, J., Xin, L., 2010. Development of the Bohai Bay Basin and destruction of the North China Craton. *Earth Science Frontiers* 17 (4), 064-089.
- Li, S. Z., Suo, Y. H., Santosh, M., Dai, L. M., Liu, X., Yu, S., 2013. Mesozoic to Cenozoic intracontinental deformation and dynamics of the North China Craton. *Geological Journal* 48, 543-560.
- Li, X. N., Li, C. Y., Pierce, I., Zhang, P. Z., Zheng, W. J., Dong, J. Y., Chen, G., Ai, M., Ren, G. X., Luo, Q. X., 2019. New slip rates for the Tianjingshan fault using optically simulated luminescence, GPS, and paleoseismic data, NE Tibet, China. *Tectonophysics*. <https://doi.org/10.1016/j.tecto.2019.02.007>.
- Li, Y. L., Yang, J. C., Xia, Z. K., Mo, D. W., 1998. Tectonic geomorphology in the Shanxi Graben System, northern China. *Geomorphology* 23, 77-89.
- Li, Y., Song, Y. G., Qian, L. B., Li, X. M., Qiang, X. K., An, Z. S., 2013. Paleomagnetic and fission-track dating of a Late Cenozoic red earth section in the Liupan Shan and associated tectonic implications. *Journal of Earth Science* 24, 506-518.
- Li, Z. C., Li, W. H., Li, Y. X., Li, Y. H., Han, W., 2016. Cenozoic stratigraphy and paleoenvironments in the Weihe area, Shaanxi Province. *Journal of Stratigraphy* 40 (2), 168-179.
- Lin, A. M., Hu, J. M., Gong, W. B., 2015a. Active normal faulting and the seismogenic fault of the 1739 M8.0 Pingluo earthquake in the intracontinental Yinchuan Graben, China. *Journal of Asian Earth Sciences* 114, 155-173.
- Lin, A. M., Rao, G., Yan, B., 2015b. Flexural fold structures and active faults in the northern–western Weihe Graben, central China. *Journal of Asian Earth Sciences* 114, 226-241.

- Lin, X. B., Chen, H. L., Wyrwoll, K. H., Cheng, X. G., 2010. Commencing uplift of the Liupan Shan since 9.5 Ma: Evidences from the Sikouzi section at its east side. *Journal of Asian Earth Sciences* 37, 350-360.
- Liu, B. J., Feng, S. Y., Ji, J. F., Wang, S. J., Zhang, J. S., Yuan, H. K., Yang, G. J., 2017. Lithospheric structure and faulting characteristics of the Helan Mountains and Yinchuan Basin: Results of deep seismic reflection profiling. *Science China (Earth Sciences)* 60 (3), 589-601.
- Liu, H. J., Xue, X. X., 2004. Discussion on the Cenozoic and its chronology in the Weihe River Basin. *Journal of Earth Sciences and Environment* 26 (4), 1-5.
- Liu, J. H., Zhang, P. Z., Lease, R. O., Zheng, D. W., Wan, J. L., Wang, W. T., Zhang, H. P., 2013. Eocene onset and late Miocene acceleration of Cenozoic intra-continental extension in the North Qinling range–Weihe graben: Insights from apatite fission track thermochronology. *Tectonophysics* 584, 281-296.
- Liu, J. H., Zhang, P. Z., Zheng, D. W., Wang, W. T., Wan, J., 2010. Pattern and timing of late Cenozoic rapid exhumation and uplift of the Helan Mountain, China. *Science China Earth Sciences* 53, 345-355.
- Liu, J., Chen, X.Q., Chi, Z.Q., Wang, Y., Min, L.R., Li, T.D., 2018. Tectonically-controlled Evolution of the Late Cenozoic Nihewan Basin, North China Craton: Constraints from Stratigraphy, Mineralogy, and Geochemistry. *Acta Geologica Sinica (English Edition)* 92, 769-785.
- Liu, M., Cui, X. J., Liu, F. T., 2004. Cenozoic rifting and volcanism in eastern China: A mantle dynamic link to the Indo–Asian collision. *Tectonophysics* 393, 29-42
- Liu, R., Ma, J. Q., Li, Q. C., Ye, P. S., 2016. Gravity, magnetic and electric comprehensive geophysical prospecting for deep structures in Hetao basin, *Journal of Geomechanics* 22 (4), 943-954.
- Liu, X. B., Hu, J. M., Shi, W., Chen, H., Yan, J. Y., 2019a. Paleogene–Neogene sedimentary and tectonic evolution of the Yinchuan Basin, western North China Craton. *International Geology Review*. DOI: 10.1080/00206814.2019.1591309.
- Liu, X. B., Shi, W., Hu, J. M., Fu, J. L., Yan, J. Y., Sun, L. L., 2019b. Paleogene–Neogene sedimentary and tectonic evolution of the Yinchuan Basin, western North China Craton. *Journal of Asian Earth Sciences* 173, 61-69.
- Long, J. Y., He, Z. T., Zhang, H., Ma, B. Q., 2017. Characteristics of structural geomorphology and segmentation of Sertenshan piedmont fault from Dahoudian to Wayaotan. *Geoscience* 31(1), 71-80.
- Ma, B. Q., Li, K., Wu, W. M., 2000. Segmentation of the Daqingshan piedmont fault. *Bulletin of*

- the Institute of Crustal Dynamics 13, 53-60.
- Menzies, M., Xu, Y.G., Zhang, H.F., et al., 2007. Integration of geology, geophysics and geochemistry: A key to understanding the North China Craton. *Lithos* 96, 1–21.
- Mercier, J. L., Carey, E., Sebrier, M., Stein, S., 1991. Palaeostress determinations from fault kinematics: Application to the neotectonics of the Himalayas-Tibet and the Central Andes. *Philosophical Transactions of the Royal Society London* 337, 41-52.
- Mercier, J. L., Vergely, P., Zhang, Y. Q., Hou, M. J., Bellier, O., Wang, Y. M., 2013. Structural records of the Late Cretaceous-Cenozoic extension in Eastern China and the kinematics of the Southern Tan-Lu and Qinling Fault Zone (Anhui and Shanxi Provinces, PR China). *Tectonophysics* 582, 50-75.
- Molnar, P., Tapponnier, P., 1975. Cenozoic Tectonics of Asia: Effects of a Continental Collision: Features of recent continental tectonics in Asia can be interpreted as results of the India-Eurasia collision. *Science* 189, 419-426.
- Northrup, C. J., Royden, L. H., Burchfiel, B. C., 1995. Motion of the Pacific plate relative to Eurasia and its potential relation to Cenozoic extension along the eastern margin of Eurasia. *Geology* 23 (8), 719-722.
- Rao, G., Chen, P., Hu, J. M., Yu, Y. L., Qiu, J. H., 2016. Timing of Holocene paleo-earthquakes along the Langshan Piedmont Fault in the western Hetao Graben, North China: Implications for seismic risk. *Tectonophysics* 677-678, 115-124.
- Rao, G., Lin, A., Yan, B., Jia, D., Wu, X., 2014. Tectonic activity and structural features of intracontinental active normal faults in the Weihe Graben, central China. *Tectonophysics* 636, 270-285.
- Ratschbacher, L., Hacker, B. R., Calvert, A., Webb, L. E., Grimmera, J. C., McWilliamse, M. O., Irelandf, T., Dong, S. W., Hu, J. M., 2003. Tectonics of the Qinling (Central China): Tectonostratigraphy, geochronology and deformation history. *Tectonophysics* 366, 1-53.
- Ren, J. Y., Tamaki, K., Li, S. T., Zhang, J. X., 2002. Late Mesozoic and Cenozoic rifting and its dynamic setting in Eastern China and adjacent areas. *Tectonophysics* 344, 175-205.
- Ren, J., Peng, J. B., Wang, F. Y., Liu, C., Feng, X. J., Dai, W. Q., 2012. The research of deep structural features of Weihe basin and adjacent areas. *Chinese J. Geophys.* 55 (9), 2939-2947.
- Riedel, W., 1929. Zur mechanik geologischer brucherscheinungen: ein Beitrag zum problem der "Fiederspa lten": Centralblatt fu r Mineralogie, Geologie, und Paleontologie, Part B, 354-368.
- Ritz, J. F., Taboada, A., 1993. Revolution stress ellipsoids in brittle tectonics resulting from an uncritical use of inverse methods. *Bull. Soc. Géol. Fr.* 164, 519-531.
- Schellart, W. P., Lister, G. S., 2005. The role of the East Asian active margin in widespread

- extensional and strike-slip deformation in East Asia. *Journal of the Geological Society, London* 162, 959-972.
- Shen, X. H., Tian, Q. J., Ding, G. Y., Wei, K. B., Chen, Z. W., 2001. The late Cenozoic stratigraphic sequence and its implication to tectonic evolution, Hejiakouzi area, Ningxia Hui Autonomous Region. *Earthquake Research in China* 17, 156-166.
- Shi, W., Cen, M., Chen, L., Wang, Y. C., Chen, X. Q., Li, J. Y., Chen, P., 2015a. Evolution of the late Cenozoic tectonic stress regime in the Shanxi Rift, central North China Craton inferred from new fault kinematic analysis. *Journal of Asian Earth Sciences* 114, 54-72.
- Shi, W., Chen, L., Chen, X. Q., Cen, M., Zhang, Y., 2019a. The Cenozoic tectonic evolution of the faulted basins in the northern margin of the Eastern Qinling Mountains, Central China: Constraints from fault kinematic analysis. *Journal of Asian Earth Sciences* 173, 204-224.
- Shi, W., Dong, S. W., Liu, Y., Hu, J. M., Chen, X. H., Chen, P., 2015b. Cenozoic tectonic evolution of the South Ningxia region, northeastern Tibetan Plateau inferred from new structural investigations and fault kinematic analyses. *Tectonophysics* 649, 139-164.
- Shi, W., Hu, J. M., Chen, P., Chen, H., Wang, Y. C., Qin, X., Zhang, Y., Yang, Y., 2019b. Yumen conglomerate ages in the South Ningxia Basin, north-eastern Tibetan Plateau, as constrained by cosmogenic dating. *Geological Journal*. <https://doi.org/10.1002/gj.3510>.
- Shi, W., Liu, Y., Chen, P., Chen, L., Cen, M., Huang, X. F., Li, H. Q., 2013. Cenozoic evolution of the Haiyuan fault zone in the northeast margin of the Tibetan Plateau. *Earth Science Frontiers* 20, 1-17.
- Shi, W., Zhang, Y. Q., Dong, S. W., Hu, J. M., Wiesinger, M., Ratschbacher, L., Jonckheere, R., Li, J. H., Tian, M., Chen, H., Wu, G. L., Qu, H. J., Ma, L. C., Li, H. L., 2012. Intra-continental Dabashan orocline, southwestern Qinling, Central China. *Journal of Asian Earth Sciences* 46, 20-38.
- Shi, W., Zhang, Y. Q., Ma, Y. S., Liu, G., Wu, L., 2006. Formation and modification history of the Liupanshan basin on the southwestern margin of Ordos block and tectonic stress field evolution. *Geology in China* 33, 1066-1074.
- Sun, P. L., Zeng, F. G., Liu, C., Zhu, Y. R., 2017. Cenozoic uplift history of the Xishan coalfield and constraints from apatite fission track dating. *Acta Geologica Sinica* 91(1), 43-54.
- Tang, Y. C., Feng, Y. G., Chen, Y. S., Zhou, S. Y., Ning, J. Y., Wei, S. Q., Li, P., Yu, C. Q., Fan, W. Y., Wang, H. Y., 2010. Receiver function analysis at Shanxi Rift. *Chinese Journal of Geophysics* 53 (9), 2102-2109.
- Tang, Y.C., Feng, Y.G., Chen, Y.S., Zhou, S.Y., Ning, J.Y., Wei, S.Q., Li, P., Yu, C.Q., Fan, W.Y., Wang, H.Y., 2010. Receiver function analysis at Shanxi Rift. *Chin. J. Geophys.* 53 (9), 2102–2109.

- Tapponnier, P., Xu, Z. Q., Françoise, R., Meyer, B., Nicolas, A., Gérard, W., Yang, J. S., 2001. Oblique stepwise rise and growth of the Tibetan Plateau. *Science* 294, 1671-1677.
- The Research Group on Active Fault System around Ordos Massif, State Seismological Bureau (RGAFSO), 1988. Active Fault System around Ordos Massif. Seismological Press, Beijing, pp. 1-335.
- Tong, H. M., Yin, A., 2011. Reactivation tendency analysis: A theory for predicting the temporal evolution of pre-existing weakness under uniform stress state. *Tectonophysics* 503, 195-200.
- Wallace, R. E., 1951. Geometry of shearing stress and relation of faulting. *Journal of Structural Geology* 59, 118-130.
- Wang, B., Zheng, H. B., He, Z., Wang, P., 2014. Study on the Bahe Formation in the Weihe Basin based on Magnetostratigraphy. *Geological Journal of China Universities* 20 (3), 415-424.
- Wang, E., Kirby, E., Furlong, K. P., 2012. Two-phase growth of high topography in eastern Tibetan during the Cenozoic. *Nat. Geosci.* 5, 640-645.
- Wang, H. F., Yang, X. C., Zhu, B. Q., Fan, S. K., Dai, T. M., 1988. K-Ar geochronology and evolution of Cenozoic volcanic rocks in Eastern China. *Geochimica* 1, 1-12.
- Wang, L. M., Dong, R. S., Zhang, Y. M., Wang, X. N., Guo, W. X., 1984. Cenozoic structures and Earthquakes in the Hetao area: Implications for the formation of the Cenozoic rifted basins around the Ordos block. *North China Earthquake Sciences* 2 (4), 8-16.
- Wang, P., Huang, Z. C., Mi, N., Xu, M., Wang, L., Li, H., 2014. Crustal structure beneath the Weihe Graben in central China: Evidence for the tectonic regime transformation in the Cenozoic. *Journal of Asian Earth Sciences* 81, 105-114.
- Wang, Q., Li, C. G., Tian, G. Q., Zhang, W. Z., Liu, C., Ning, L. Y., Cheng, Z. G., He, C. Y., Yue, J., 2002. Tremendous change of the earth surface system and tectonic setting of salt-lake formation in Yuncheng Basin since 7.1 Ma. *Sci. China (Ser. D: Earth Sci.)* 45 (2), 111-122.
- Wang, Q., Zhang, P. Z., Freymueller, J., Bilham, R., Larson, K. M., Lai, X. A., You, X. Z., Niu, Z. J., Wu, J. C., Li, Y. X., Liu, J. N., Yang, Z. Q., Chen, Q. Z., 2001. Present-day crustal deformation of China constrained by global positioning system measurements. *Science* 294, 574-577.
- Wang, W. T., Kirby, E., Zhang, P. Z., Zheng, D. W., Zhang, G. L., Zhang, H. P., Zheng, W. J., Chai, C. Z., 2013. Tertiary basin evolution along the northeastern margin of the Tibetan Plateau: Evidence for basin formation during Oligocene transtension. *Geological Society of America* 125, 377-400.
- Wang, W. T., Zhang, P. Z., Kirby, E., 2011. A revised chronology for Tertiary sedimentation in the Sikouzi basin: Implications for the tectonic evolution of the northeastern corner of the

- Tibetan Plateau. *Tectonophysics* 505, 100-114.
- Xie, F. R., Cui, X. F., Zhao, J. T., Chen, J. C., Li, H., 2004. Regional division of the recent tectonic stress field in China and adjacent areas. *Chin. J. Geophys.* 47, 654-662.
- Xie, G. H., Wang, J. W., Tatsumoto, M., Basu, A. R. 1989. Petrochemistry and isotope geochemistry of Hannuoba basalts and Datong volcanos. *Geochimica* 4, 277-286.
- Xing, Z. Y., Zhao, B., Tu, M. Y., Xing, J. S., 2005. The formation of the Fenwei rift valley. *Earth Science Frontiers* 12 (2), 247-262.
- Xu, J. Y., Ben-Avraham, Z., Kelty, T., Yu, H. S., 2013. Origin of marginal basins of the NW Pacific and their plate tectonic reconstructions. *Earth Science Reviews*. doi: 10.1016/j.earscirev.2013.10.002.
- Xu, Q. Q., Ji, J. Q., Zhao, W. T., Yu, X. J., 2017. Uplift-exhumation history of Daqing Mountain, Inner Mongolia since Late Mesozoic. *Acta Scientiarum Naturalium Universitatis Pekinensis* 53, 57-65.
- Xu, T., Yang, J. X., Liu, Y., Shi, W., Wei, W., 2013. The sedimentary characteristics in the Late Pleistocene in southern Ningxia and its tectonic significance. *Earth Science Frontiers* 20, 36-45.
- Xu, X. W., Ma, X. Y., 1992. Geodynamics of the Shanxi Rift system, China. *Tectonophysics* 208, 325-340.
- Xu, X. W., Ma, X. Y., Deng, Q. D., 1993. Neotectonic activity along the Shanxi Rift system, China. *Tectonophysics* 219, 305-325.
- Xue, H. Y., Yan, J. Q., 1983. The contemporary crustal stress field around the Ordos Block. *Acta Geophysica Sinica* 27 (2), 144-152.
- Ye, H., Zhang, B., Mao, B. F., 1987. The Cenozoic tectonic evolution of the Great North China: Two types of rifting and crustal necking in the Great North China and their tectonic implications. In: Froidevaux, C., Tan T. J. (Eds.), *Deep Internal Processes and Continental Rifting*. *Tectonophysics* 133, 217-227.
- Yin, A., 2010. Cenozoic tectonic evolution of Asia: A preliminary synthesis. *Tectonophysics* 488, 293-325.
- Yin, G., Lu, Y. C., Zhao, H., Li, W. L., Li, L., Guo, S. L., 2001. The tectonic uplift of the Hua Shan in the Cenozoic. *Chinese Science Bulletin* 46 (19), 1665-1668.
- Yue, L. P., Deng, T., Zhang, Y. X., Wang, J. Q., Zhang, R., Yang, L. R., Heller, F., 2004. Magneto stratigraphy of strato-type section of the Baode stage. *J. Stratigr.* 1, 51-63.
- Zhang, A.L., Yang, Z.T., Zhong, J., Mi, F.S., 1995. Characteristics of late Quaternary activity along the southern border fault zone of Weihe graben basin. *Quat. Int.* 25, 25-31.
- Zhang, J., Cunningham, D., Cheng, H. Y., 2010. Sedimentary characteristics of Cenozoic strata

- in central-southern Ningxia, NW China: Implications for the evolution of the NE Qinghai-Tibetan Plateau. *Journal of Asian Earth Sciences* 39, 740-759.
- Zhang, P. Z., Burchfiel, B. C., Molnar, P., Zhang, W. Q., Jiao, D. C., Deng, Q. D., Wang, Y. P., Royden, L., Song, F. M., 1990. Later Cenozoic tectonic evolution of the Ningxia-Hui Autonomous Region, China. *Geological Society of America Bulletin* 102, 1484-1498.
- Zhang, P. Z., Burchfiel, B. C., Molnar, P., Zhang, W. Q., Jiao, D. C., Deng, Q. D., Wang, Y. P., Royden, L., Song, F. M., 1991. Amount and style of late Cenozoic deformation in the Liupan Shan area, Ningxia Autonomous Region, China. *Tectonics* 10, 1111-1129.
- Zhang, X. J., 1983. The stratigraphical sequence of Linhe region in Neimeng Autonomous Region: Cenozoic strata. *Petroleum Exploration and Development* 4, 1-8.
- Zhang, Y. Q., Liao, C. Z., Shi, W., Hu, B., 2006. Neotectonic evolution of the peripheral zones of the Ordos basin and geodynamic setting. *Geological Journal of China Universities* 12, 285-297.
- Zhang, Y. Q., Ma, Y. S., Yang, N., Shi, W., Dong, S. W., 2003. Cenozoic extensional stress evolution in North China. *Journal of Geodynamics* 36, 591-613.
- Zhang, Y. Q., Mercier, J. L., Vergdly, P., 1998. Extension in the graben systems around the Ordos (China), and its contribution to the extrusion tectonics of south China with respect to Gobi-Mongolia. *Tectonophysics* 285, 41-75.
- Zhang, Y. Q., Teng, J. W., Wang, Q. S., Zhang, Z. J., Gao, R., 2013. Hetao Basin and its adjacent region of crustal structure and deep dynamical process. *Earth Physics Progress* 28 (5), 2264-2272.
- Zhao, H. G., Liu, C. Y., Wang, F., 2007. Uplift and evolution of Helan Mountain. *Science China (Ser. D)* 50 (Suppl. 2), 217-226.
- Zhao, J. F., Liu, C. Y., Wang, X. M., Ma, Y. P., Huang, L., 2009. Uplifting and evolution characteristics in the Lüliang Mountain and its adjacent area during the Meso-Cenozoic. *Geological Review* 55 (5), 673-683.
- Zhao, W., Hou, G., Hari, K. R., 2016. Two episodes of structural fractures and their stress field modeling in the Ordos Block, northern China. *Journal of Geodynamics* 97, 7-21.
- Zhao, X. C., Liu, C. Y., Zhao, Y., Deng, H., Zhang, Q. H., 2016. Response of the Ningnan area to the Eocene peripheral rifting breakup event of the Ordos Basin. *Geological Science and Technology Information* 35 (6), 24-37.
- Zheng, D. W., Zhang, P. Z., Wan, J. L., Yuan, D. Y., Li, C. Y., Yin, G. M., Zhang, G. L., Wang, Z. C., Min, W., Chen, J., 2006. Rapid exhumation at ~8 Ma on the Liupan Shan thrust fault from apatite fission-track thermochronology: Implications for growth of the northeastern Tibetan Plateau margin. *Earth and Planetary Science Letters* 248, 198-208.

- Zheng, W. J., Zhang, P. Z., He, W. G., Yuan, D. Y., Shao, Y. X., Zhen, D. W., Ge, W. P., Min, W., 2013. Transformation of displacement between strike-slip and crustal shortening in the northern margin of the Tibetan Plateau: Evidence from decadal GPS measurements and late Quaternary slip rates on faults. *Tectonophysics* 584, 267-280.
- Zhu, D. G., Meng, X. G., Shao, Z. G., Lei, W. Z., Wang, J. P., Han, J. E., Yu, J., Lv, R. P., 2008. Ages of Neogene starta in the Baode-Jingle area, Shanxi, China. *Geological Bulletin of China* 27 (4), 510-516.
- Zhu, W. Y., Wang, X. Y., Chen, Z. Y., Xiong, Y. Q., Zhang, Q., Ye, S. H., Ma, Z. J., Chen, J. Y., Xu, H. Z., Wei, Z. Q., Lai, X. A., Liu, J. N., Jin, B. R., Ren, J. W., Wang, Q., 2000. Crustal motion of Chinese mainland monitored by GPS. *Sci. China D* 43, 394-400.

Figure Caption

Fig. 1. Geological outline map of the Eastern Asia continent (A), and simplified structural and geomorphic map of the Ordos Block in the central Eastern Asia continent shown by Digital elevation model (DEM) (B). DEM data originated from <https://earthexplorer.usgs.gov/>

Fig. 2. Cenozoic structures and stratal distribution of the Ordos Block and its periphery (resulted from 1:200000 Ningxia, Neimenggu, Shanxi, Hebei, Shaanxi regional investigation). SNB: South Ningxia Basin; YCB: Yinchuan Basin; JLTB: Jilantai Basin; HTB: Hetao Basin; WHB: Weihe Basin; DTB: Datong Basin; XDB: Xinzhou-Dingxiang Basin; TYB: Taiyuan Basin; LFB: Linfen Basin; YCB: Yuncheng Basin. F₁₋₁: Liupanshan Fault; F₁₋₂: Haiyuan Fault; F₁₋₃: Xiangshan-Tianjingshan Fault; F₁₋₄: Yantongshan Fault; F₁₋₅: Niushoushan-Luoshan Fault; F₂₋₁: Yellow River Fault (Yinchuan Basin); F₂₋₂: Yinchuan-Pingluo Fault; F₂₋₃: Luhutai Fault; F₂₋₄: Helanshan Eastern Piedmont Fault; F₂₋₅: Helanshan Western Piedmont Fault; F₃₋₁: Langshan Fault; F₃₋₂: Seertengshan Fault; F₃₋₃: Yellow River Fault (Hetao Basin); F₃₋₄: Wulashan Fault; F₃₋₅: Daqingshan Fault; F₃₋₆: Helingeer Fault; F₄₋₁: Yanggao-Tianzheng Fault; F₄₋₂: Kouquanshan Fault; F₄₋₃: Liulengshan Fault; F₄₋₄: Yuxian Fault; F₄₋₅: Hengshan Fault; F₄₋₆: Wutaishan Fault; F₄₋₇: Xizhoushan Fault; F₄₋₈: Jiaocheng Fault; F₄₋₉: Taigu Fault; F₄₋₁₀: Huoshan Fault; F₄₋₁₁: Yunzhongshan Fault; F₅₋₁: Qinling Piedmont Fault; F₅₋₂: Weihe Fault; F₅₋₃: Kouzhen Fault; F₅₋₄: Huashan Piedmont Fault; F₅₋₅: Zhongtiaoshan South Piedmont Fault; F₅₋₆: Zhongtiaoshan North Piedmont Fault; F₅₋₇: Hancheng Fault.

Fig. 3. Cenozoic stratal sequences correlation of the Cenozoic basins around the Ordos Block.

Fig. 4. The geological map of the Liupanshan region in the southwest margin of the Ordos Block and field view of the Cenozoic deformation. (A) The three sets of faults at the Loc. B15 and NE-SW compressive stress field. (B) Reverse strike-slip faults affecting red clay bed and fault striation data. (C) Thrusting of Late Cretaceous conglomerate over the Cenozoic sandstone and mudstone. Stereonet projection is lower-hemisphere, equal-angle (Wulff) in A and B.

Fig. 5. The geological map of the South Ningxia Basin and structural section (S₂). (A) - (F) Fault kinematic features in the Haiyuan Fault. (A) Syn-depositional structures in the Late Oligocene–Early Miocene mudstone (Qingshuiying Fm.) dominated by

NW-SE extension. (B) Syn-sedimentary normal faults in the Middle Miocene mudstone of the Zhangenpu Fm., east segment of the Haiyuan Fault (H118), indicating a NW-SE extension. (C) Showing southwestward thrusting of Silurian phyllite onto Miocene-Pliocene red conglomerate along the west segment of the major Haiyuan Fault at Loc. H146. (D) Exhibiting nearly E-W striking folds covered by Early Pleistocene conglomerate in the interior of the Laolongwan Basin. A hammer (35 cm long) or a person (170 cm high) for scale. See the sites in the geological map. Fig. 5 is modified from Shi et al. (2015).

Fig. 5. Continued. (E) Two sets of faults in gypsum-bearing sandstone (Qingshuiying Fm.) at Loc. H39, associated with early NW-SE extension and later NW-SE compression, respectively. (F) Outcrop showing nearly horizontal fault striations in fault gouge in the interior of the main Haiyuan Fault (Loc. H144), suggesting an ENE–WSW compression. (G) Outcrop-scale fold related to faulting suggesting NE–SW shortening. (H) Two-generation faults in the Qingshuiying Formation mudstone, early strike-slip activation and late normal faulting. (I) Cross section showing a northeastward shortening along the detachment layer in the underlying mudstone of the Qingshuiying Fm. prior to the Late Pleistocene. The fault-slip vectors determine three stages of stress kinematic regimes deformation, NW-SE extension and NE-SW compression. (J) Upright NW-striking fault typical of dextrally strike-slip activation. (J₁) expressing two sets of gypsum veins growing in the red, medium-thinly-bedded mudstone (Qingshuiying Fm.) east of Tongxin, including nearly vertical syntaxially veins and horizontal shearing veins, which indicates early NW-SE extension (J₂) and young NE-SW compression (J₃, J₄), respectively, based on their intersection relationship. (K) An upright, nearly N-S-striking fault cutting the Ganhegou Fm. deposits in the west of the Yantongshan Fault (Loc. E05) showing a right-lateral strike-slip activation due to NE-SW shortening. (L) Outcrop displaying the two groups of faults in the red, bearing-gypsum mudstone (Zhangenpu Fm.) west of the Niushoushan Mt. (H219), normal faults and strike-slip faults, suggesting early NW-SE extension and early ~E-W compression, respectively, as inferred from the cross-cutting relationships of fault planes.

Fig. 6. Cenozoic structural features of the Yinchuan Basin and structural cross section (COC, 1983; Li et al., 2005). (A) Fault scarps along Helanshan Eastern Piedmont Fault and two-stage deformation (old NW-SE compression and young

NE-SW extension) observed by two sets of striation from the fault scarps. (B) Syn-depositional normal faults in the Late Oligocene–Early Miocene mudstone (Qingshuiying Fm.) controlled by NW-SE extension near to the east of the Yellow River Fault (Loc. Y01) and NE-SW extension after NW-SW extension, based on the fault kinematic analysis. (C) Two sets of faults grow in the red sandstone (Qingshuiying Fm.) near the Yellow River Fault (Loc. W04) indicating NW-SE extension and NE-SW compression. (D) The normal faults in the conglomerate-bearing sandstone of the Zhangenpu Fm. (N_{1z}) and the Ganhegou Fm. (N_{1-2g}) in the interior of the south Yinchuan Basin linking with NW-SE extension. (E) Normal faults and strike-slip faults present within the Miocene mudstone (N_{1z}) at Loc. E348 south margin of the Yinchuan Basin, which are in accordance with old NW-SE extension and young NW-SE compression, respectively in terms of the interrelationships of the fault planes.

Fig. 7. Simple geological map of the Jilantai and Hetao Basins and Cenozoic deformation. (A) The Oligocene–Early Miocene mudstone (Qingshuiying Fm.) in the middle segment of the Liulengshan Fault (Loc. LS11) contain two groups of normal faults, related to early NW-SE extension and later NE-SW compression and NW–SE extension in terms of the fault-slip vectors, respectively. (B) Faults in the Oligocene–Miocene mudstone near the Yellow River Fault (Loc. WH14) are linked with early NW-SE extension and late transtension (NE-SW compression and NW-SE extension). (C) – (F) Cenozoic activation of the Seertengshan Fault. (C) Outcrop showing two groups of normal faults, one group of faults (F_1) cutting the Proterozoic gneiss, indicating NW-SE extension prior to Early Pleistocene, the other group of faults (F_2) cutting the Early Pleistocene conglomerate showing early NE-SW extension and later ~N-S extension. (D) Two sets of normal faults in the Miocene mudstone are presented by early NW-SE extension and later NE-SE extension, respectively (Loc. SE14). (E) Normal faults in the Late Pleistocene lacustrine sediments with the OSL age of 79.1 ka exhibit early NE-SW and later NNE-SSW extension (Loc. SE10). (F) Two groups of normal faults in the Late Pleistocene lacustrine sediments show early NE-SW and later NNE-SSW extension (Loc. SE11). (G) – (H) The Wulashan Fault characteristic of fault scarps cutting Proterozoic gneiss correlating with earliest NW-SE extension, and fault scarps cutting Early Pleistocene conglomerate linking with early NE-SW and late NNE-SSW extension (Loc. D17). (I) – (J) Fault scarps marking the Daqingshan

Fault. The Loc. D19 showing a nearly N-S extension on the fault (I), and the Loc. D20 indicating early NW-SE extension and later N-S extension here (J). (K) Fault in the Late Pleistocene loess suggesting nearly N-S extension. Structural section S₄ and S₅ after COC (1983), and S₄ after Li et al. (2005).

Fig. 7. Continued.

Fig. 8. Sketch geological map of the Shanxi Basin, structural section and Cenozoic deformation. (A) – (C) Deformation of the Liulengshan Fault (F₄₋₃), featured by fault scarps (A), Quaternary basalt erupted along the fault (B), and early NW-SE extension and late NE-SW extension controlling here (Loc. D10). (C) The Liulengshan Fault characteristic of 10–18-m-high fault scarp composed of Jurassic granite, recording ~N-S extension (Loc. D30). (D) The Kouquanshan Fault presented by fault 10–20-m-high scarp (Loc. D45), two sets of striations showing the evolution of the fault, early NW-SE extension and later NNW-SSE extension (E). Structural section S₇ modified from (GSBSX, 2002).

Fig. 9. Simplified geological map of the Linfen Basin, structural section and structural investigation. Luoyunshan fault characteristic of fault scarps (A), and pure dip-slip and oblique-slip faulting, associated with NW–SE and NNW–SSE extension, respectively at Loc. HS86 (B). (C) An E-W trending normal fault to the south of the Linfen Basin, documenting NE-SW extension (Loc. HS90). S₈ after Xu et al. (1993).

Fig. 10. Sketch geological map of the Weihe Basin and structural features. (A) NE-striking syn-depositional faults in the Honghe Fm. (E₂) suggesting NW-SE extension in the Eocene. (B) An E-W-striking fault in the interior of the Weihe Basin, linking with NE-SW extension (Rao et al., 2014), and here ¹⁴C (1) age from Rao et al. (2014) and ¹⁴C (2) from Li et al. (2015). (C) NW-striking normal faults in the Q₂ interbedded sandstone and gravel in the interior of the Weihe Basin (HS29), presented as NE-SW extensional activation. (D) The Qinling Piedmont Fault characteristic of the two-stage extension, including early NW-SE extension and later NE-SW extension as indicated by fault kinematic analysis at HS25. (E) The Huashan Piedmont Fault featured by nearly N-S extensional movement at HS31. (F) The Kouzhen Fault affecting the deposit of loess, presented by early NW-SE and late nearly N-S extension (Lin et al., 2015a). (G) The Hancheng Fault marked by NW-SE striking extension prior to the Late Pleistocene and NNW–SSE directed extension in the Holocene (Loc. SX4). (H) The North Zhongtiaoshan Fault presented by a group of high-angle normal faults cross-cutting late Pleistocene loess and gravel-bearing sandy clay, related with NNW-SSE extension at Loc. H97. (I) The

North Zhongtiaoshan Fault in the Miocene-Pliocene red clay undergoing two-episode extensional activity, i.e., early NE-SW and later NNW-SSE extension at Loc. H92.

Fig. 10. Continued.

Fig. 11. The Late Pleistocene–Holocene transtensional stress field with ENE–WSW compression and NNW–SSE extension around the Ordos Block, derived from analysis of fault-slip data. (A) Stereonet projection of the mean azimuths of maximum and minimum stress axes (σ_1 , σ_2 , and σ_3 , respectively), indicating a transtensional stress regime with an NNW–SSE extension and ENE–WSW compressional shortening field in the southwest of the Ordos Block. (B) Stereonet projection of the mean azimuths of maximum and minimum stress axes (σ_1 , σ_2 , and σ_3 , respectively), showing a NNW–SSE extensional stress field in the faulted basins around the Ordos Block. (C) Stereonet projection of the mean azimuths of maximum and minimum stress axes (σ_1 , σ_2 , and σ_3 , respectively) exhibiting a transtensional stress regime with a NNW–SSE extension and ENE–WSW compression in the periphery of the Ordos Block. Stereonet projection is Equal area, lower hemisphere. See Fig. 3 for legend.

Fig. 12. The Late Pleistocene NE–SW extensional stress field around the Ordos Block, based on fault kinematic analysis. Same legend as Fig. 3.

Fig. 13. The Late Miocene–Early Pleistocene transtensional stress field featured by NE–SW compression and NW–SE extension around the Ordos Block, obtained from calculation of fault-slip data. (A) Mean stereonet projection of three principal stress axes giving a NE–SW compressional stress regime in the southwest of the Ordos Block. (B) Mean stereonet projection of three principal stress axes documenting a NW–SE extensional stress field in the faulted basins around the Ordos Block. (C) Mean stereonet projection of three principal stress axes showing a transtensional stress regime with a NW–SE extension and NE–SW compression in the periphery of the Ordos Block. Equal area, lower hemisphere projection for stereonet. See Fig. 3 for legend.

Fig. 14. The Late Miocene fault-slip data indicating NW–SE compressive event around the Ordos Block, resulted from fault-slip vectors. Same legends as Fig. 3.

Fig. 15. The Oligocene–Middle Miocene NW–SE extension around the Ordos Block, deduced from fault-slip vectors. Same legends as Fig. 3.

Fig. 16. Stress field sequence and deformation stages around the Ordos Block

mainly suggesting a two-phase tectonic evolution history.

Fig. 17. Cenozoic tectonic evolution models around the Ordos Block. A1-The Oligocene–Late Miocene (10.5 Ma) sedimentary basin formation. A2-The Late Miocene (10.5–9.5 Ma) sedimentary basin inversion. B1-The early Late Miocene (9.5 Ma)–Early Pleistocene mountain building. B2-The Late Pleistocene paleo-lake formation. B3-Strike-slip activity on the four major faults since the end of the Late Pleistocene.

Fig. 18. The deformation regime in the periphery of the Ordos Block. (A₁₋₁), (A₁₋₂) The pure shear model of the periphery of the Ordos Block at the early stage; (B₁₋₁), (B₁₋₂) The simple shear model of the periphery of the Ordos Block at the late stage (modified from Riedel (1929) and Davis et al. (1999)).

Fig 1

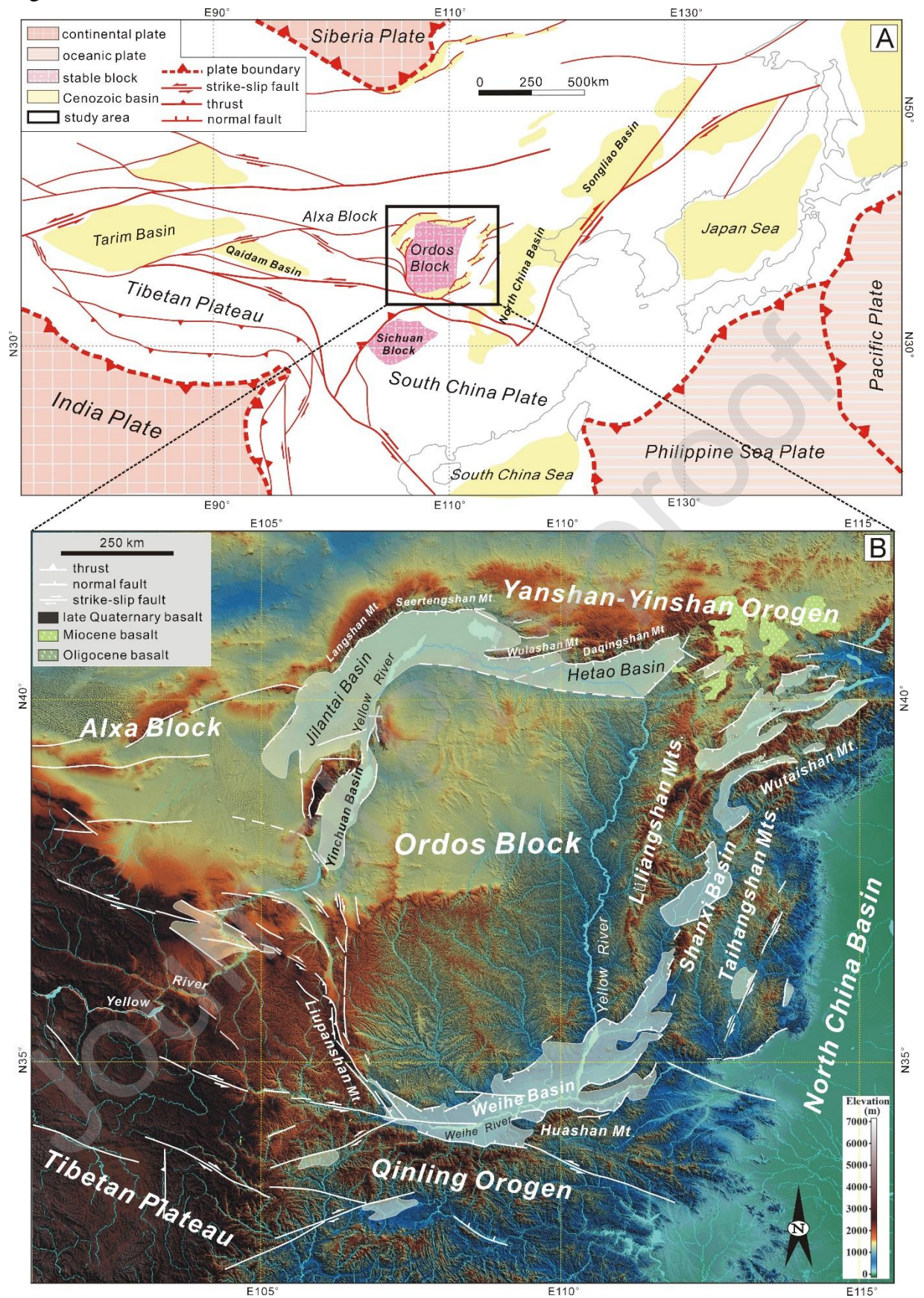


Fig 2

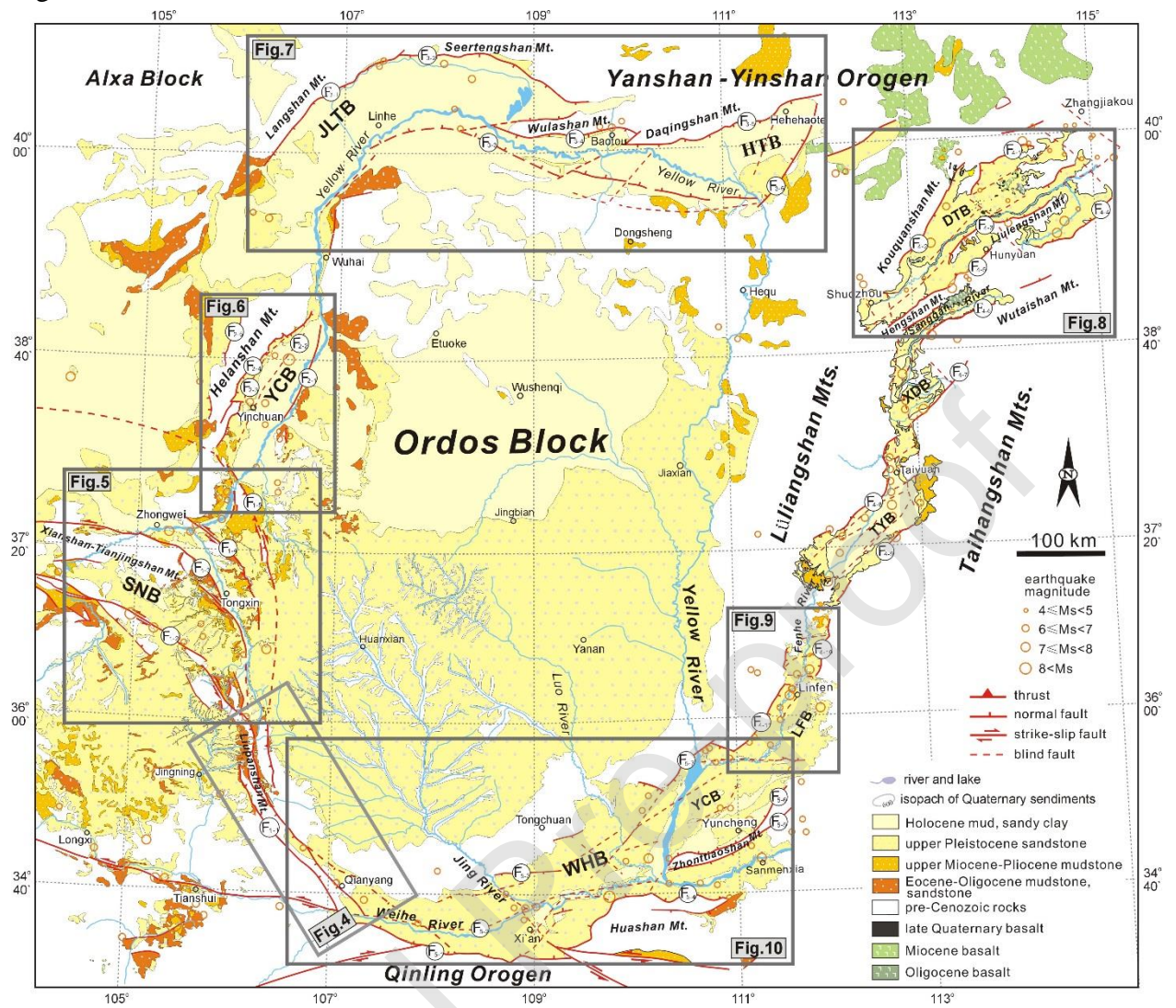
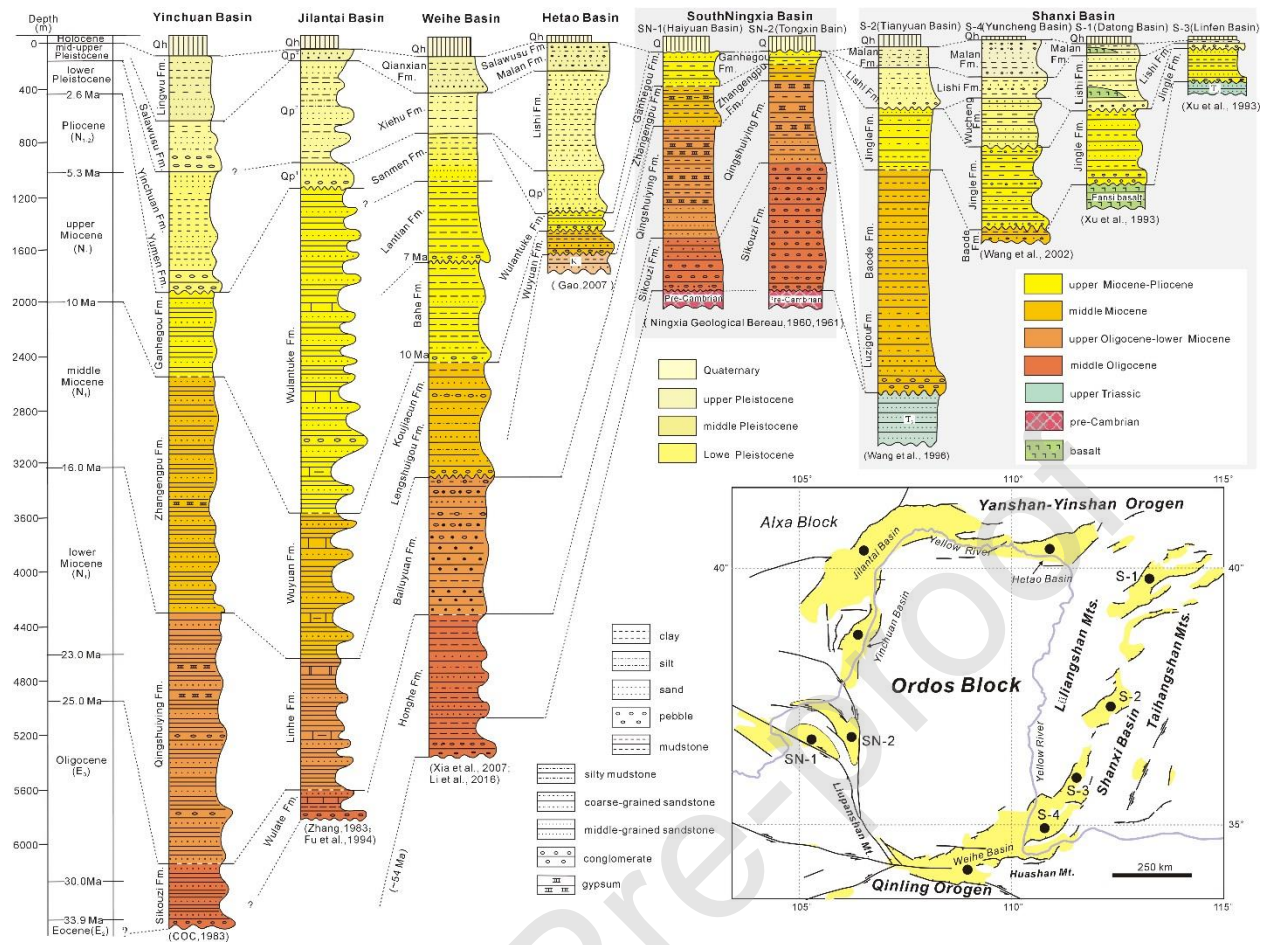


Fig 3



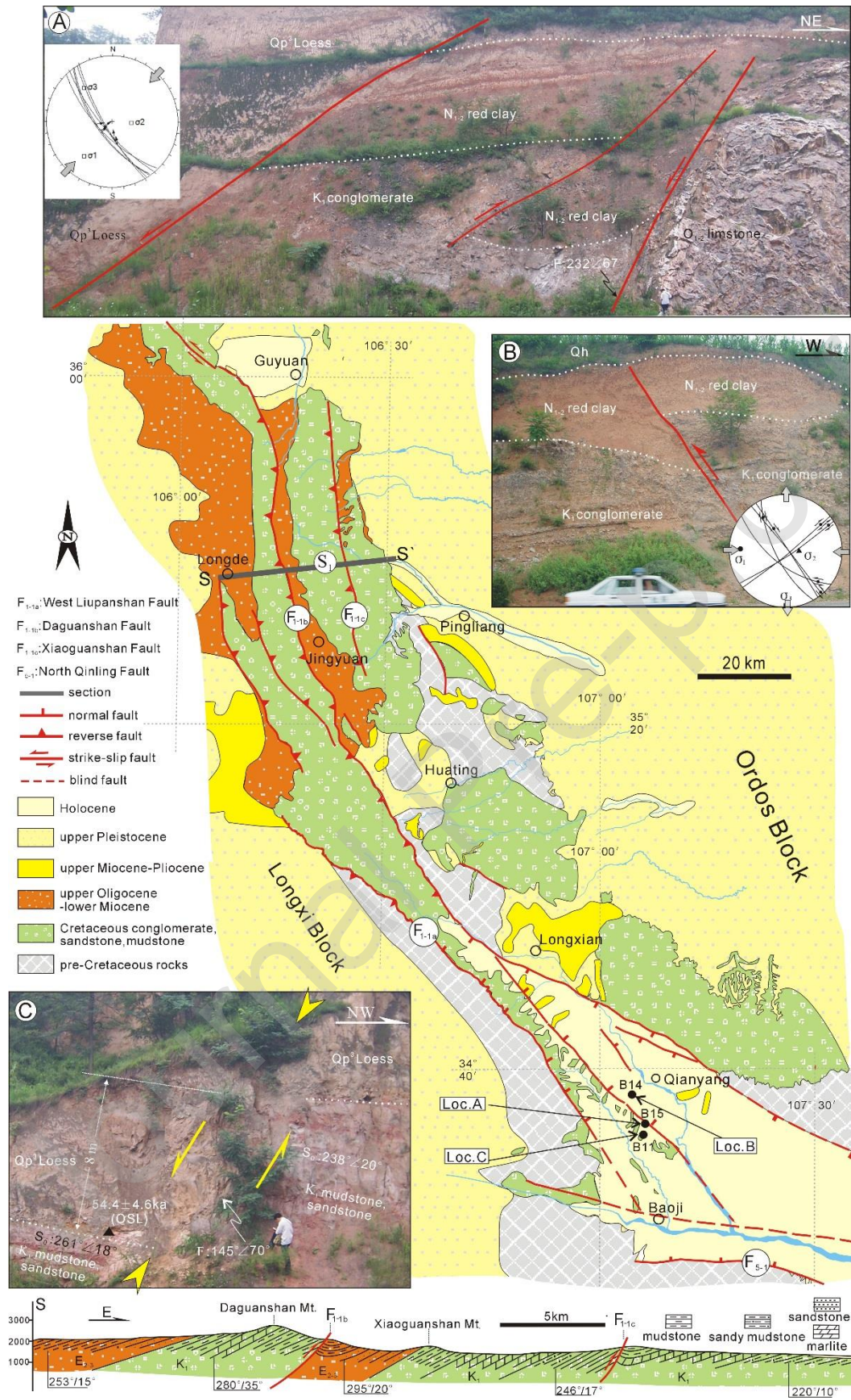


Fig 5

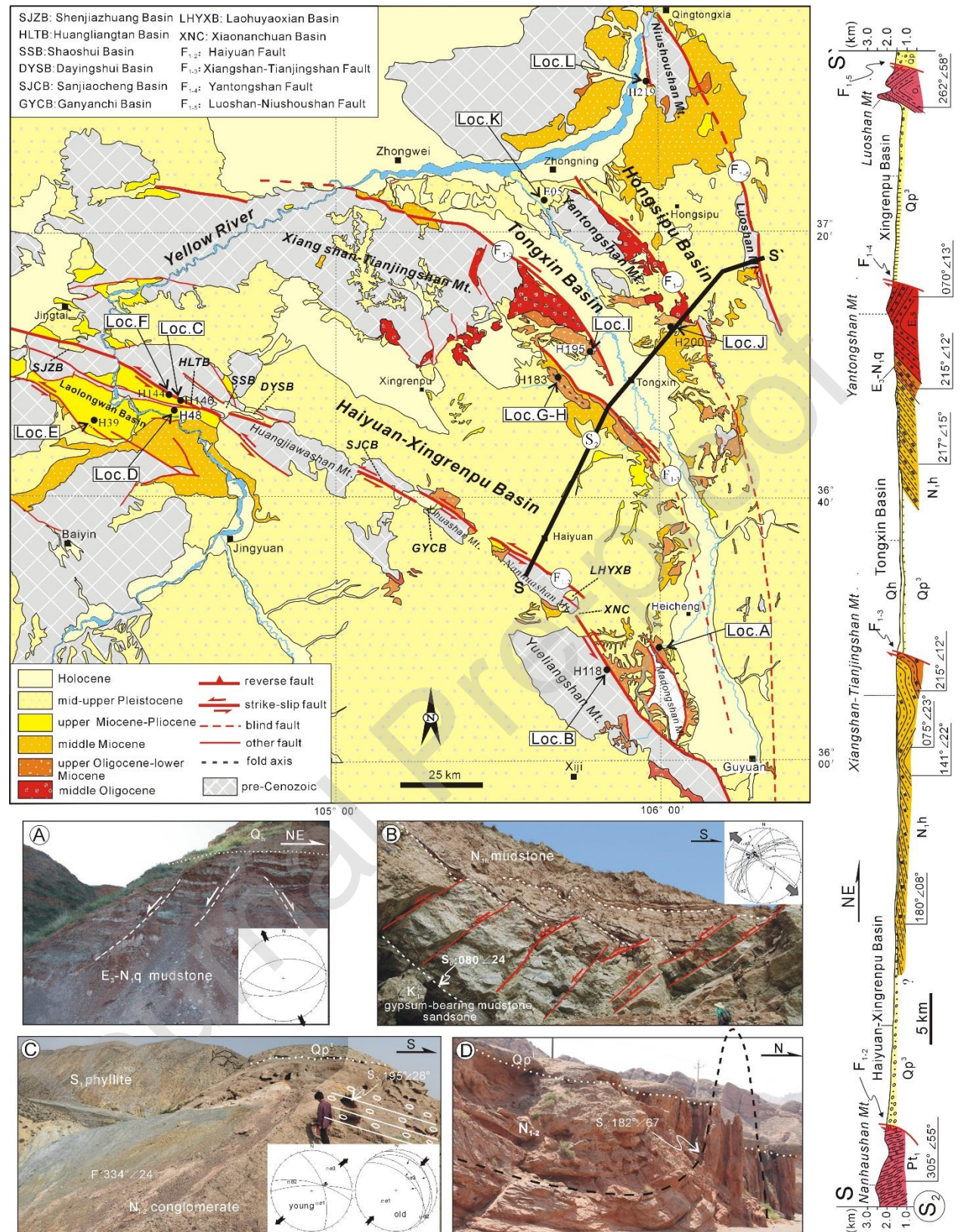


Fig 6

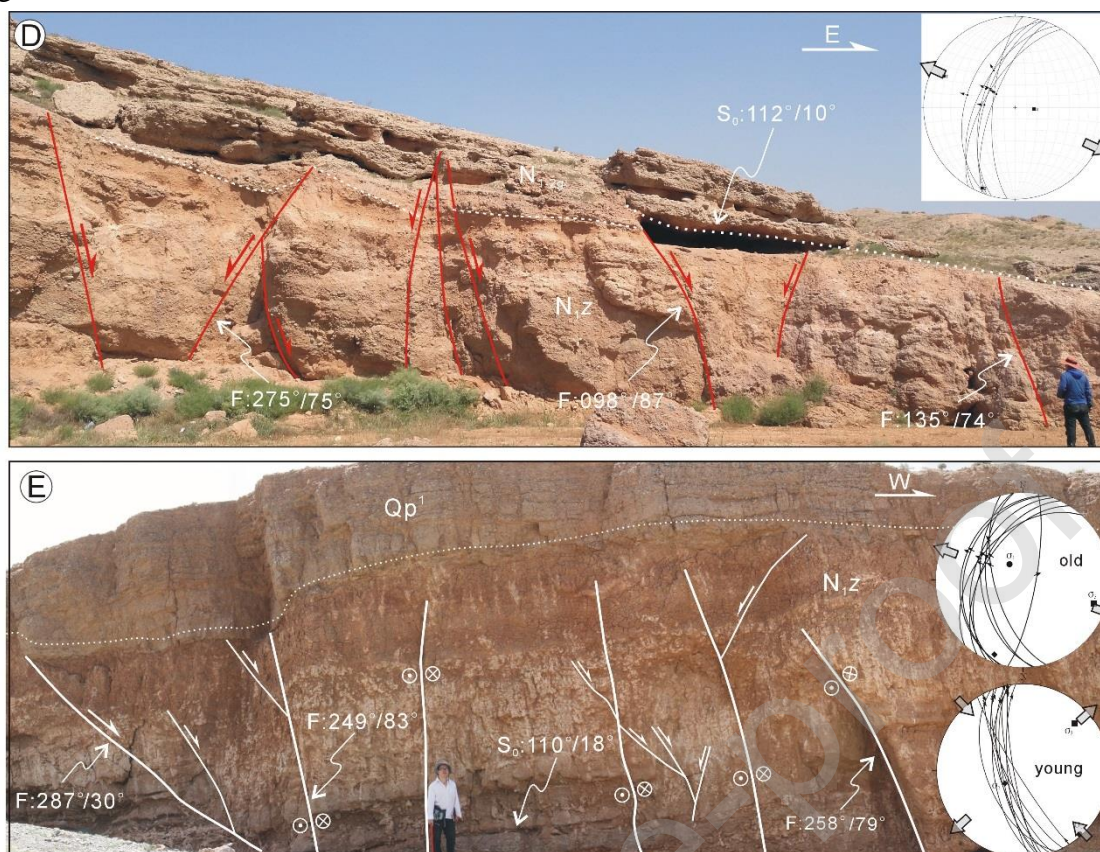


Fig 7

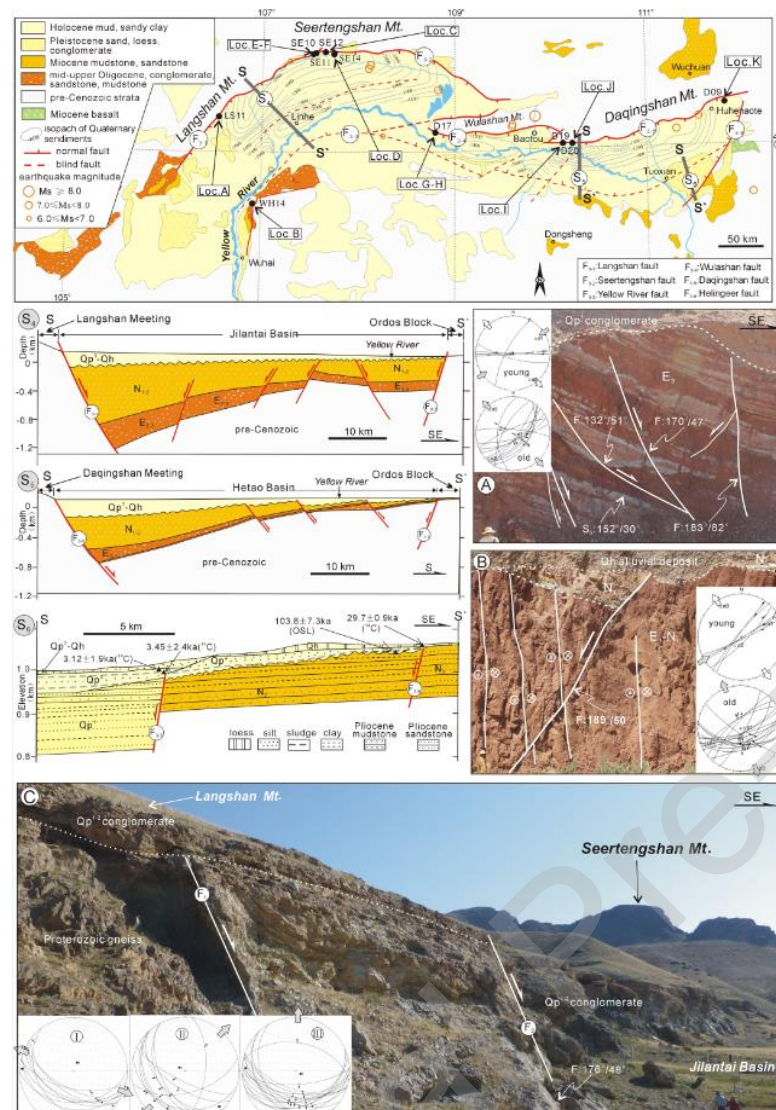


Fig 7

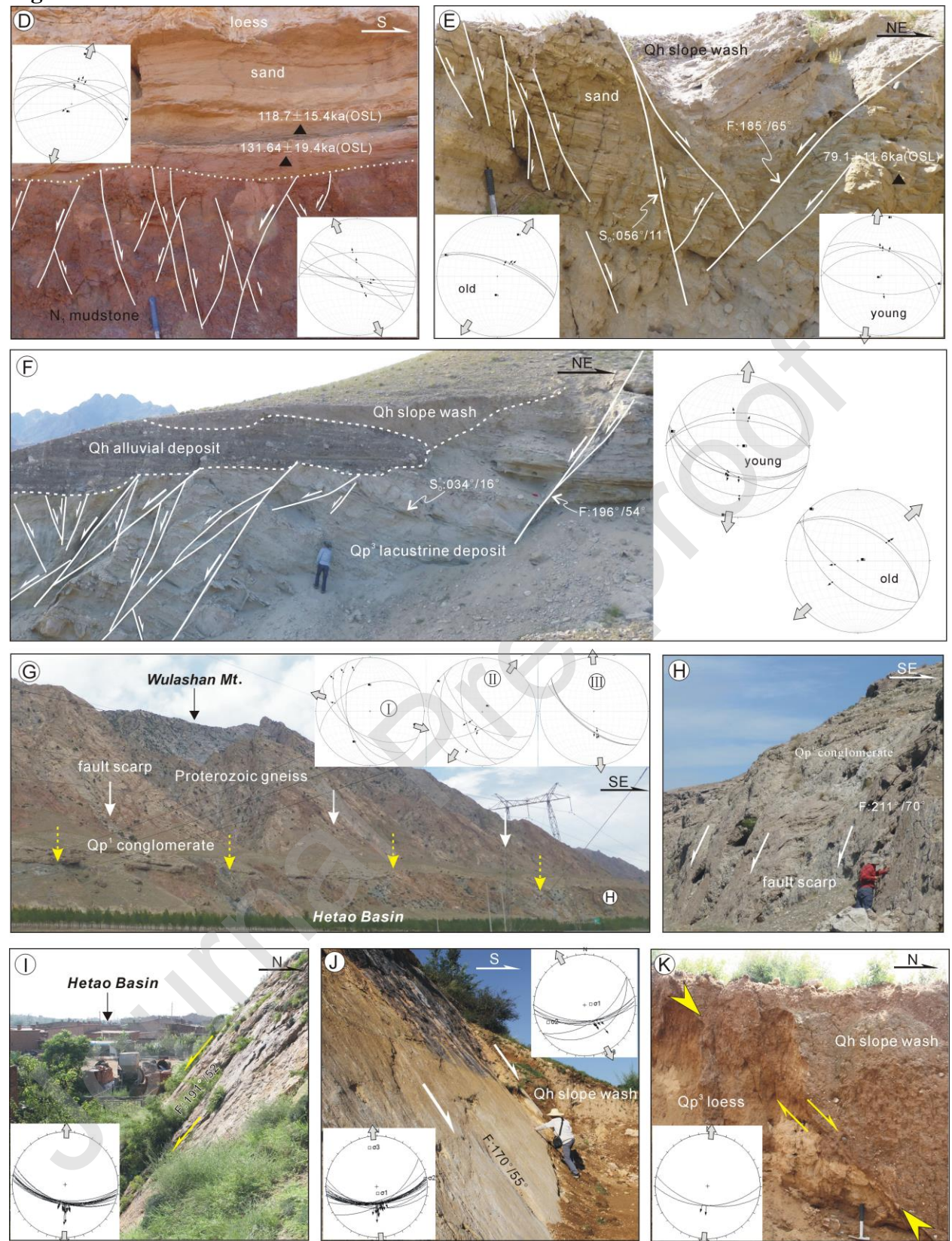


Fig 8

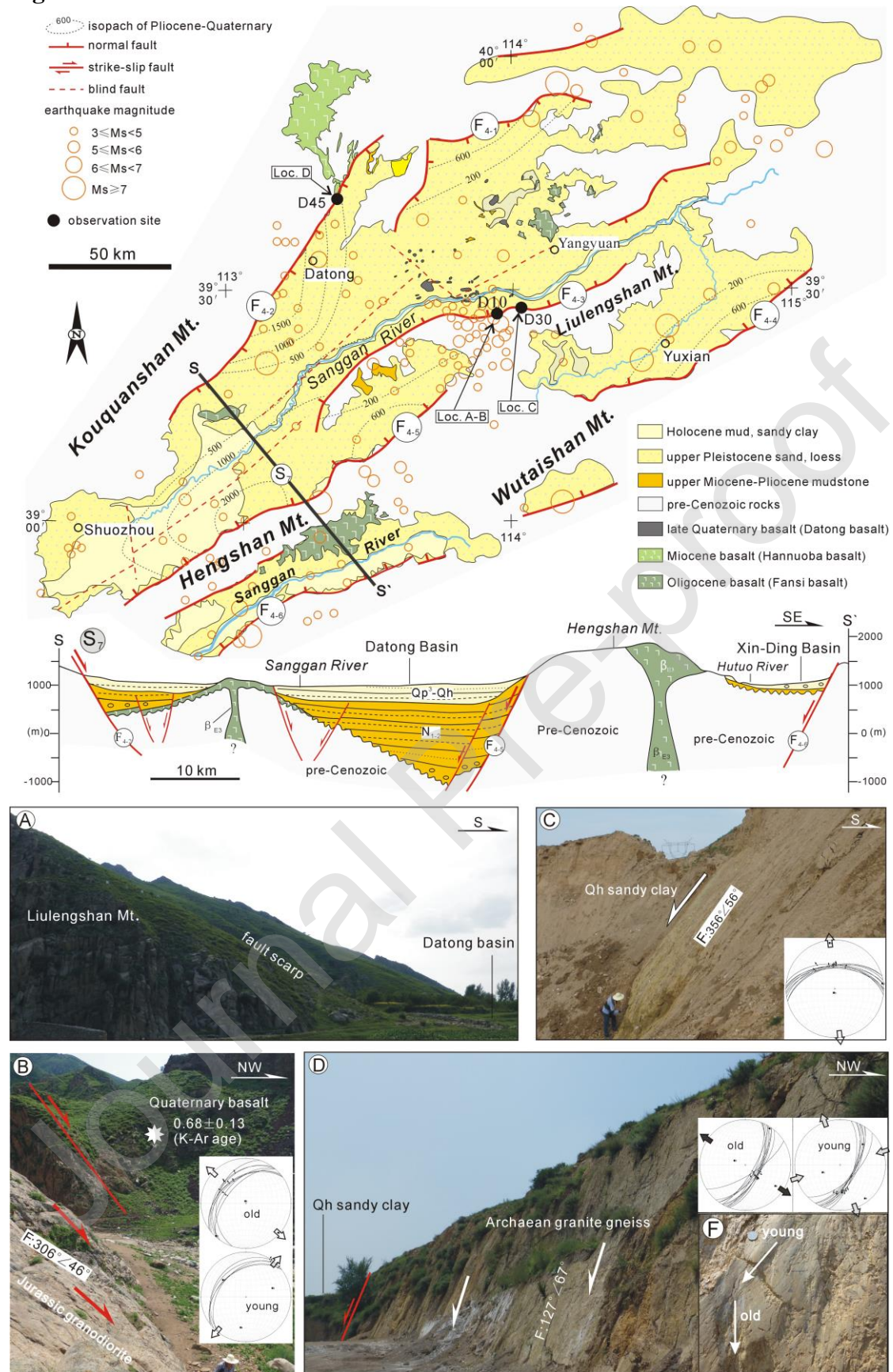


Fig 9

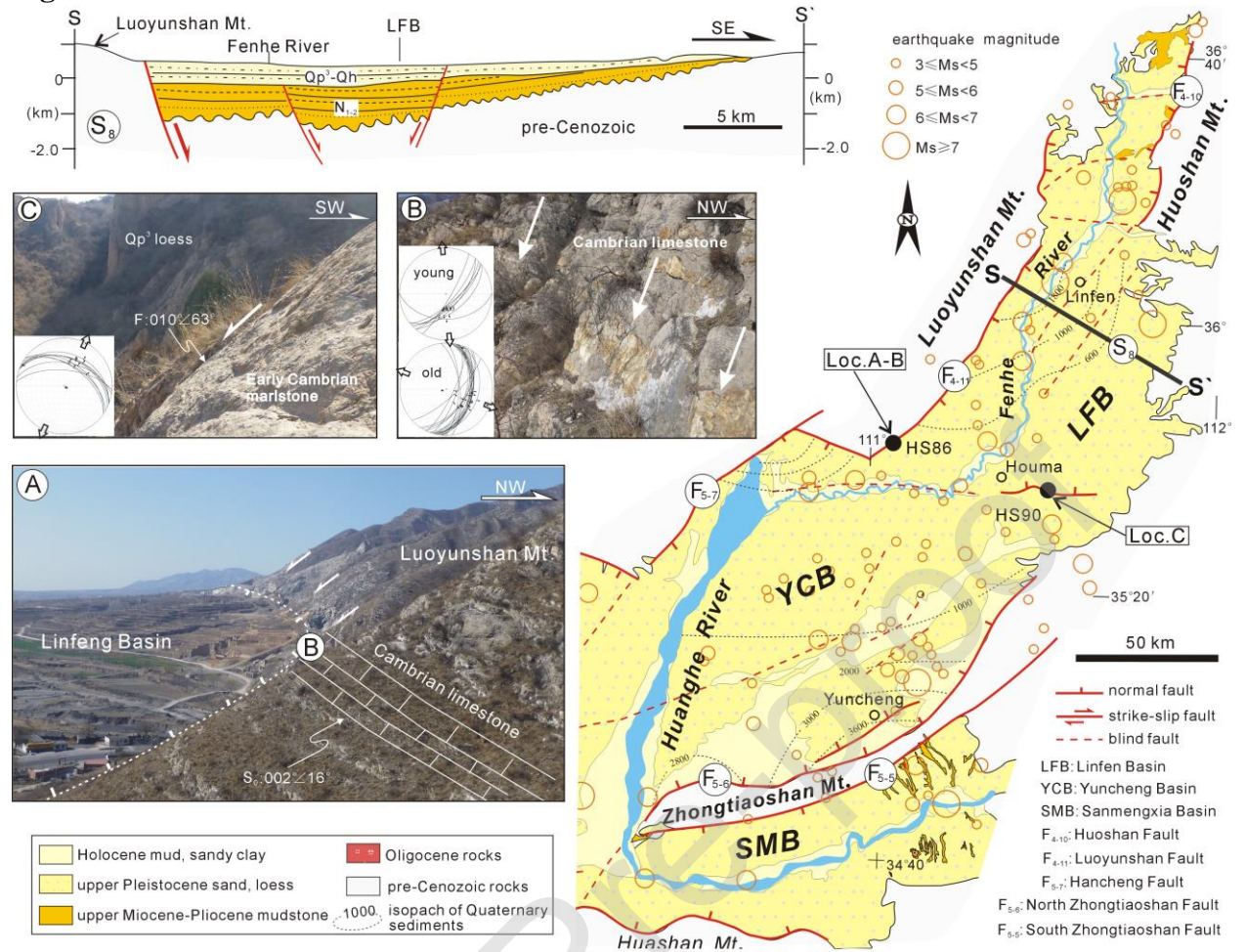


Fig 10

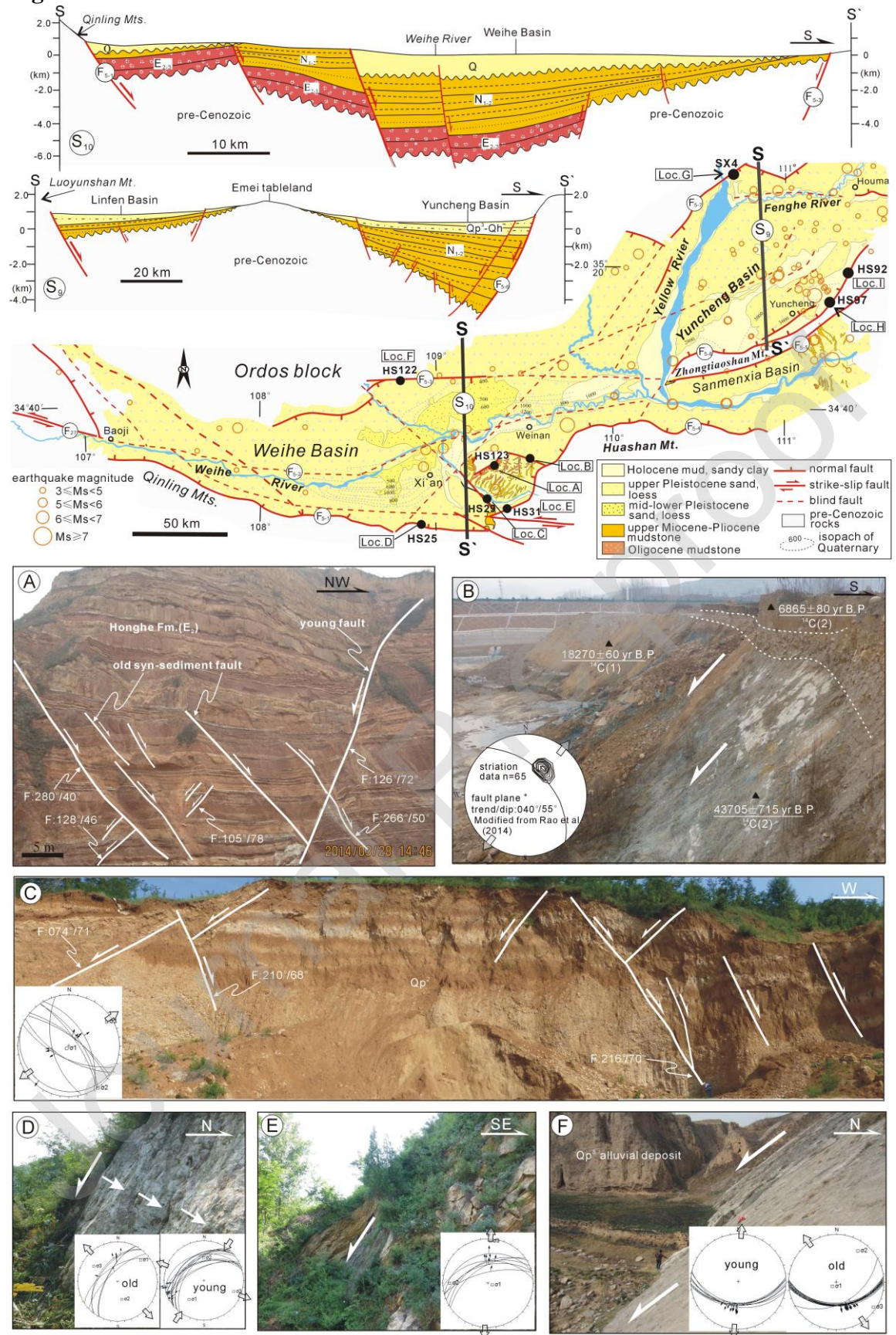
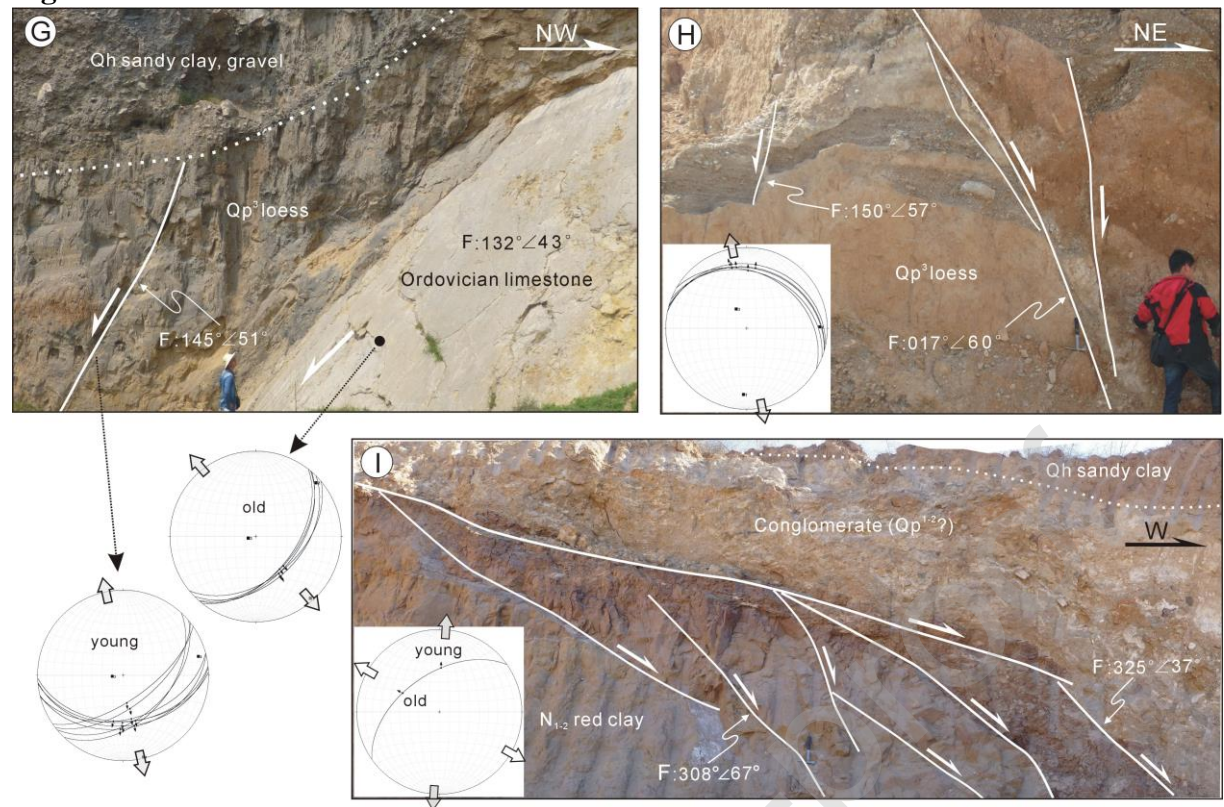


Fig 10



Yanshan - Yinshan Orogen

Ordos Block

Helanshan Mt.

Weihe River

Luliangshan Mts.

Wutaishan Mt.

Yinchuan

Xi'an

Taiyuan

100 km

Legend:

- ▲ maximum stress axes (σ_1)
- intermediate stress axes (σ_2)
- minimum stress axes (σ_3)
- ▲ mean σ_1 at $078^\circ \angle 02^\circ$
- mean σ_2 at $200^\circ \angle 72^\circ$
- mean σ_3 at $172^\circ \angle 14^\circ$

Inset Box A (N=69):

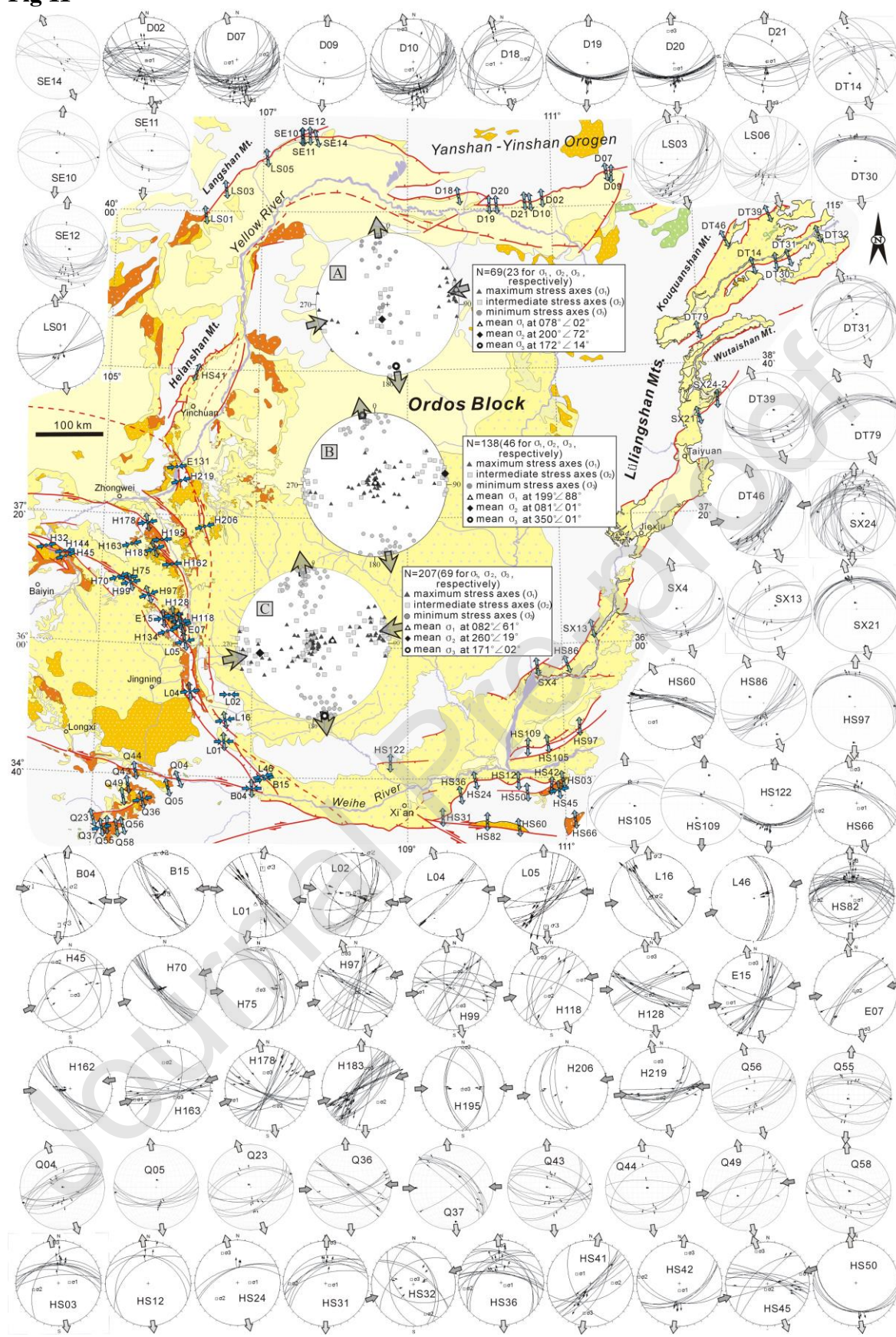
- ▲ maximum stress axes (σ_1)
- intermediate stress axes (σ_2)
- minimum stress axes (σ_3)
- ▲ mean σ_1 at $189^\circ \angle 88^\circ$
- mean σ_2 at $08^\circ \angle 01^\circ$
- mean σ_3 at $350^\circ \angle 01^\circ$

Inset Box B (N=138):

- ▲ maximum stress axes (σ_1)
- intermediate stress axes (σ_2)
- minimum stress axes (σ_3)
- ▲ mean σ_1 at $082^\circ \angle 61^\circ$
- mean σ_2 at $260^\circ \angle 19^\circ$
- mean σ_3 at $171^\circ \angle 02^\circ$

Inset Box C (N=207):

- ▲ maximum stress axes (σ_1)
- intermediate stress axes (σ_2)
- minimum stress axes (σ_3)
- ▲ mean σ_1 at $082^\circ \angle 61^\circ$
- mean σ_2 at $260^\circ \angle 19^\circ$
- mean σ_3 at $171^\circ \angle 02^\circ$



[illegible]

The figure is a detailed geological map of the Yanshan-Yinshan Orogen, showing the distribution of stress axes and principal stress directions. The map includes the following features:

- Geological Features:** Major mountain ranges (Langshan Mt., Seertengshan Mt., Luliangshan Mts., Taihangshan Mts., Huashan Mt.) and rivers (Yellow River, Weihe River) are labeled. The Qinling Orogen is shown to the south.
- Stress Axes Data:** Three data sets are provided:
 - N=75 (25 for σ_1 , σ_2 , σ_3 , respectively):**
 - Maximum stress axes (σ_1) represented by black triangles.
 - Intermediate stress axes (σ_2) represented by grey squares.
 - Minimum stress axes (σ_3) represented by white circles.
 - Mean σ_1 at $044^\circ \angle 04^\circ$.
 - Mean σ_2 at $129^\circ \angle 06^\circ$.
 - Mean σ_3 at $088^\circ \angle 85^\circ$.
 - N=135 (45 for σ_1 , σ_2 , σ_3 , respectively):**
 - Maximum stress axes (σ_1) represented by black triangles.
 - Intermediate stress axes (σ_2) represented by grey squares.
 - Minimum stress axes (σ_3) represented by white circles.
 - Mean σ_1 at $237^\circ \angle 73^\circ$.
 - Mean σ_2 at $033^\circ \angle 01^\circ$.
 - Mean σ_3 at $134^\circ \angle 09^\circ$.
 - N=210 (70 for σ_1 , σ_2 , σ_3 , respectively):**
 - Maximum stress axes (σ_1) represented by black triangles.
 - Intermediate stress axes (σ_2) represented by grey squares.
 - Minimum stress axes (σ_3) represented by white circles.
 - Mean σ_1 at $224^\circ \angle 28^\circ$.
 - Mean σ_2 at $259^\circ \angle 10^\circ$.
 - Mean σ_3 at $134^\circ \angle 18^\circ$.
- Principal Stress Directions:** Numerous circular diagrams (Wulff nets) are shown around the map, each representing the principal stress directions at a specific location. These are labeled with codes such as LS11, D02, D07, D08, D10, D11, D18, D20, SE17, HL75, HL72, HL62, HL55, HL45, HL38, HL32, HL08, HL04, HL03, WH10, WH14, WH08, WH04, WH01, HL55, HL38, HL62, HL45, HL32, HL72, HL89, HL83, DT36, DT34, DT45, DT47, DT10, DT31, DT11, DT17, DT74, SX25, DT10, DT17, DT31, DT32, S4, DT111, DT36, DT34, DT45, DT47, DT74, SX18, SX15, HS87, HS90, HS92, HS101, HS107, Q07, Q09, Q18, Q39, Q47, Q60, Q69, SX18, HS107, J02, B06, G04, LD04, P02, HS25, HS90, HS87, HS92, HS101, H13, H36, H57, H63, H72, H74, H93, H99, SX25, H123, H142, H166, H195, H200, E01, E05, E06.
- Scale and Orientation:** A scale bar indicates 100 km. A north arrow is present. The map includes latitude and longitude coordinates.

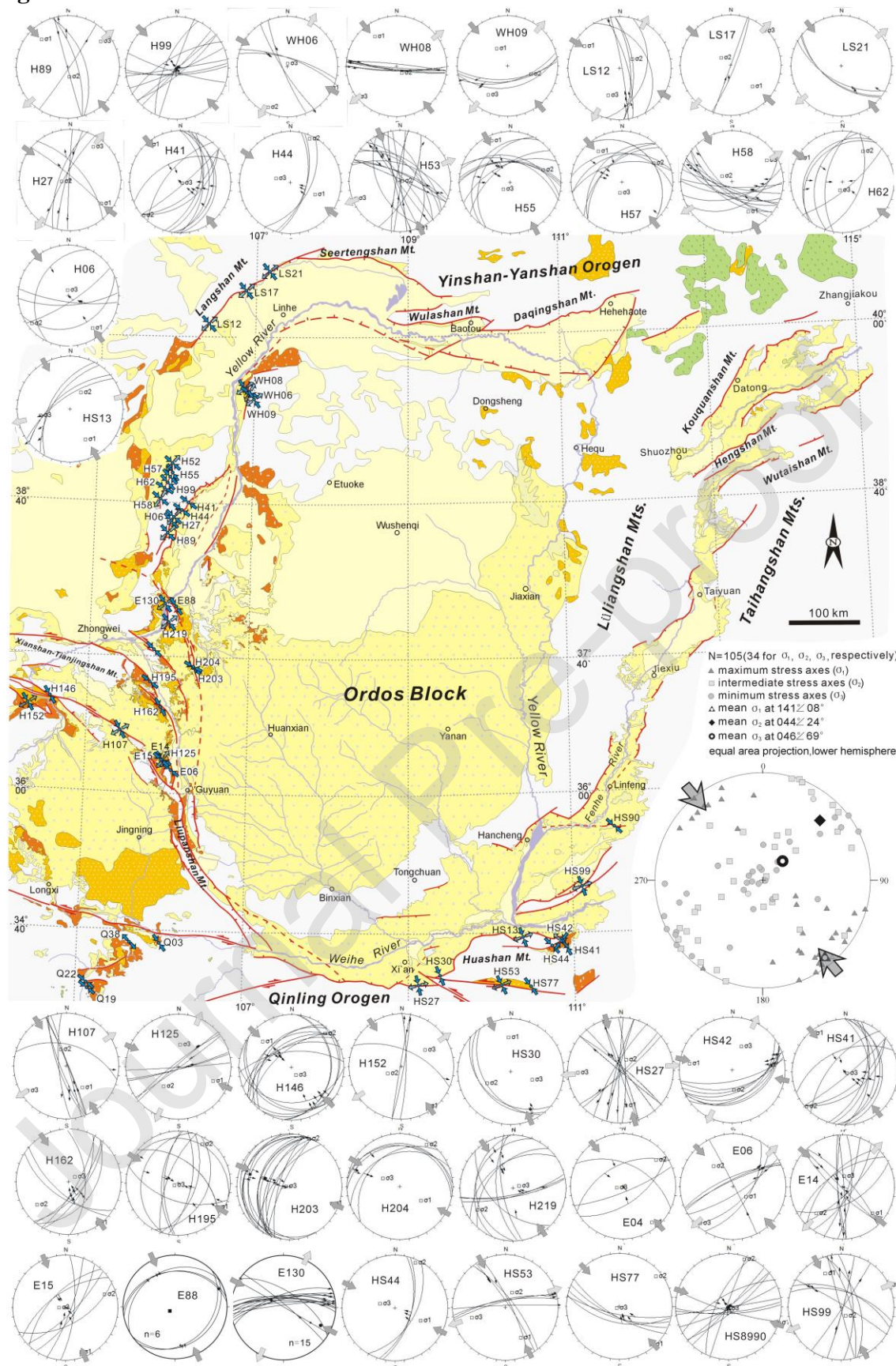
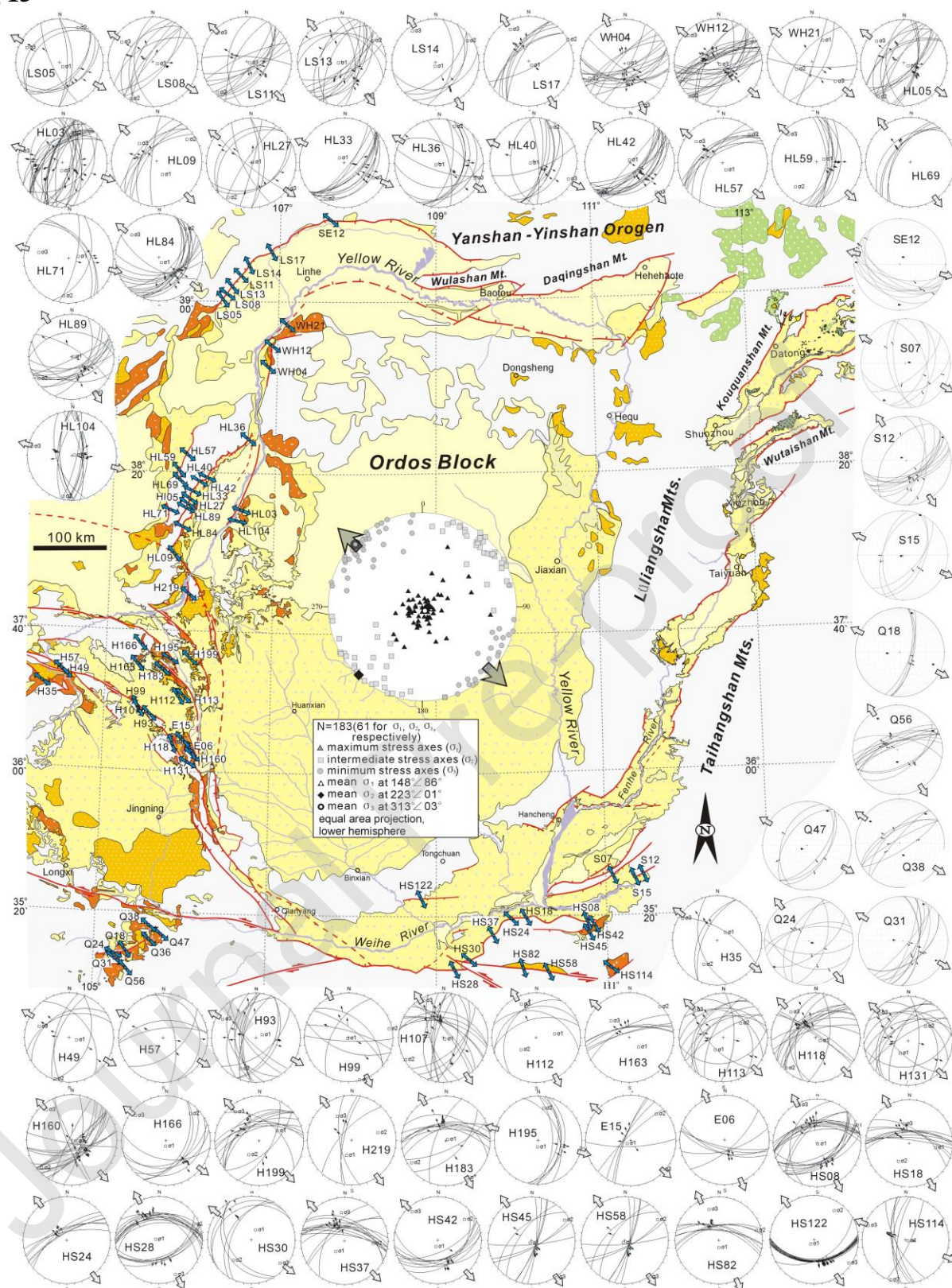




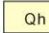
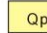



Fig 15





	Stratigraphy lithology	Age(Ma)	tectonic stress field	tectonic evolution stage	tectonic evolution sub-stage	tectonic-sedimentary response	dynamics setting
Quaternary	Qp ¹⁻²	0-0.01		pull-apart basin formation	repull-apart activity of basins (B3)	NNW-SSE dextral shearing and pull-apart basin reconstruction around the Ordos block and intensive strike-slip activity on primary faults in the west of the Ordos block.	predominant far-field effect of northeast-ward growth of the Tibetan Plateau
	Qp ³	0.01-0.78			paleo-lake occurrence in the basins (B2)	NE-SW extension and occurrence of paleo-lakes	
	Qh	0.78-2.58			formation of pull-apart basins (B1)	N-S dextral shearing and pull-apart basins formation in the east and northeast of the Ordos block (Shanxi basin, Hetao basin), and intensive NE-SW shortening and mountain building in the west of the Ordos block.	
Pliocene		2.58-5.33					
		5.33-9.5					
Miocene		9.5-10.5		NE-striking faulted basin formation and inversion	basin inversion (A2)	gentle NW-SE compression and short-term crustal shortening.	main far-field effect of the NW-ward subduction of the Pacific Plate
		10.5-15					
Eocene-Oligocene		15-20			NE-striking faulted basin formation (A1)	NW-SE extension and the formation of NE-striking basins in the northwest and southeast of the Ordos block (e.g. Jilantai basin, Yinchuan basin, Weihe basin), depression basins in the west of the Ordos block.	
		20-23.03					
		23.03-25					
		25-~50					
		~50	?	regional tectonic uplift		?	?


 Qh
Holocene


 Qp³
Upper Pleistocene


 Qp¹⁻²
Lower-Mid Pleistocene


 Late Miocene-Pliocene


 Middle Miocene

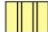
 Upper Oligocene-Lower Miocene


 Middle Oligocene

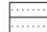
 sedimentary gap

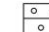
 minimum principle stress direction


 maximum principle stress direction


 Late Pleistocene loess

 mudstone

 sandstone

 conglomerate

 avulsion

 parallel unconformity


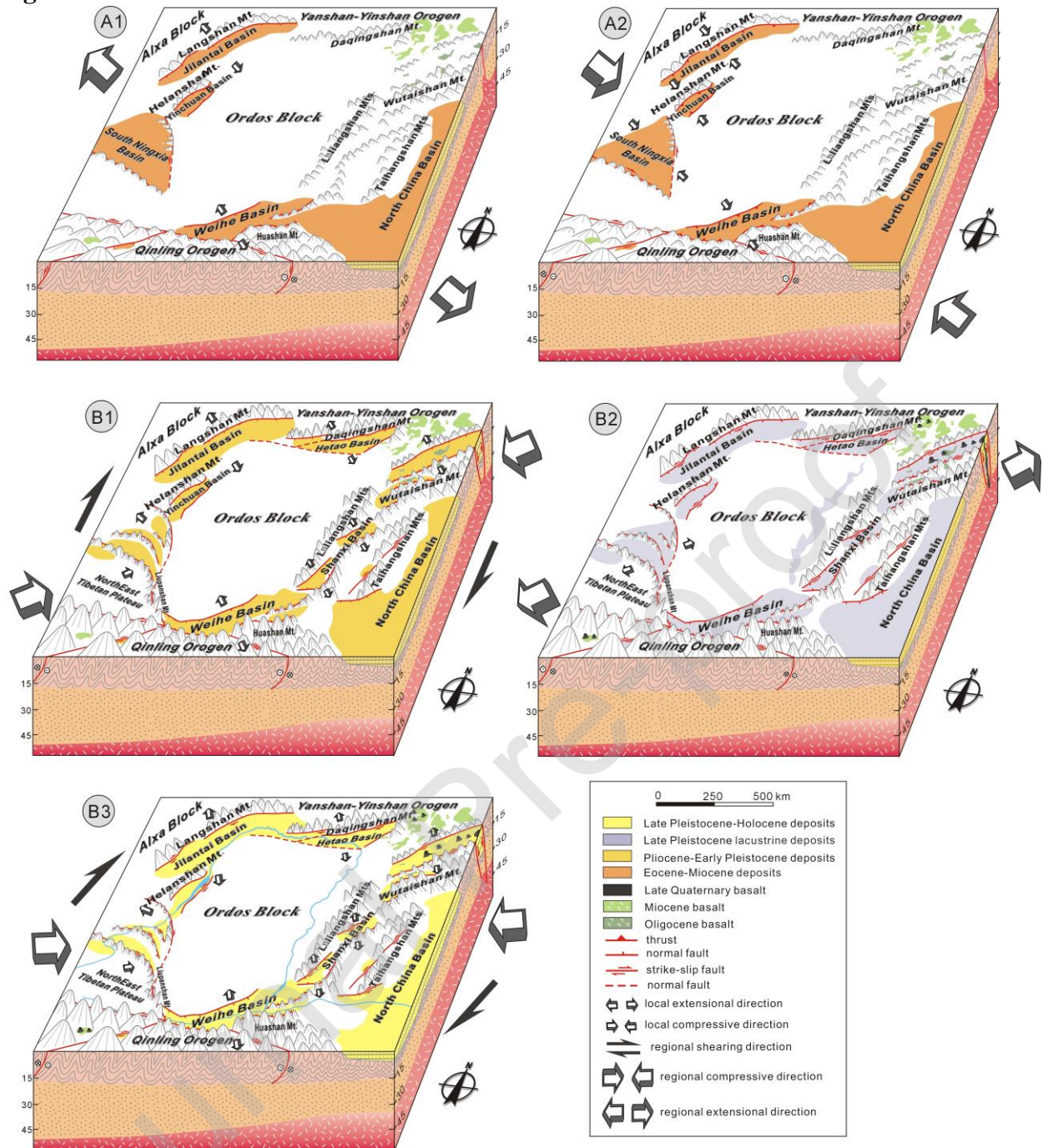
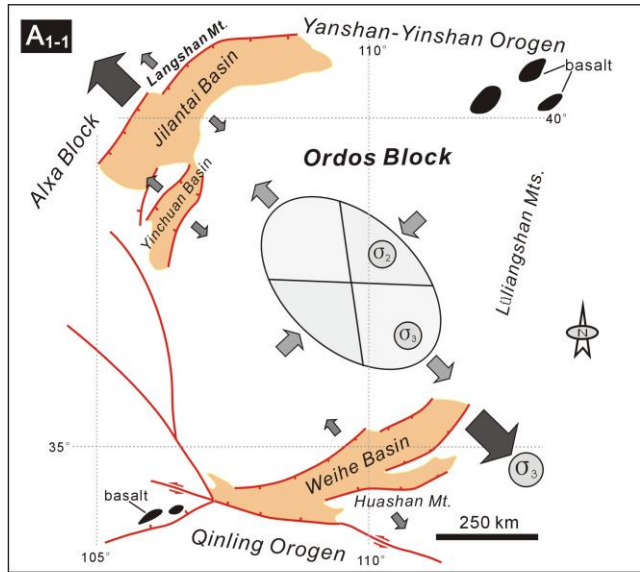
 angular unconformity

Fig 17





R-Riedel shear
R'-conjugate Riedel shear
P-shear fracture
D-main shear
T-tension fracture
S-compressive zone
 σ_1 -maximum principal stress
 σ_2 -intermediate principal stress
 σ_3 -minimum principle stress

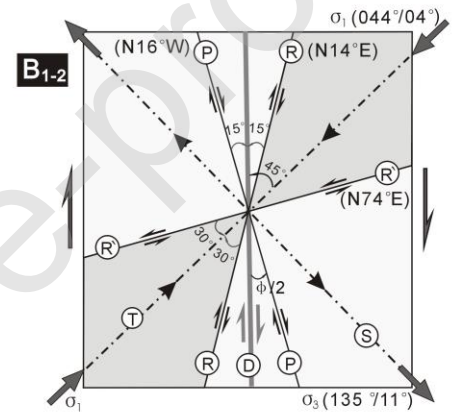
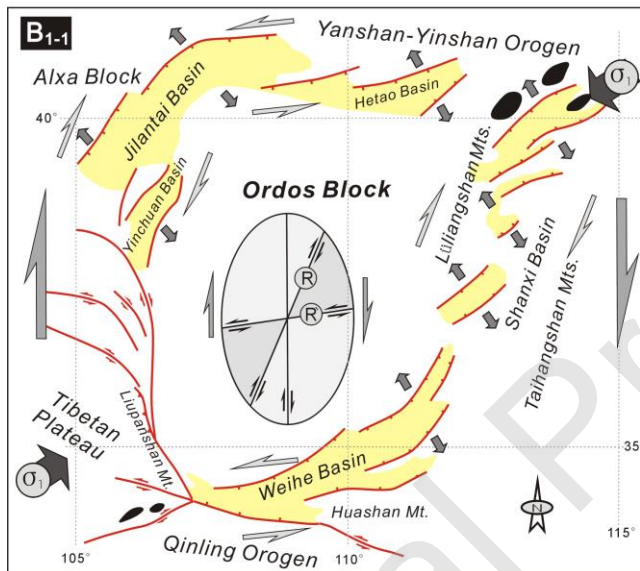
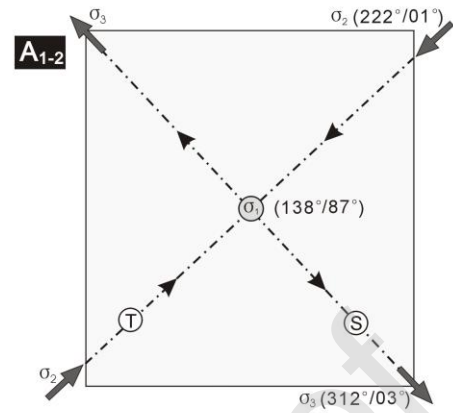


Table 1. Cenozoic strata frames of the Cenozoic basins around the Ordos Block.

Strata epoch		Age (Ma)		South Ningxia basin	Yinchuan basin	Jilantai basin	Hetao basin	Shanxi basin		Weihe basin
Holocene	Upper			Lacustrine deposit	Lacustrine deposit	Lacustrine deposit	Dishaogou Fm.	Alluvial deposit		Banpo Fm.
	Lower			Lingwu Fm.	Lingwu Fm.		Dagouwa Fm.			
Pleistocene	Upper		0.0	Malan Fm.	Shuidonggou Fm.	Malan Fm.	Malan Fm.	Malan Fm.	Daton g basalt	Malan Fm.
			0.1	Salawusu Fm.	Salawusu Fm.	Salawusu Fm.	Qianxian Fm.			
	Middle		0.7	Helan Fm.	Helan Fm.	Helan Fm.	Lishi Fm.	Lishi Fm.		Xiehu Fm.
				Yinchuan Fm.	Yinchuan Fm.	Yinchuan Fm.				Sanmen Fm.
Lower			Yangjuanpu Fm.	Yumen Fm.	Yumen Fm.	Alluvial deposit	Wucheng Fm.			
Neogene	Pliocene		2.5	Ganhegou Fm.	Ganhegou Fm.	Wulantuke Fm.	Wulantuke Fm.	Jinle Fm. Baode Fm.		Lantian Fm.
			5.3							Bahe Fm.
	Miocene		23.0	Zhangengpu Fm.	Zhangengpu Fm.	Wuyuan Fm.	Wuyuan Fm.	Hannuoba basalt		Koujiacun Fm.
				Qingshuiyi Fm.	Qingshuiyi Fm.					Lengshuiyou Fm.
Paleogene	Oligocene		33.9	Ng Fm.	ng Fm.	Linhe Fm.		Fansi basalt		Bailuyuan Fm.
				Sikouzi Fm.	Sikouzi Fm.	Wulate Fm.				
	Eocene			56.60						

	Paleocene								
--	-----------	--	--	--	--	--	--	--	--

Journal Pre-proof